Deliverable 16.2: Updated State-of-the-art report & Summary of major conclusions from the MAGIC work package

Work Package 16

This project has received funding from the European Union's Horizon 2020 research and innovation programme 2014-2018 under grant agreement N°847593

http://www.ejp-eurad.eu/

Document information

Project Acronym	**EURAD**
Project Title	**European Joint Programme on Radioactive Waste Management**
Project Type	**European Joint Programme (EJP)**
EC grant agreement No.	**847593**
Project starting / end date	**1st June 2019 – 30 May 2024**
Work Package No.	**16**
Work Package Title	**Chemo-Mechanical AGIng of Cementitious materials**
Work Package Acronym	**MAGIC**
Deliverable No.	**16.2**
Deliverable Title	**Updated State-of-the-art report & Summary of major conclusions from the work package**
Lead Beneficiary	**IRSN**
Contractual Delivery Date	**May 2024**
Actual Delivery Date	**May 2024**
Type	**Report**
Dissemination level	**PU**
Authors	**Alexandre Dauzères (IRSN), Olivier Helson (Andra), Sergey Churakov (PSI), Alain Sellier (LMDC), Erika Neeft (COVRA), Kristel Mijnendonckx (SCK-CEN), Andrea Cherkouk (HZDR), Guido Deissmann (FZJ).**

To be cited as:

Dauzères A., Helson O., Churakov S., Sellier A., Neeft E., Mijnendonckx K., Cherkouk A., Deismann G., Updated State-of-the-art report & Summary of major conclusions from the MAGIC work package. Final version as of 22.05/2024 of deliverable D16.2 of the HORIZON 2020 project EURAD. EC Grant agreement no: 847593.

Disclaimer

Acknowledgement

This document is a deliverable of the European Joint Programme on Radioactive Waste Management (EURAD). EURAD has received funding from the European Union's Horizon 2020 research and innovation programme under grant agreement No 847593.

Status of deliverable		
	By	Date
Delivered (Lead Beneficiary)	Alexandre Dauzères (IRSN)	March 2024
Reviewed (internal review)	MAGIC board members	April 2024
Reviewed (Reviewers)	Andres Idiart (Amphos 21)	May 2024
Approved (PMO)	Bernd Grambow	May 2024
Submitted to EC (Coordinator)	Coordinator (Andra)	May 2024

Executive Summary

The present report aims to consolidate all the key and noteworthy results achieved by the partners working over the past three years in the MAGIC work package (WP). It is the result of the analysis of five deliverables containing the entirety of the detailed scientific production of the WP. While MAGIC has been structured into tasks depending on the scale at which the chemo-mechanical ageing of cementitious materials in a geological disposal environment was studied, this report provides a different perspective. Indeed, it cross-references all the results from all tasks with a contextualization related to the life cycle to which the concretes will be exposed: from the operational phase to the long-term phase.

Due to its structure, this report will allow the reader both to identify the initial objectives of MAGIC based on the initial state of the art provided at the beginning of the project and to quickly understand the studies conducted with a systematic and concise recall of the experimental or modelling conditions chosen and a synthetic description of the noteworthy results. For more details, the reader can simultaneously refer to the technical deliverables that helped create this synthesis and were provided by the tasks.

This report concludes with a 6-page summary that highlights the added value in terms of knowledge development that the MAGIC WP has contributed to the understanding of chemo-mechanical ageing of cementitious materials in geological disposal conditions. This includes the development of knowledge on the chemo-mechanical ageing of concrete during the operational and long-term phases of disposal; the impact of microbial activity; the improvement of multi-scale modelling, particularly the chemo-mechanical modelling at the structural scale.

Table of content

List of figures

List of Tables

Glossary

AAR	Alkali aggregate reactions
ANN	Artificial Neural Networks
ASR	Alkali silica reactions
ASTM	American Society for Testing and Materials
ATP	Adenosine Triphosphate
BSA	Biogenic sulphuric acid
CASH	Calcium Aluminate Silicate Hydrates
CDF	Cumulative Distribution Function
CEBAMA	Cement Based Materials
CEM	Cement (CEM I, CEM II…)
CFL	Courant-Friedrichs-Lewy
CH	Calcium Hydroxide: Portlandite
CI	Cement-clay Interaction
CIGEO	Industrial Centre for Geological Disposal
CKD	Cement Kiln Dust
CNT	Classical Nucleation Theory
CORI	Cement Organic Radionuclide Interactions
COX	Callovo-Oxfordian clay
CSH	Calcium Silicates Hydrates
DDL	Diffuse double layer
DEM	Discrete Element Method
EC	European Commission
EDS	Energy dispersive spectroscopy
EPS	Extracellular Polymeric Substances
ESEM	Environmental Scanning Electron Microscopy
EU	European Union
EURAD	European Joint Programme on Radioactive Waste Management
FDM	Finite Difference Method
FE	Finite Element
FEM	Finite Element Method
FFT	Fast Fourier Transform
GC	Gouy-Chapman (model)
GDF	Geological disposal facilities
GEM	Gibbs Energy Minimization
HCP	Hydrated Cement Paste
HET	Heterogeneous
HLW	High-Level Waste
HON	Homogeneous
HPF	Hyperalkaline Plume in Fractured Rock
ILW	Intermediate Level Waste
ISA	Iso-Saccharinic Acid
ITZ	Interfacial Transition Zone
LAC	Low Alkaline Cement
LB	Lattice Boltzmann (method)
LBM	Lattice Boltzman Modelling
LCS	Long-Term Cement studies project
LLW	Low Level Waste
LMA	Law of Mass Action
MAGIC	The chemo-mechanical aging of cementitious materials
MGC	Modified Gouy Chapman model
MICP	Microbial induced calcite precipitation
MS	Member states
MSH	Magnesium Silicate Hydrate
NN	Neural Networks
NRUS	Nonlinear Resonant Ultrasound Spectroscopy
NS	Navier-Stokes

OPA	Opalinus Clay
OPC	Ordinary Portland Cement
OTU	Operational Taxonomic Unit
PB	Poisson Boltzmann
PDF	Probability Density Function
R&D	Research and Development
REV	Representative Elementary Volume
RH	Relative humidity
RUS	Resonant Ultrasound Spectroscopy
SEM	Scanning Electron Microscope
SNT	Supersaturation-Nucleation-Time
SOB	Sulphur-oxidizing bacteria
SOTA	State of the art
SRB	Sulphate reducing bacteria
TGA	Thermo-Gravimetry Analysis
THM	Thermo-hydro-mechanical
URL	Underground Rock Laboratory
VFA	Volatile fatty acids
WP	Work Package
XAS	X-ray absorption spectroscopy
XRD	X-ray diffraction analysis

1. General Introduction – From the conclusion of the initial SOTA to the objectives of MAGIC

In many radioactive waste disposal concepts, cementitious materials are widely used, for example as structural support material for access galleries and disposal drifts or cells (e.g., concrete/shotcrete), as well as grouts/mortars used as containment material for low and intermediate level wastes (Neeft et al. 2020). Thus, these cementitious materials can be in contact with both, the host rock clay or granitic formation as well as bentonite components (NEA, 2012; Neeft et al., 2020; Szabó-Krausz et al., 2021). Concretes, mortars, and grouts are used for structural and containment purposes in high-level and low-intermediate level radioactive waste repositories. Cement-based materials are envisaged for a large number of disposal facilities for intermediate level wastes across Europe and are already used as liners in disposal cells or as part of waste containers in many member states' existing facilities for low-level waste / near-surface disposal. Extensive feedback on the durability of concrete is available from the vast experience in civil engineering. However, a specific approach during the design and construction of a repository in terms of stringent safety requirements is of key importance. In addition, further understanding is required to support their use as a backfill material for radioactive intermediate and high level wastes in geological disposal, particularly to understand their contribution to the overall system performance during late post-closure time frames.

The mechanical behaviour of cementitious materials is strongly influenced by the boundary conditions imposed by the geotechnical system and the host rock (i.e. water saturation, temperature, etc.), during both the operational phase and the post-closure transient period (period with saturation progress). To assess the performance of the cementitious components, studies must be extended over long periods of time, considering various operating conditions. Cementitious materials are planned to be used as engineered barriers (i.e. buffer, plugs), as conditioning materials (waste packages and waste matrices) and as structural elements. These multiple uses require further understanding of their long-term behaviour, taking into account the mechanical initial state and including the impacts of all relevant physical and bio-geochemical processes (e.g. microbes) on their degradation. Furthermore, over the long term, ground- and pore-waters, with aggressive chemical ions, are a key driving factor for cementitious materials deterioration. The mineralogical and microstructural changes generated by these aggressive environments might have consequences on the mechanical behaviour of the cement matrix.

1.1 Previous conclusion in the initial SOTA

The initial state of the art report (SOTA) produced by the MAGIC WP (D16-1) summarized three decades of extensive Research & Development (R&D), allowing to identify the key reactive mechanisms, the alteration processes and consequences on the microstructure in cementitious materials emplaced in underground environment. It mentioned that the evolution under complex coupled perturbation phenomena were still not fully explored and understood and that recent innovations in terms of material formulations (low-pH cements notably) required dedicated R&D to better understand how their long-term performance is influenced by the host rock and the near-field conditions (i.e., degree of pore saturation, chemical evolution of the barriers, microbial impacts, loading and gas formation). Nowadays, most of the experimental data were limited to the short-term material evolution. Long-term mechanical integrity of the cementitious material remained largely unknown, despite existing data on ageing of Roman cements or natural analogues, provide evidence that the ageing of cementitious materials can be a very slow process, if well manufactured in response to the environment.

The collective work in the initial SOTA summarized the main conclusions according to the following themes:

- **About the physico-chemical evolution of concrete**

The main reactive processes controlling the chemical evolution of cementitious materials are globally well understood at the interface with the host rock or directly with the natural water:

- In saturated conditions: leaching, carbonation, magnesium and sulphate attacks, sometimes chloride attack (in function to the environment and concentration in sulphate) are the main processes identified.
- In unsaturated conditions, carbonation is the main process.

A deleterious impact of the ingress of sulphate species (sulphate attack) can be prevented with an appropriate choice in the type of cement formulation. If some studies focused on these disturbances, the impact of chemical changes on microstructure evolution and transport properties remains challenging. For example, the intensity of the pore clogging is influenced by the type and amount of salt and by the pore structure of the substrate. Several continuum scale reactive transport models have been developed to simulate these coupled disturbances (especially leaching and carbonation process). Recent works focused on Mg attack modelling accounting for the improved knowledge in the field of precipitation of Si-Mg phases (e.g. M-S-H). The predictive capability of such models depends on the accuracy of input parameters and their changes as the pore-structure evolves. If these essential parameters could be obtained from a pore-scale simulation able to resolve heterogeneities in cement paste microstructures, it is still an open issue, how to extract these essential parameters.

Only recently, a proper coupled description of reactive transport in unsaturated systems is feasable, accounting for multiphase transport, evaporation and porosity changes. This SOTA lists a few limitations in using reactive transport within cementitious materials in unsaturated conditions. The long-term processes impacting the cementitious materials exclude a simple approach and require multiscale modelling to take into account the relevant reactive pathways identified at the nano/micro and mesoscale, including the skeleton evolution. Indeed, the classical REV approach with a single porosity seems not to be capable to correctly simulate the behaviour of complex materials like concrete composed of several porosity levels (capillary, C-S-H…) in the long term.

- **About the microbial interactions with concrete**

Limited research has been performed to characterize microbial interactions with cementitious materials. Especially studies in relation to nuclear waste disposal remain scarce. Microbial degradation of cementitious materials has been shown in various environments such as sewage pipes, marine structures and wastewater treatment systems. Cementitious materials impose a highly alkaline environment, which inhibits microbial activity. However, several processes affect the chemical evolution of cementitious materials, which can result in a local decrease in pH, enabling microbial activity. Furthermore, concrete is a quasi-brittle material in which the formation of cracks gives microorganisms space to migrate and attach along the surfaces. In such a case, a biofilm can be formed. Microbial degradation of cementitious materials is mainly caused by the biological production of organic and inorganic acids, which can react with the cement.

- **About the mechanical evolution of concrete**

The main part of studies relative to cementitious materials in geological disposal environment focuses on the chemical and microstructural evolutions. But cementitious materials will play essentially a mechanical role in repositories and consequences of the chemical and microstructural changes on the mechanical properties were under-explored.

The mechanical behaviour of underground cementitious structures depends on various parameters: boundary conditions and construction methods. The assessment of long-term performance requires to take into account the host rock loading and the stiffness evolution of the structure. This evolution is

depending on the chemical and microbial perturbations, the level of loading and also the concrete formulation.

In the case of reinforced concrete, corrosion causes mechanical damage to the concrete under the combined effect of the corrosion-induced expansion (generating internal mechanical stresses) and the loss of cross-sectional area and bonding of the steel, which causes the structure to lose its load-bearing capacity. Previous experimental results highlighted the heterogeneity of the corrosion product layers and the evolution of the mechanical properties of the layers with time and ageing conditions. A specific effort has to be made to understand this behavior.

The multiscale characterization and especially the coupled approach at nano/microscale with RUS, nano/micro indentation, and by SEM/EDS is a key to recover data to feed numerical chemo-mechanical modelling. Currently, studies on the micro-mechanical consequences of groundwater on cementitious materials are very scarce (mainly in pure water, nitric acid solutions or sulphated water). These works highlight a non-negligible evolution of elastic mechanical properties of the cement matrix subjected to an aggressive solution but the results obtained are hard to interpret for their significance in the context of disposal of radioactive waste. Disposal representative experimental results are difficult to obtain from short term experiments.

The use of numerical approaches to determine the mechanical behaviour of cementitious materials has gained growing interest in recent years, due to the continuous increase of computational power. Characterising the mechanical properties of cementitious materials requires understanding the evolution of the microstructure and corresponding phase assemblage of the cement paste in the context of its disposal environment.

Many studies have been devoted to the analysis and description of the evolution of the microstructural and mechanical properties of cementitious materials when subjected to the contact of groundwater and argillite. At the nano-microscale, the different minerals (phase assemblage) composing the hydrated cement paste should in principle be considered since the paste holds the aggregates together. The mechanical strength of concrete is determined by the content of aggregates, the strength of these aggregates and how well these aggregates are attached to the cementitious phase in concrete. At the nanoscale, the use of approaches based on molecular dynamics is widely accepted. At the microscale, more advanced and versatile methods (micromechanics and upscaling, Mori-Tanaka method, homogenization schemes …) have been developed to estimate the properties evolutions.

Carbonation and leaching have antagonistic effects on porosity and some mechanical parameters. Both processes are integrated in multi-scale models but treated separately experimentally. This raises several questions:

- Will one process dominate the other? If so, over what period of the concrete's life?
- Would one process dominate in the short term and the other in the longer term?
- Has their superposition been treated experimentally?

Whatever the scale considered, an accurate description of the microcracking and its repercussions on both mechanical and diffusive properties is essential to the simulation of the coupled response of cementitious materials.

- **About the chemo-mechanical coupling in concrete**

The multiscale chemo-mechanical modelling was not sufficiently supported in the past as part of the geological disposal context. Two main reasons explain this situation: (i) the limitation of the power of the modelling tools, (ii) the isolation of teams and researchers between chemistry and mechanics with difficulties to communicate. In the SOTA, this part was considered beyond the boundaries of the disposal context, at the pore/microstructure scales, mesoscale and the macroscale. A special attention was paid

to identify what are the key limits and gaps remaining to obtain representative chemo-mechanical models of concrete in geological disposal context.

The pore scale modelling

The pore-scale modelling is relatively young, and there are many limits and gaps. The pore scale approach requires new conceptualizations that might be different from more established continuum approaches. This is true for both, chemical and mechanical processes. Typically, pore scale models have discrete phases, but they also might include sub-scale elements (for example amorphous phases) that are treated differently. Because of the heterogeneity of cement paste microstructure, the number of voxels/elements of pore-scale models is large. The need for computationally efficient approaches is paramount. The most obvious approach is to use parallelization and more powerful computers, but the physical limit of small time steps at lower spatial scales results in huge amounts of iterations and requires broader solutions. One mitigation strategy is an effective geochemistry calculation. The solution time of non-linear equations for the geochemical system can be reduced using tabulated values or abstracted chemical systems. The number of time steps can be reduced by adjusting the chemical systems.

Another field that needs attention is the validation of pore-scale models. Most experiments provide continuum or effective values (e.g. mass of a specific solid phase) or information without spatial information, for example pore size distribution. It is very difficult to obtain spatial information of a property at precisely the same location in an evolving material after the geochemical alteration reaction. For this reason, pore scale models are usually validated using averaged values. However, it is important to underline that this is an indirect validation where a part of the important information is lost during averaging. In the future, more efforts need to be devoted to the experimental techniques that can directly support validation of pore scale models.

As mentioned, coupling between chemistry and mechanics is very recent on the pore scale. This coupling can result in a complex spatial-temporal evolution of composition, microstructure and morphology in materials. The relationships are interconnected as for example not only the formation of secondary phases cause stresses, but also the stresses influence the conditions of the formation of secondary phases. Reliable chemo-mechanical models are not very common, especially not in a multiscale framework.

The challenge of upscaling

Appropriate upscaling is another challenge. The purpose of pore-scale models is to support the choice of parameter values and constitutive laws on larger scales. The upscaling in this sense usually stretches beyond pure mathematical principles and includes the development of conceptual models and concepts that are appropriate for use on larger scales.

Previous structural chemo-mechanical models decoupled the macroscopic modelling from the mesoscopic phenomena. However, in order to compare concrete properties made of different matrices, a non-linear analytical homogenisation model for the chemical-mechanical behaviour of concrete is required to be implemented. Such a model must be able to assess the solid phases of cement paste as a function of the chemical state of concrete, and this must be reflected in the mechanical properties. Furthermore, during the chemical damage processes (leaching, carbonation, NaCl ingress…in the hydrated cement paste), this model should also consider the amount and nature of aggregates on macroscopic residual mechanical properties.

The specific case of reinforced concrete

Until now, the phenomenological modelling of reinforcement corrosion was decoupled from the chemical state of the concrete. Hence the goal in this chemo-mechanical model consist in predicting the progress of steel corrosion as a function of the chemical state of the concrete at the interface and in localised

cracks, deducing its effect in terms of steel anchorage and its contribution on the mechanical performances of reinforced concrete.

Another phenomenon to be considered and incorporated into this model is the cracking of reinforced concrete, along with predicting its impact on the transport properties (permeability, diffusion coefficient, water retention curve…) of the concrete.

The implementation solution

The goal is the implementation in a Thermo-Hydro-Chemo-Mechanical finite element code able to compute the evolution of a tunnel during several thousand years. Once implemented, it will allow a more accurate prediction of the lifetime of radioactive waste disposal structures, but also the simulation of their very long-term behaviour under natural mechanical loading and physicochemical degradation caused by the host rock water. Different chemistry of binders could be considered as variables to perform comparative studies of envisioned solutions.

1.2 Initial objectives and outcomes of the MAGIC WP

Based on this SOTA review, the cementitious materials studied in MAGIC have different initial properties due to their function in the deep geological disposal facility. As indicated in deliverable 16.4, there are three main categories of materials selected:

- Concrete linings of tunnels ensure safety during the operating phase and must therefore guarantee mechanical stability for over a hundred years. Liners need to support the convergence of the geological environment in the case of clay rocks. This component is exposed to atmospheric carbonation and drying under the effect of ventilation. In the long term the failure of this component can have an impact on the extension of the excavation damaged zone of the host rock (Armand et al., 2014). The expected extension is not the same whether the void between containers and liners is empty or filled with material (e.g. sand). It is therefore important to study the influence of chemical degradation, induced by multi-ionic attacks caused by the environment through contact with water/rock. This can lead to degradation by leaching, carbonation, sulphate attack, etc. This type of structure is also subject to degradation by corrosion of the reinforcement, the propagation of which is not well known, depending on cracking and the initial quality of the steel/concrete interface (Castel et al., 2006).

- Sealing plugs have a mechanical function, which consists of containing the swelling pressures of the clay core (bentonite) (Lebon, et al., 2013). In this case, the re-saturation of the swelling clay core can charge the groundwater with sulphates and chlorides and therefore alter the concrete components in contact with the bentonite pore water (María Cruz Alonso et al., 2017). In the case of closure structures, the use of low pH concrete is a solution to prevent chemical evolution of clay materials with time (host rock and bentonite) (Pernicova et al., 2023). The advantage is twofold in the case of plugs, as low pH concretes have the advantage of low heat of hydration and therefore avoid reaching excessively high temperatures during setting that could alter mechanical and transfer properties. Depending on the geometry of the closure structure, the plugs are cast directly in contact with the host rock, and the swelling of the clay core can apply an axial force that mechanically solicits the interface (Stavropoulou et al., 2020). Chemical degradation of concrete can affect the mechanical behaviour of the interface between the concrete and the host rock by altering the first few centimetres of the component.

- Backfill and buffer-like materials are also studied in MAGIC. Backfill fills voids and helps dissipate heat providing a material with a higher thermal conductivity than concrete, while buffer provides an alkaline environment to limit the corrosion rate of the carbon steel overpack (Li et al., 2023), under anaerobic conditions (Tyupina et al., 2023). The buffer's protection against corrosion includes a period during which the waste emits heat in amounts that the host rock is

heated by the wastes. The buffer also contributes to the radiological shielding facilitating handling during the operational phase (Bel et al., 2006).

The MAGIC WP was built to increase the confidence in chemo-mechanical simulations by reducing uncertainties in input data and understanding of key coupled processes (for both young and aged materials). Specific conditions for waste disposal (microbial activity, chemical and mechanical stress, variable saturation, etc…) are taken into account by addressing implementation needs and safety aspects, e.g. regarding selection of materials, dimensioning, and (long-term) behaviour of seals and plugs.

The MAGIC WP has four main objectives:

1- To quantify the chemo-mechanical multi-scale evolution of cementitious materials under the chemical degradation expected in repository environments.

2- To identify the main reactive pathways at the repository scale during the re-saturation phase and at saturated conditions.

3- To obtain a reference chemo-mechanical model of Portland and low-pH concretes exposed to relevant disposal environments, considering representative boundary conditions.

4- To estimate the extent of the impact of microbial activity on concrete properties (low-pH and Portland cement) in partially and fully saturated media.

Linked to these objectives, a list of expected outcomes was determined:

- To obtain an experimental dataset, from the microscale to the scale of concrete specimen samples, clearly highlighting the link between the chemical degradation of selected cementitious materials under coupled representative disturbances and the evolution of their mechanical parameters: compressive and tensile strengths, Young's modulus, cracks formation and their dynamics of propagation, evolution of samples initially under creep or damaged.

- To clearly identify the main reactive mechanisms and their consequences on the mechanical behaviour of Low-pH and Portland cementitious formulations with and without a microbial impact.

- To be able to model the mechanical behaviour under chemical evolution of the cementitious materials formulations selected at the experimental scale.

- To determine a mechanical constitutive law of the cementitious material, taking into account the chemical and hydrodynamical evolutions and processes occurring at different scales.

- To model the long-term mechanical evolution of cement-based materials exposed to a set of disposal conditions while taking into account the chemical evolution of the system.

This report is organized in four chapters. In order to exhibit the complementarity at the different scales studied in the MAGIC WP, this report is not organized per Task but in function to the successive environments encountered by the cementitious materials during their life cycle. After this introduction recalling the key conclusions of the initial SOTA and the objectives that followed, the second and third chapters are dedicated to the results of the chemo-mechanical evolution of cementitious materials during the operating and the post closure phases of the disposal facility, respectively. The fourth chapter focuses on the impact of the microbial activity. The fifth chapter presents the modelling of the base cases before to conclude on the added value of the WP about concrete structure ageing.

This final report of the MAGIC WP is a synthesis of 5 technical deliverables produced by all partners. Its objective is to give to the reader the easiest understanding of the main highlights and results of the WP in relation to the main initial questions and expected outcomes of the WP.

For more details about the experimental or modelling conditions, and detailed calculations, please refer to the corresponding deliverables.

2. The chemo-mechanical evolution of cementitious materials during the operating phase of the disposal facility

During the operating and early post closure period, cementitious materials evolve under unsaturated conditions. In this context, the main identified chemical process is atmospheric carbonation. This chemical reaction can lead to a chemical gradient from the surface of the concrete structure to the steel reinforcements. An uncontrolled evolution can lead to an increase of the corrosion rate and may have an impact on the mechanical properties of the cementitious structure. The conception phase takes this evolution into account and technical decisions can prevent such an evolution (formulations, steel embedding).

The partners working in the MAGIC work package on reactivity in unsaturated media have proposed additional experiments to identify the key chemical and microstructural changes and their consequences on the mechanical behaviour of the cementitious material from the nanoscale to the structure scale to feed the modelling development.

2.1 From the nanoscale to the macroscale, experimental approaches and main results

2.1.1 Impact of the carbonation of the cementitious material

The carbonation process on cementitious materials has multiple impacts on the mechanical behaviour of concrete associated to mineralogical and microstructural changes as stated previously and in the state of the art of the MAGIC program (Deliverable 16.1, §1.1.1 and 2.3.2). The reaction of carbon dioxide with portlandite and C-S-H (Bary and Sellier, 2004) leads to calcite production associated with pore filling by calcite and carbonation shrinkage as well as modifications of mechanical characteristics of C-S-H phases which are experiencing decalcification.

These different effects may lead to opposite evolutions in the mechanical behaviour of concrete under carbonation. The densification due to filling of pores or even initial pre-existent microcracks tends to increase the strength of concrete and the Young's modulus (Merah and Krobba, 2017) whereas C-S-H decalcification and subsequent shrinkage (Kangni-Foli et al., 2021) in a heterogeneous material (cementitious matrix, aggregates, air voids) could generate new micro-cracks and a decrease in mechanical properties (Cheng et al., 2016).

In addition, concrete materials used in deep geological disposal facilities are frequently submitted to (partial) drying, at least during a period of their lifetime. This could develop drying shrinkage (Bisschop and Van Mier, 2002) even before any carbonation or loading process. This shrinkage is linked to potential microcracking between constituents of concrete (mainly matrix shrinking around "rigid" aggregates) but also due to presence of heterogeneous hydraulic gradients. For example, in tunnel linings, the intrados side would be submitted to a drying environment but due to the low mass transfer properties of concrete, the progression of the desaturation front towards the core of lining is expected to be very slow. As a result, a shrinking concrete near the intrados around a non-shrinking core would lead to "structural" microcracking. In the same way, this structural effect could appear for differential carbonation shrinkage between the exposed side and the inner part of a concrete lining.

These material and structural shrinkages, due to drying and carbonation, could affect in a different way the mechanical behaviour and could also enhance the kinetics of carbonation towards the core of a structure (or sample). Therefore, all these chemo-thermo-hydro-mechanical phenomena act in a complex manner with couplings and competitive effects at different scales. This still need to be better accounted for.

At small scale, the CEA developed an experimental program dedicated to provide all the data and information that were necessary for the simulations of the cracking of the cement paste (C_3S and C-S-

H pastes). The objective of modelling was finally to simulate the accelerated carbonation tests (3 % CO_2) carried out in an IRSN thesis (Kangni-Foli, 2019) taking advantage of model pastes (C_3S and C-S-H pastes). A lot of data were needed for such simulations. The CEA's experiments focused on the influence of carbonation on the change in water desorption isotherms of cement-based materials. It must be recalled here that there exist some results showing the impact of carbonation on the water retention curve. These results were however obtained after the materials were completely carbonated and they do not give all the information needed for the modelling: there is still a need to understand the intermediate states of carbonation. The objectives of this work were to: (1) design and setup a new methodology to ensure intermediate uniform carbonation states within samples and (2) measure the water desorption isotherms at different intermediate states of carbonation.

The main idea was to take advantage of a commercial Dynamic Vapour Sorption device (DVS Intrinsic from SMS Ltd) that was modified so that the user can select the carrier gas: either pure nitrogen (N_2) or a mix of N_2 and CO_2 (Figure 2-1). A DVS is a device that allows weighing constantly and accurately a sample that is subjected to a gas flux at controlled environmental conditions. The use of the two different carrier gases makes it possible either to measure either the carbonation or the water desorption isotherm using a single device. The sample tested in the DVS is a finely divided material, i.e. the material to be tested is powdered before use (the grains were less than 200 µm in diameter in this specific case). This is important because it means that CO_2 diffusion within the grains is fast and is not the limiting step of carbonation signifying that the rate of CO_2 reaction within the grains is the limiting step. The main consequence is that uniform carbonation states can be reached within the grains depending on the CO_2 exposition time. The disadvantage is that concrete itself is not tested. A translation of the experimental results into disposal representative outcomes needs to be made. This translation needs to cover tens, hundreds or thousands of years after which the same magnitude of reaction would have taken place in the cementitious phase of concrete, as observed in this laboratory experiment.

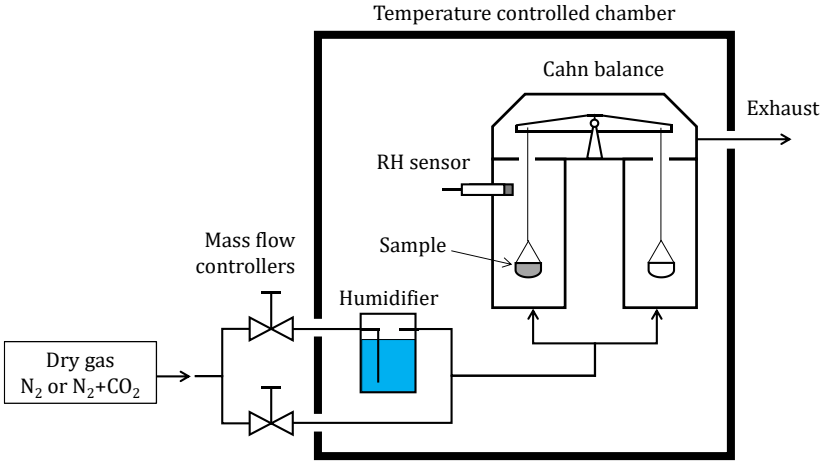

Figure 2-1: Schematic view of the modified DVS, a three-way valve was added so that the user can select the carrier-gas either N_2 or a mix of N_2 and CO_2.

The DVS was used with CEM V/A (see deliverable D16-9 for more information) and with the two model pastes designed and tested in a previous work (Kangni-Foli, 2019). The first one is an ordinary mature C_3S paste with a water-to-cement ratio equal to 0.5 and the second one is a C-S-H paste prepared using C_3S and nanosilica in stoichiometric amounts so that the C/S of the C-S-H was equal to 1.4. The main advantage of these two materials is that their mineralogical compositions are extremely simple: the C-S-H paste only contained C-S-H with C/S = 1.4 whereas the C_3S paste contains portlandite and C-S-H (with C/S ≈ 1.7). The advantage of using model materials is that it makes quantification much more straightforward and easier. Note that these materials were prepared especially for the MAGIC project and kept more than a year under water before use.

In practice, a small sample of model paste (a few tens of mg) was first re-saturated by adding demineralized water, then introduced into the DVS and equilibrated at 55% RH under nitrogen flow. Once equilibrium was reached (i.e. constant mass), a mixture of nitrogen and CO_2 (3 wt%) was injected for a period decided by the user in order to reach different states of carbonation. After that, the sample was once again re-saturated using demineralized water and reinserted in the DVS to measure the water desorption isotherm under N_2 flow.

After the accelerated carbonation phase and measurement of the desorption isotherm in the DVS, the sample was recovered for analysis by XRD and TGA. In a first time, the sample was mounted on a zero background XRD holder and then the diffractogram was collected using Cu-Kα radiation between 5° and 70°. The diffractogram was used to identify the mineral phases present and quantify them using the Rietveld method. Finally, thermogravimetric analysis was performed between 25°C and 1150°C with a heating rate of 10°C/min under N_2 flow (80 mL/min). The amount of $CaCO_3$ was then evaluated using the tangential method considering the mass loss between 600°C and 1000°C.

Results show the mass gain of the C-S-H paste during the accelerated carbonation phase of the five tests. When exposed to CO_2 the C-S-H quickly gains weight during the first days in line with CO_2 binding. It is noteworthy that the mass gain slightly decreases after nearly a week of carbonation. The results obtained using TGA and XRD clearly show that the level of carbonation[1] of C-S-H paste samples increased with the duration of exposure to CO_2. Note that the results could provide an estimation of the reaction rate of the C-S-H.

Figure 2-2 highlights possible helpful results for the modelling. However, it needs to be kept in mind that the results are obtained with cement paste and not with concrete. The reaction rims made during hardening between the aggregates and cementitious fluid (Jackson et al., 2017) may provide a denser and more refined pore structure than cement paste alone. The figure presents the resulting water retention as a function of carbonation time for both model cement pastes. The isotherms are strongly impacted for the C-S-H paste: carbonation reduces the amount of water retained over the whole RH-range and the intensity of the decrease increases with the carbonation time in line with C-S-H dissolution and solid densification (due to CO_2 fixation). Unlike the C-S-H paste, the isotherm of the C_3S paste is hardly modified at low RH: portlandite helps protecting the C-S-H from carbonation and dissolution. The effect of carbonation is however more marked at high RH (over 50%) probably in line with portlandite dissolution that tends to coarsen the pore-structure. Quantifying the carbonation rates appeared more difficult than for C-S-H paste, mainly due to the presence of different inflections in the thermogravimetric curve associated with the probable presence of different types of $CaCO_3$ (and maybe amorphous). The values obtained were however of the order of 30% for 3 days of carbonation and of 45-50% for 15 and 21 days of carbonation. Note that these values remain limited even after three weeks of carbonation in the DVS. **This indicates that the carbonation rate of the C_3S paste is much lower than that of the C-S-H paste, due to the protective presence of portlandite. The presence of portlandite in the cementitious materials is a key with respect to carbonation intensity**. From a practical point of view, much longer - and prohibitive - times would be required to achieve higher carbonation levels. In other words, the carbonation procedure used here is perfectly suited for the C-S-H paste but not for the C_3S paste.

[1] The carbonation level is defined as the ratio of the amount CO_2 fixed (mol) to the total amount of Ca (mol).

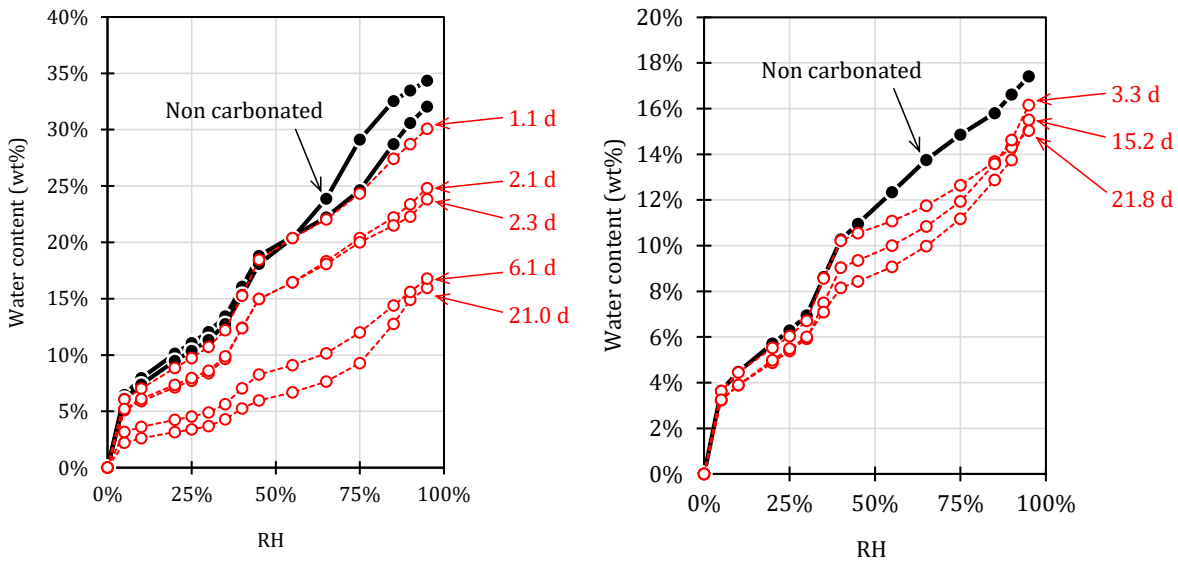

Figure 2-2: Effect of carbonation on the water retention curve in the C-S-H paste (left), b/ the C_3S paste (right) at room temperature.

These results provide a clearer picture of the effect of carbonation on water retention in cementitious materials. The release of free water during carbonation is an important point - that remains unfortunately unaccounted for - as the amount of water affects not only CO_2 transport (and therefore the carbonation rate) but also deformation (and therefore potentially cracking). This is taken into account in the modelling.

A complementary work was conducted by LAMCUBE to obtain a better understanding of carbonation effects with a focus on the microstructure evolution from the microscale to the mesoscale. A specific laboratory testing programme on mortars constituted of Portland cement was designed. Uniaxial and triaxial compression tests were performed with microtomographic monitoring. Digital Volume Correlation (DVC) was used to determine the local strain fields and cracks in the tested samples with different carbonation degrees. Uniaxial creep tests were also conducted. For the realization of those tests, specific experimental devices were designed and fabricated (see deliverable D16.5).

The tested mortar samples were cast according to the specification jointly designed with other partners (LMDC, Andra) in order to optimize the carbonation process. Sand up to 1 mm size was used as aggregate. The aggregate size is rather small, which should have an impact on mechanical properties and cracking under loading. The main specifications are “Water absorption of sand = 0.5%”, “Efficient water / Cement = 0.579” and “Sand / Cement = 2”. Samples initially cured at room temperature and approximately 100% humidity for 28 days were conserved in lime-saturated water before testing. The initial state of each sample was scanned by X-ray micro-tomography and the obtained results used as the reference state. The carbonation of samples was completed at 20°C with 65% Relative Humidity (RH) and 50% CO2 concentration in a specifically designed climatic chamber. Three carbonation percentages (volume) were considered (0%, 50% and 100%). The carbonated samples were again examined with X-ray micro-tomography to determine the microstructural modification due to carbonation. It was found that the carbonation process induced non-uniform shrinkage in the samples. The rate of shrinkage was faster when the carbonation level became higher than 50%. The local shrinkage bands are mainly located in the cement portion of the interfacial zone between cement and sand. A few dilation bands can also be observed in the initial crack zones of some samples. There is some slight expansion of cracks during the carbonation process.

According to the uniaxial compression tests, the uniaxial compressive strength of the mortar is between 60 and 65 MPa at 28 days-cure (cylindrical samples size: 25mm height – 5 mm of diameter). With the help of the DVC analysis, the distributions of both axial and radial strains are clearly non-uniform inside the samples, due to the material heterogeneity. The high deformation zones are mainly located in the porous cement agglutinated zones. The axial strain field is dominantly compressive but dilatant zones are observed also. At the same time, the distribution of radial strain seems more complex containing dilatant and compressive zones. An example of radial strain distribution is shown in Figure 2-3.

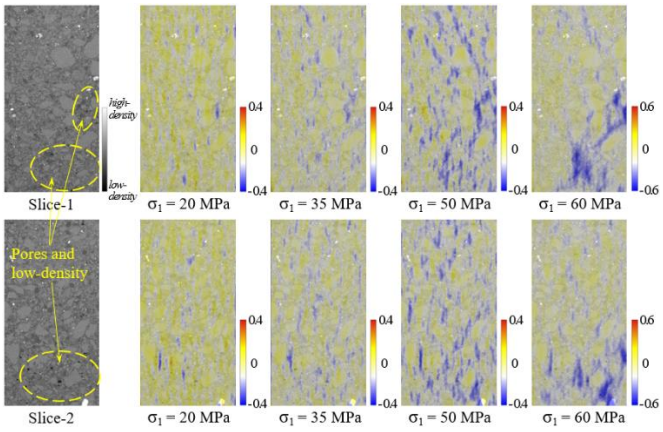

Figure 2-3 - Distributions of accumulated radial strain (in %) along two orthogonal vertical slices in sample S1-1

The general trends of stress-strain responses of the mortar in triaxial compression tests are very similar to those in the uniaxial compression tests. However, as for most frictional materials, the failure strength increases with the confining pressure, approximately by 25% for 3 MPa and 50% for 6 MPa. As for the uniaxial compression, the local strain fields are also clearly non-uniform inside the samples. Moreover, it is found that initial cracks are present in some samples. These ones affect the deformation during the subsequent loading process. The initial cracks are compressed in the axial direction and induce a large axial compressive strain. In some zones, the initial cracks lead to large compressive axial and large dilatant radial strain. An example of strain fields in a triaxial compression test with 3 MPa confining pressure is presented Figure 2-4.

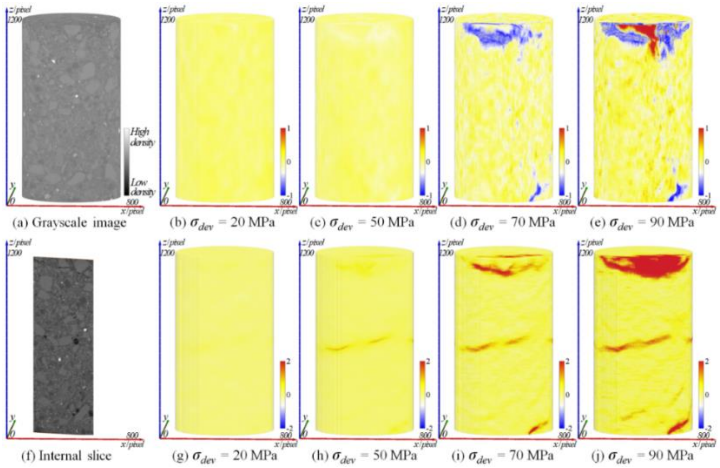

Figure 2-4 - Distributions of accumulated radial (b~e) and axial (g~j) strains (in %) of sample S1-3s in a triaxial compression test with 3 MPa confining pressure

Comparisons between sound and carbonated samples are performed. **It is found that there is no clear difference of the deformation mechanism. However, as the carbonation process induces**

additional material heterogeneities, the strain distributions of carbonated samples exhibit a higher heterogeneity. Some strongly strain concentration zones are observed. At the same time, there is an increase of mechanical strength due to carbonation. For instance, the uniaxial failure strength is increase by 10% for the 50% carbonated samples but nearly 40% for the fully carbonated ones.

In parallel, at macroscale, LAMCUBE in collaboration with ANDRA and LMDC focused on an experimental approach to evaluate the effect of atmospheric carbonation on residual mechanical properties of concrete. Moreover, drying shrinkage related microcracking was also taken into account. Hence, an experimental campaign has been planned for this purpose and aimed in particular at:

- Generating different carbonation states with an accelerated protocol in concrete samples to evaluate how carbonation extent may affect its mechanical properties.
- Characterizing mechanical properties under uniaxial and triaxial compression, three-point bending and creep to quantity the effects of carbonation on elastic and strength properties.
- Evaluating the role of pre-existing (micro)cracks before carbonation on mechanical properties to address this potential phenomenon in concrete linings.

Three major results are selected. Firstly, after a phase to adapt the carbonation process to ensure the achievement of different carbonation states (sound, 50% carbonation and 100%+ carbonation), a series of uniaxial compression tests has been performed to evaluate the modification in the mechanical behaviour of 4 concrete samples (representative of the whole tested samples) with carbonation (Figure 2-5).

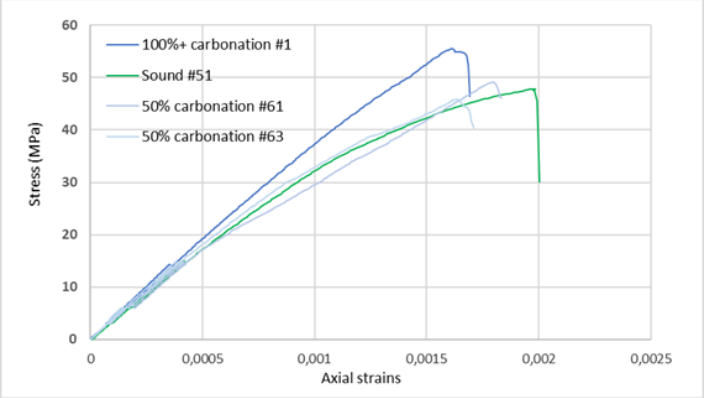

Figure 2-5 - Stress-strain curves in uniaxial compression for samples #1, 51, 61 and 63 (different carbonation states)

It appears that the behaviour of 100% + carbonated sample #1 has a higher strength and a more linear stress-strain curve compared to sound (sample #51) or partially carbonated samples (samples #61 end #63).

A quantitative comparison is done of individual properties (E, v, failure strength Rc) for samples under uniaxial compression and grouped by carbonation states. Average failure strength of sound samples is 47.8 MPa, higher than for saturated samples without pre-drying (41 MPa). A 50% carbonation does not change this value (47.3 MPa). For a 100%+ carbonation state, the increase is +25% compared to sound samples. For the Young's modulus, a 3% increase between sound and 50% carbonation is observed, and +10% for 100%+ carbonation. The Poisson's ratio v appears to be unaffected by carbonation and stays around 0.24-0.26.

The creation of solid calcite inside the existing porous network (and potential initial microcracks) may help filling the gaps and both reduce friction of cracks (solid phase continuity between the edges of cracks) and limit the creation of new ones (decreasing porosity and therefore higher strength). This can be linked to the increase in strength, Young's modulus, a more linear strain-stress curve and a more

brittle failure for 100%+ carbonated samples. For the partial carbonation state (50%), the effect of carbonation on the mechanical behaviour remains small compared to the 100%+ state. For the failure strain, if 50% of the cross section of the sample remain sound, the failure strength of this inner part should be identical to sound samples and will be the cause of the failure (weakest link effect, the outer part has a better strength but cannot fully support the load once the inner part has reached its peak value).

Secondly, triaxial compression tests were performed to check the influence of a triaxial loading state on residual properties of carbonated samples. In Table 2-1, quantitative properties measured are listed on samples under triaxial and uniaxial compression, according to the sample state of carbonation. The Poisson's ratio v seems unaffected neither by the confining pressure nor the state of carbonation (between 0.24 and 0.26). The Young's modulus E remains similar at sound state and 50% of carbonation both with or without confining pressure (37-38 GPa).

Table 2-1 - Comparison of triaxial and uniaxial compression results according to carbonation

Confining	Sample state	Sample number	Rc (MPa)	E (GPa)	v (-)
Pc = 3 MPa	100 %+ carbonation	12	93.0	40.5	0.25
	50 % carbonation	62	74.2	37.4	0.25
	Sound	51	74.0	37.0	0.26
Pc = 0 MPa	100 %+ carbonation	Average 2 samples	59.6	40.9	0.26
	50 % carbonation	Average 3 samples	47.3	38.3	0.24
	Sound	Average 2 samples	47.8	37.1	0.26

However, a same increase due to 100%+ carbonation is observed and tends to confirm the findings in uniaxial compression. The confining pressure does not change the value of the elastic modulus (perhaps a slight decrease is indicated but statistically significant conclusions cannot be drawn as only one sample has been tested in triaxial tests). The most important change due to the addition of a confining pressure concerns the peak strength which is about 55% higher in comparison with uniaxial compression, whatever the level of carbonation. **This large effect of confining pressure would indicate that it may exist a potential "structural confining" of the inner part of a specimen due to an important carbonation shrinkage in the outer part (at high level of C-S-H decalcification), leading to an increase in strength**.

Finally, previous experiments on samples without pre-damage at different states of carbonation under uniaxial compression tests are compared to pre-damaged samples before carbonation (Figure 2-6). A clear decrease of 23% in the failure strength of the pre-damaged sample is observed and a decrease of 6% for the Young's modulus. **However, the behaviour of the pre-damaged sample is more or less comparable to the one observed on the 100%+ carbonated sample (predominance of a linear behaviour up to peak strength), even if this pre-damaged sample is not carbonated. This could be an indication that existing cracks may limit the extent of creation of new cracks during the uniaxial compression test.** The non-linearity could be more tied to this creation of new cracks rather than sliding between edges of existing cracks. Therefore, the effectiveness of this protocol is confirmed. The Poisson's ratio remains in the same range as in previous tests (0.24-0.26) without any clear effect. Additional tests are required to improve the statistical significance of these comparisons, mainly by comparing the mechanical behaviour of pre-damaged samples submitted to carbonation.

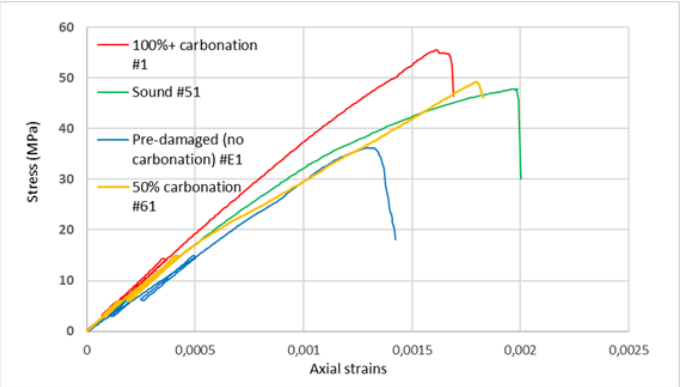

Figure 2-6 - Comparison of axial stress-strain curves for different samples under different conditions in uniaxial compression

SCK-CEN, COVRA and FZJ investigated the impact of carbonation on the compressive strength of two types of concrete: a buffer-like concrete and backfill concrete. Buffer-like concrete was made with CEM III/B. The porosity for buffer-like concrete made with CEM III/B was 12-13% (only capillary pores). The buffer-like concrete was expected to have a too small size of pores to allow microbial activity inside the concrete specimen (discussed in Part 4 of the present report). A buffer-like concrete specimen made with CEM III/A (a blend of OPC (35-64 wt%) and Blast Furnace Slag (36-65 wt%)) was investigated. This specimen was manufactured in 1993. Only concrete (with aggregates) was considered. All cubical samples were made with siliceous aggregates with a size at least ten times smaller than the edge of the specimens. The edges of these samples were 5 cm, 10 cm and 15 cm.

The experimental approach consisted in 40 initially saturated buffer-like concrete specimens dried at 11 different relative humidities at 20°C and 9 different relative humidities at 5°C for about 1000 days in air. In order to investigate the effect of a different distribution in size of pores, a similar amount of initially saturated backfill concrete specimens with the same type of cement (CEM III/B) and content but different porosity than buffer-like concrete was also dried. Since the carbonation rims were negligible in size, the porosity was determined from the initial weight and the final weight at the lowest relative humidity of 6% i.e. a gravimetrical measurement. The degree of saturation in equilibrium with each relative humidity was also gravimetrically determined. The volume of pores with a certain size was calculated with the Young-Laplace relationship. The compressive strength was measured after 1000 days and compared with the strength measured of other specimens after 28 days. The concrete specimens were split by hand and a photograph was taken of the freshly cracked surface to measure the oxygen penetration front and again after spraying with a phenolphthalein solution in order to measure the carbonation front.

Main results (Figure 2-7) exhibit that buffer-like concrete has only capillary pores i.e. the difference in content in water between 98% relative humidity and submerged is almost negligible. Its strength was measured to increase with decreasing degree of saturation. The contribution of the suction force could be well predicted by the volume of pores that had a certain radius as presented in the Figure 2-7c (Neeft et al., 2021).

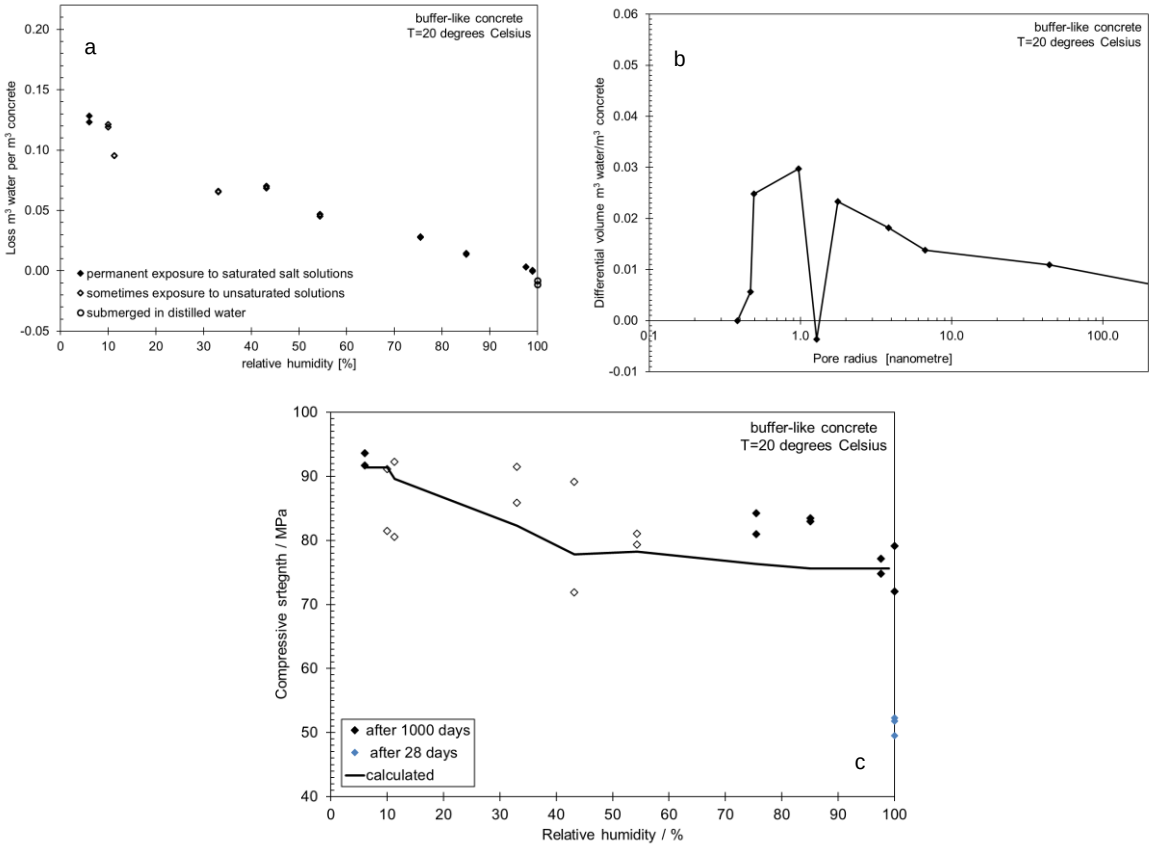

Figure 2-7- For the buffer-like concrete: a/ Evolution of the water content in function to the relative humidity; b/pore size distribution; c/ compressive strength evolution in function to the relative humidity

The compressive strength of the 30 years old buffer-like specimen made with CEM III/A was also high i.e. about 80 MPa with the thick centimetre sized carbonation fronts.

Backfill concrete has apart from capillary pores also pores with a larger size by which the difference in water content between 98% relative humidity and submerged is not negligible. Its strength was also measured to increase with decreasing degree of saturation but the contribution of the suction force of the capillary pores was blurred by the larger pores.

2.1.2 Consequences on the rebar corrosion

Steel corrosion is one of the main degradation phenomena of reinforced concrete structures. The stability of a metal in contact with concrete interstitial solution depends on the pH of the solution and also on the electrical potential of the metal (Pourbaix, 1963). The concrete pore water has high pH thanks to its alkalinity, but it could decrease to a value below 9 during carbonation and dissolution of portlandite. In the presence of water and oxygen, reinforcement bars can be de-passivated leading to steel corrosion. Concrete carbonation induces generalised corrosion which provokes a reduction of the reinforcement section and steel-concrete bond. Thus, the mechanical behaviour of reinforced concrete is degraded (stiffness, ductility, and load bearing capacity). The formation of expansive corrosion products induces pressure on the concrete surrounding the reinforcement and mechanical damage will depend on the modulus of the corrosion products (Dehoux et al., 2015). When stress is higher than the tensile strength, cracking occurs. This cracking affects the mechanical behaviour of the structural elements and represents new penetration paths for aggressive agents. In the Cigéo context, atmospheric carbonation simulations of intermediate-level long-lived radioactive waste (ILW) concrete

packages (Thouvenot et al., 2013) shows that the concrete alteration is about 2 to 3 cm over a period of 100 years, which is non negligible considering the thickness of the concrete cover.

The quality of the steel-concrete interface (SCI) is considered as a major parameter controlling the spread of steel corrosion. Previous researchers concluded that SCI defects are required to initiate corrosion by favouring oxygen and aggressive agents as chlorides to reach the rebars (Page, 2009; Angst et al., 2011). Two origins of defects of SCI are known. The first one stands for imperfections during concrete placing and formation of gaps caused by plastic settlement and collection of bleeding water, a phenomenon known as top bar effect (Soylev and François, 2005). The second one corresponds to a mechanical damage which occurs during mechanical loading when cracking occurs due to high tensile stress (Castel and François 2011). This damage is located in the area of SCI around crack tips.

The couplings between steel-concrete bond and the spread of steel reinforcement corrosion require to be studied under conditions representative of those of repository structures leading to atmospheric carbonation or carbonation under water. The analysis must focus on the couplings between the degradation of the SCI, of mechanical origin or due to defects linked to the concrete material settlement, on the initiation and propagation of corrosion, and the behaviour of the resulting steel-concrete bond.

An experimental programme is led by ANDRA, LAMCUBE and LMDC to study the degradation of the steel-concrete bond due to steel corrosion in conditions representative of reinforced structures in a repository design. The objectives of the study of reinforced concrete behaviour were to analyse the coupled effects of previous SCI degradation, mechanical damage or top bar effect, on corrosion initiation and onset, and also the corrosion effects on the steel-concrete bond. 100×100×400 mm reinforced concrete prisms with or without top bar effect were tested by three point-bending tests to create a flexural crack favouring carbonation to reach the SCI. Two levels of loading were applied to induce two distinct mechanical damages of SCI, characterized by the residual crack width after unloading, w1 (200-300 µm) and w2 (400 µm). In case of top bar effect prisms, only the w1 residual crack width was applied. The accelerated atmospheric carbonation was 3 % ±0.5 % CO_2, 57 % RH ±3 % RH and 20 °C ±1 °C. The carbonation evolution was 3 mm at 7 days, 7 mm at 28 days and finally 10 mm at 70 days, end of the phase. Each prism was sawn to provide two pull-out test specimens used to characterize the steel-concrete bond.

Top bar effect and impact of the mechanical damage

Figure 2-8 presents the evolutions of CMOD (Crack Mouth Opening Displacement) measurements vs bending moment applied for the three families of prisms:

These graphs can be divided into two phases. The first phase (A) represents a linear behaviour of the reinforced concrete prism until a value of the bending moment inducing a flexural cracking. This crack appears when the stress reaches the tensile strength of concrete in the central part of the prism, in the lower fibre. The second phase (B) corresponds to the composite behaviour of a cracked reinforced concrete element, with the softening post-cracking behaviour of the concrete coupled with the steel reinforcement contribution. Thus, the curve decreases and then increases thanks to reinforcement action. In case of prisms with top bar effect, bending moment values to reach the targeted crack width value are smaller than the value leading to cracking. This reveals that rebar anchorage length on the support in this configuration of three-bending test is not sufficient. The rebar probably slips because of lower bond with concrete due to top bar effect.

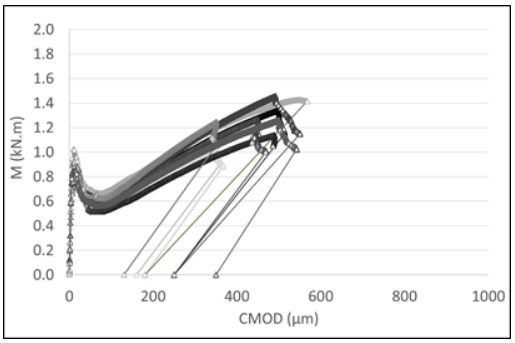

Residual targeted crack width w1: SCI with lowest mechanical damage

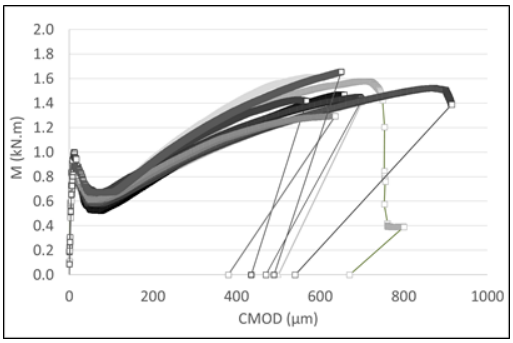

Residual targeted crack width w2: SCI with highest mechanical damage

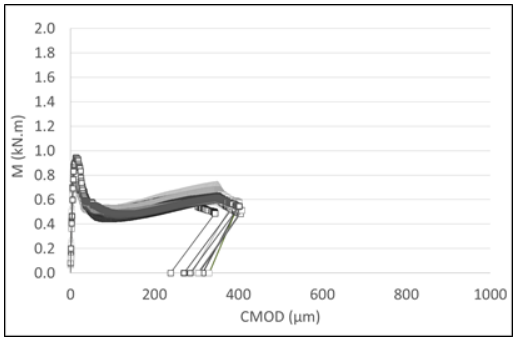

Top bar effect with residual targeted crack width w1

Figure 2-8 - Evolutions of CMOD measurements vs. bending moment

The objective was to reach a crack width higher than the targeted value considering the elastic reversible behaviour when unloading. The wedges were placed just before unloading to maintain the desired crack width after unloading. However, even with the placement of wedges, some variability on the residual crack width values is observed, whatever the prism family. It was rather difficult to place the wedges, because of the tortuosity and the variability of the crack width along the depth of the prism, on its lower side. Then, residual cracks can be different even with the same value before unloading.

Figure 2-9 presents the values of the residual crack width for:

- each prism: n°1 to 3
- for each family: w1, w2, or w1 with top bar effect (TP)
- for prisms used for reference pull-out tests without carbonation, for prisms which were stored in the only Phase A, and for prisms which were stored successively under Phases A and B.

To improve the precision, the residual crack width had been measured on the two sides at the bottom of cracks using a video microscope. Experimental problems occurred during tests for two prims. There are no values of crack width for w1-ref-3 and TP-w2-ref-3.

Globally, the residual crack width values correspond to the interval of values desired:

- w1 ≈ 200-300 µm (targeted): 227 µm (± 58 µm) for w1 and 258 µm (± 31 µm) for w1 with top bar effect
- w2 ≈ 400 µm (targeted): 373 µm (± 113 µm)

The spread of the results is not negligible. Then, the samples have been gathered by group based on their future storage conditions. The samples with the highest values of crack width are subjected to phases A and B to induce more steel corrosion.

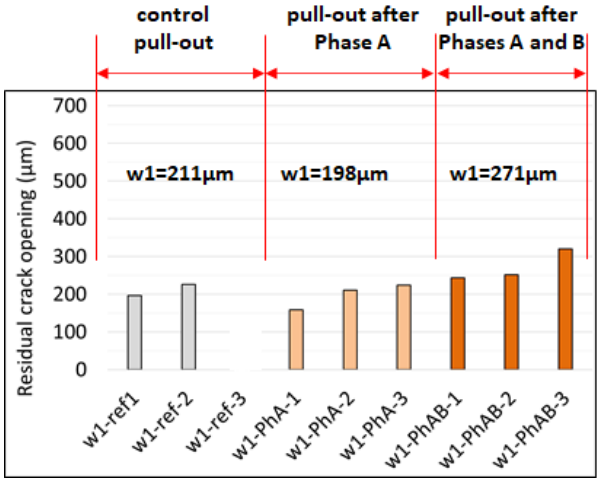

residual targeted crack width w1:
Mean value w1 = 227 µm

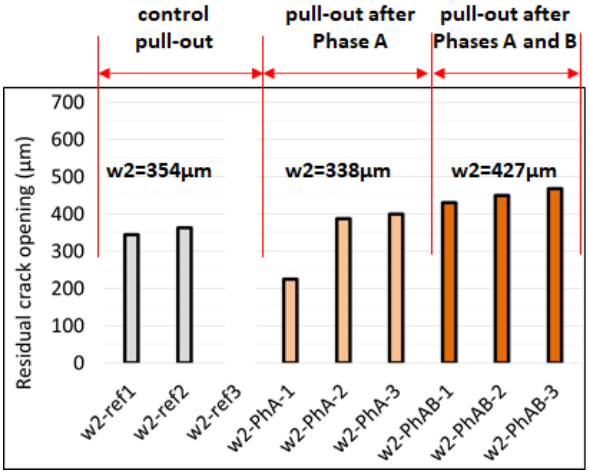

residual targeted crack width w2:
Mean value w2 = 373 µm

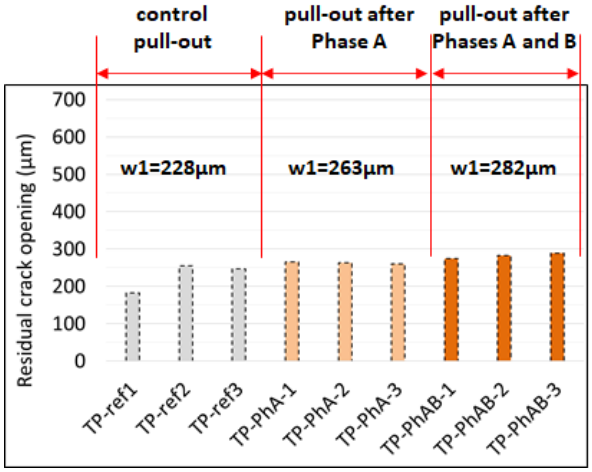

top bar effect with residual targeted crack width w1: Mean value w2 = 258 µm

Figure 2-9 - Residual crack width values for each prism, each degradation type of SCI, and each future storage condition

Figure 2-10 presents the evolutions of shear stress value vs the slip between steel rebar and concrete for the reference pull-out test samples, after autogenous curing and without carbonation. The shear stress is calculated from the force value and anchorage length of the rebar (60 mm) in concrete.

The curves are classical for pull-out tests with a linear phase followed by a second one characterized by a progressive decrease of the rate until a maximum value of the shear stress and a plateau. A greater variability is observed for pull-out test sample with w2 and top bar effect groups of samples, compared to w1 group (except to 2 tests).

The failure is by concrete splitting for w1 and w2 group whereas the rebar slips for top bar effect group revealing the presence of decohesion at SCI.

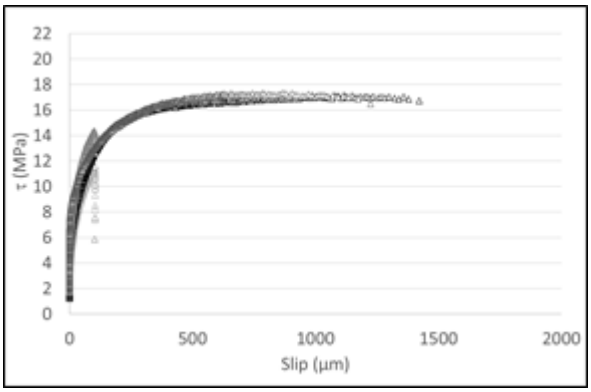

w1: failure by concrete splitting

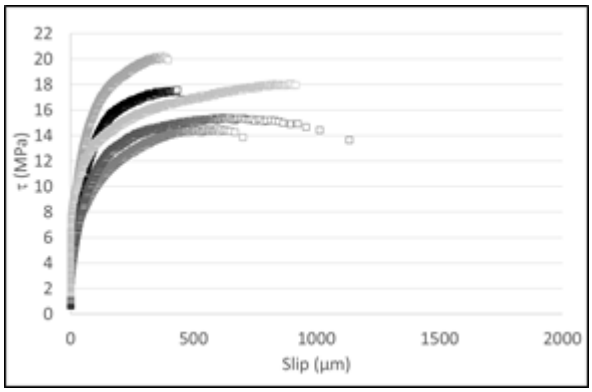

w2: failure by concrete splitting

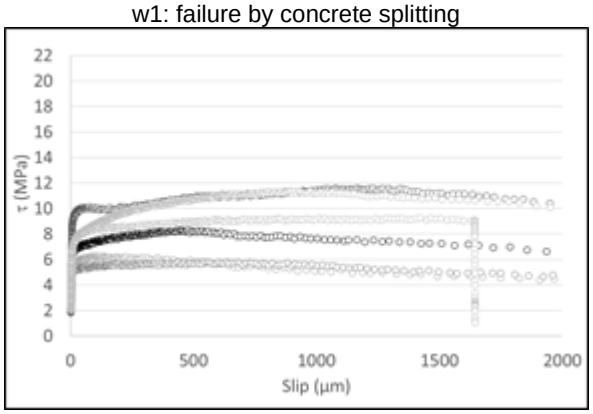

top bar effect with crack width w1: failure by rebar slipping

Figure 2-10 - Evolution of shear stress vs slip of steel rebar for each reference pull-out test samples without carbonation and for each degradation type of SCI

Effect of corrosion according to exposure conditions and the initial state of the concrete (top bar effect and/or level of crack opening)

During the phase A of accelerated atmospheric carbonation, a rainbow indicator was used to analyse the carbonation depth on concrete blocks cast with other samples, and also at SCI after pull-out test. This indicator is more precise and non-toxic compared to phenolphthalein. It turns green when the pH is lower than 11 and purple when higher.

The measures on the concrete blocks stored in the same conditions of phase A show a carbonation depth of: 3 mm at 7 days; 7 mm at 28 days; 10 mm at 70 days, i.e. at the end of the phase A.

The analysis at the SCI using the rainbow indicator after breaking the samples following the pull-out test does not show carbonation. However, it takes more seconds to turn to purple in case of w2 and top bar effect groups in comparison with w1. This could demonstrate that the pH is closer to 11 in that case and that carbonation is more advanced due to SCI decohesion.

Figure 2-11**Erreur ! Source du renvoi introuvable.** presents the evolutions of shear stress value vs the slip between steel rebar and concrete for the pull-out test samples after phase A of atmospheric carbonation.

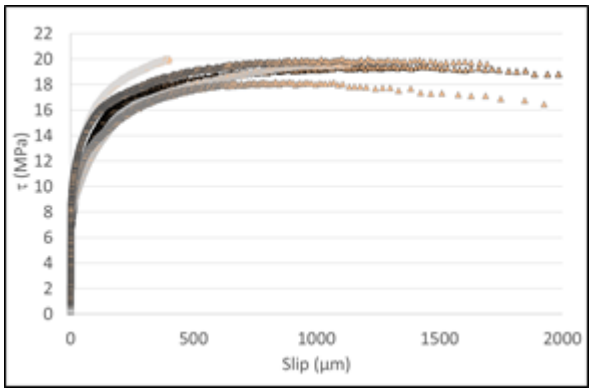

w1: failure by concrete splitting

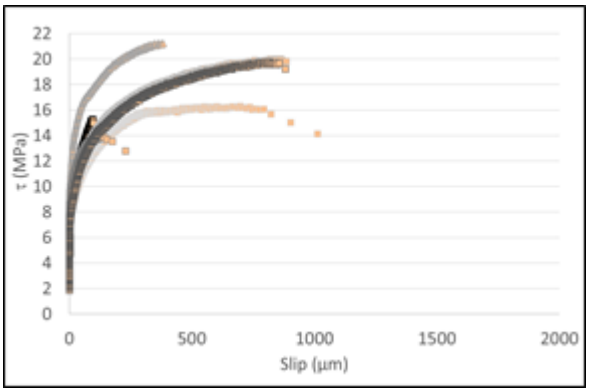

w2: failure by concrete splitting

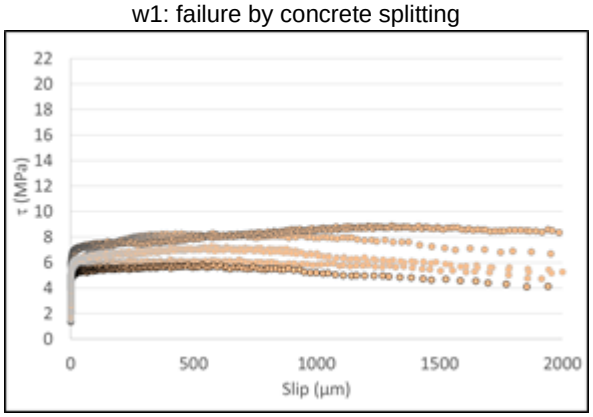

top bar effect with crack width w1:
w1: failure by rebar slipping

Figure 2-11 - Evolution of shear stress vs slip of steel rebar and for each degradation type of SCI after phase A

The results are relatively similar to those for the reference samples without carbonation in terms of curve forms, type of failure, and variability greater for w2 and top bar effects groups of samples.

The Figure 2-12 synthetise the maximum values of the shear stress for each group, in case of reference conditions without carbonation and after phase A of atmospheric conditions.

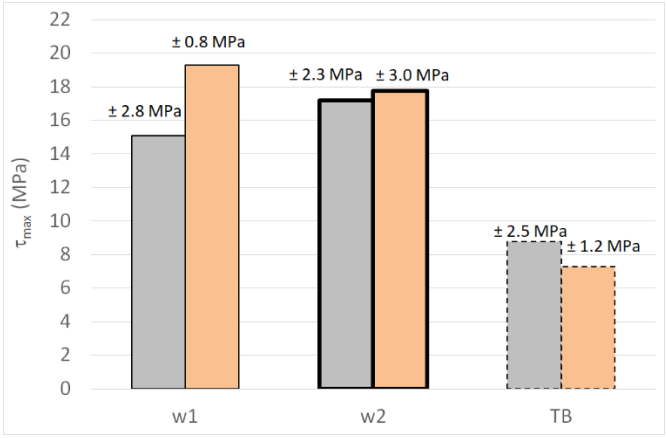

Figure 2-12 - Comparison of the mean value of maximum shear stress (with standard deviation) for each degradation type of SCI (w1, w2 and top bar effect group “TP”), for reference samples (in grey) and after phase A (in orange)

The results for reference samples without carbonation show a slightly higher mean value of the maximum shear stress for crack width w2 compared to that of w1. The larger crack opening does not seem to have caused more damage of SCI. However, the difference and the variability of the results in

case of w2 group of samples have to be take into account to moderate this analysis. The probable higher damage around the crack tip could also induce presence of concrete particles which could increase the friction. The results for the top bar effect group clearly reveal the strong impact of the decohesion due to material behaviour at fresh state in case of reinforcement rebar located at height in a formwork.

After the phase A of atmospheric carbonation, the maximum shear stress increases significantly for w1 group and slighter for w2 group, whereas it decreases for top bar effect group.

These behaviours cannot be attributed to carbonation, as it is not detected at the SCI, or maybe with a lower pH for w2 and top bar effect revealing a beginning of carbonation. The explanation is probably the lower mean values of crack width for the w1 and w2 groups subjected to atmospheric carbonation compared to those of reference samples (Figure 2-9):

- w1 group: 198 µm for reference condition without carbonation, and 211 µm for phase A group
- w2 group: 354 µm for reference condition without carbonation, and 338 µm for phase A group

In case of top bar samples, it is the opposite since the mean value of crack width for the reference group, 228 µm, is lower than for the phase A group, 263 µm, explaining the lower value of the maximum shear stress instead of a carbonation effect.

The main results about the rebar corrosion and the consequences on the mechanical behaviour are the following:

- **Control specimens without carbonation**: the failure is by concrete splitting for w1 and w2 groups whereas the rebar slips for top bar effect group due to the presence of decohesion at SCI. A slightly higher mean value of maximum shear stress for w2 group is observed compared to that of w1 one. Higher SCI damage could induce the presence of concrete particles which could increase the friction. Top bar effect significantly decreases the maximum shear stress.
- **Specimens subjected to carbonation condition**: the failure and the shear stress vs slip curves are similar to those of control specimens. After 70-day carbonation condition, the maximum shear stress increases for w1 group and slighter for w2 group, whereas it decreases for top bar effect group. However, this tendency cannot be explained by carbonation since it is not detected at the SCI. It is probably due to differences in residual crack width values, and differences in SCI mechanical damages, for control and carbonated samples.

2.2 The modelling at small scale

2.2.1 Modelling the chemo-mechanical evolution of cement paste carbonation

Carbonation is a complex degradation process to model which involves severe feedback mechanisms between hydraulic, chemical, mechanical and thermal effects. Water consumption and production and carbonation of concrete has been modelled in EURAD ACED (Huang et al., 2021). In a prior MAGIC publication (Seigneur et al., 2022), it was demonstrated that reactive transport alone was not able to represent the long-term effect of carbonation without incorporating the appearance and propagation of cracks. This implies that a fully coupled Thermal-Hydraulic-Mechanical-Chemical (THMC) approach is required to accurately model carbonation.

A literature review of past attempts to THMC approaches revealed that much remained to be done in this topic. In general, past attempts usually included two shortcomings:

They never included a two-way dynamic feedback between chemistry and mechanics.

The THC (or reactive transport part) is usually simplified as it does not take into account the water production and consumption.

For concrete in general, water reactivity plays an important part for the durability of concrete and cementitious materials, as we have shown in Seigneur et al., (2022) for carbonation. Also, the induced pore-pressure is important to consider for a chemo-mechanical coupling, as emphasized by the drying shrinkage observed in these materials. The capacities of the modelling code HYTEC with respect to water reactivity were able to solve the second shortcoming (Seigneur et al., 2018). From this, a poromechanical calculation can be implemented with CAST3M, thanks to the HYTEC computation of pore pressure and mineralogical composition. We have chosen a damage approach in CAST3M which can be converted into crack openings which would then be fed back in HYTEC through the double-porosity approach available in HYTEC (Figure 2-13).

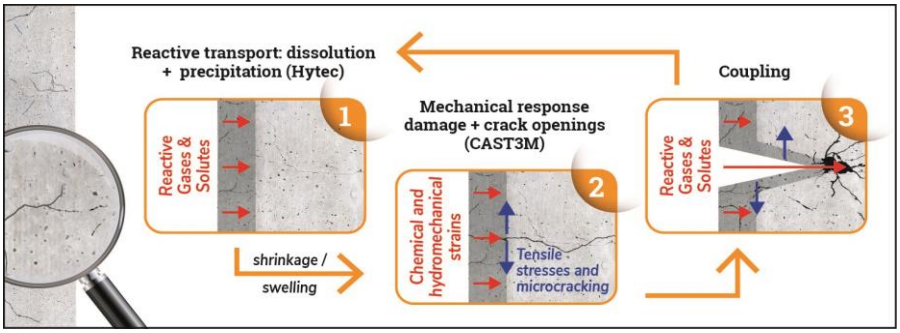

Figure 2-13 - Illustration of the approach

The experimental approach was dedicated to provide calibration data and validation results of our approach when applied to simulate the accelerated carbonation. For this, we use results from the PhD Thesis of Kangni-Foli (Kangni-Foli, 2019; Kangni-Foli et al., 2021). In addition, through the experimental work of CEA described in part 2.1.1, additional characterizations have been performed to constrain and inform the modelling approach. In particular, sorption isotherms and additional microtomography analyses have been obtained. Our work focused on two model cementitious materials that were studied within the previously cited PhD Thesis. The first one is a hydrated C_3S paste, the simplest possible cementitious material to prepare. The second one is a pure C-S-H paste, representative of low-pH cement, which exhibits a higher level of cracking.

Regarding the numerical approach, it is centred on the development of a Python program which alllows the two codes (HYTEC and CAST3M) to communicate. Carbonation is simulated by HYTEC for a certain duration (until porosity varies by 0.1% at any point in the domain.), then HYTEC results are translated into internal stresses (through pressure field, mineralogical evolution, and, above all, carbonation shrinkage) to CAST3M. In CAST3M, a poromechanical damage approach is used, for its simplicity and extrapolability to larger scale problems. Thus, CAST3M computes a damage and a strain field, which are then translated into the development of cracks, whose apertures are controlled by the strains. Then, the cornerstone of our approach is that the information of crack aperture at every cell is applied in HYTEC through the evolution of dual porosity, whose properties (permeability, diffusion) are computed based on the apertures. This approach has several advantages, which overcomes the past limitations of chemo-mechanical coupling approaches from the literature:

- It is based on a physical approach: the damage and internal stresses are parametrized using the processes (carbonation and drying shrinkage, external loading) responsible for the appearance of cracks;
- The use of dual porosity approaches to model fractured porous media is general and does not require the use of upscaled behaviour laws (diffusion, …);
- The fact that the coupling from CAST3M towards HYTEC is performed over the opening of a dual porosity allows for a two-way physical coupling and greatly simplifies the mass balance and geochemical problems;

- The approach allows to close previous cracks (from mineral precipitation or stress evolution);
- Its physical roots make it, theoretically, applicable to other cement pathologies;
- It can be adapted to other reactive transport or mechanical simulators. Indeed, HYTEC presents all the features relevant for the coupling (water production by the dissolution of cement hydrates, water evaporation and the subsequent drying).

The deliverable D16.8 describes in detail the numerical and modelling approaches. Results are illustrated in Figure 2-14 for the C_3S paste and Figure 2-15 for C-S-H paste.

This coupling approach was developed by a first postdoc using carbonation as an illustration of the soundness and applicability of our approach (Socié et al., 2022). In that article, the degradation front of a model C_3S cement paste, exhibiting a more pronounced degradation along its edges, is compared to our model results (Figure 2-14). **This comparison yielded satisfactory results and provided an explanation for the front disturbance. Because HYTEC provides a complete THC description, this coupling thus constitutes a first fully coupled THMC approach, with a high potential for use in other contexts.**

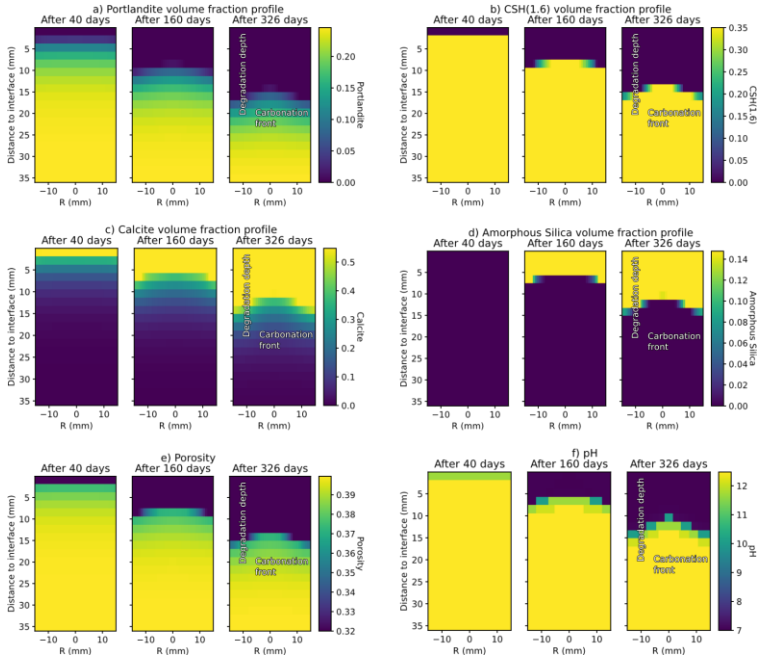

Figure 2-14 - Mineralogical spatial maps after 40, 160 and 326 days of accelerated carbonation of the C_3S paste.

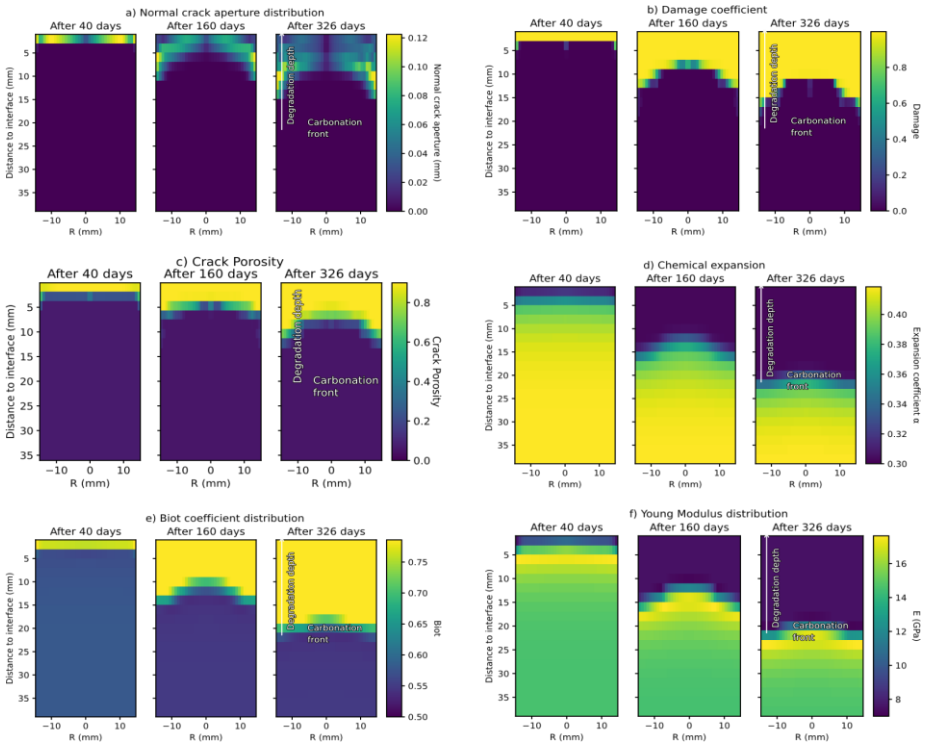

Figure 2-15 Mechanical spatial maps after 40, 160 and 326 days of accelerated carbonation of the C_3S paste.

This approach relies on the description of several behaviour laws or homogenization schemes to compute effective properties (e.g. Young's modulus) as the materials evolve (Stora et al., 2008). Also, many different approaches could be considered to describe the appearance and propagation of cracks within a material. Therefore, the second part of the work consisted in studying in depth all of these behaviour laws and to apply them in a quantitative way to cement samples from the PhD thesis from Kangni-Foli (2019), with an emphasis on representing materials exhibiting significant cracking, like low-pH cements. To this end, the work focused on being able to provide accurate relations to model the evolution of certain properties (e.g. Young's modulus). **Also, the poromechanical model was adapted to be able to reproduce measured macroscopic deformation and shrinkage.** This was done through a literature review of how a C-S-H phase evolves (shrinkage) during carbonation and its implication for a cement material which includes inclusions of other minerals.

2.2.2 Development of an elastoplastic model based on analytical homogenization procedures to describe the mechanical behaviour

LAMCUBE, in parallel to the experimental work (see 2.1.1) has developed an upscaling approach by homogenisation method from micro to macro scale with an intermediate mesoscopic step to represent the aggregates of the concrete matrix. Effective properties are derived by analytical averaging methods. In addition, artificial neural networks (ANNs) are used to predict the effective elastic properties of concrete. An important parameter of the chemo-mechanical processes is the fracture strength, which has also been estimated by ANNs. The deliverable D16-8 gives the details about the methodology.

Simplified micro-structure considered

The estimation of macroscopic mechanical properties is inherently based on the description of microstructures and the local mechanical properties of constituent phases. It is worth noticing that the microstructures of concrete materials are typically complex. For example, different types of C-S-H are formed in cement pastes. Voids and inclusions of different sizes are distributed at various scales. The

macroscopic mechanical properties of concrete materials are fundamentally influenced by the local characteristics of constituent phases, their morphology, porosity, and the volumetric fraction of inclusions. Considering all these micro-structural parameters simultaneously poses challenges.

Building upon the methods introduced above, we consider here concrete materials containing a class of pores and a family of inclusions, each situated at different scales. The representative elementary volume (REV) of the concrete material is defined. At the macroscopic scale, the material is represented as a homogenized equivalent medium (HEM), the strength properties of which need to be predicted. At the mesoscopic scale, aggregates are distributed in a quasi-continuous cement paste matrix. At the microscopic scale, the cement paste contains a family of pores.

2.2.3 Chemical mechanical coupling

For the description of chemical mechanical coupling with the micro-mechanics-based modelling, the effects of chemical degradation are directly described by the evolution of microstructures. More precisely, due to chemical leaching, a part of solid calcium is dissolved and the related volume is transformed into an increase of porosity. As the mechanical properties are explicitly functions of porosity, its increase will directly affect the elastic properties and failure strength. Inversely, due to carbonation, there is a decrease of porosity and production of additional solid calcite grains. The elastic modulus and failure strength are then increased.

Experimental data from Task 2 and Task 3 to quantify the chemical degradation effects on micro-structural evolution and mechanical properties changes will be used for validation.

2.2.4 Elastic properties

When investigating the elastic properties of concrete, it is essential to consider another prevalent microstructural configuration, which involves the coexistence of pores and inclusions at the same scale. Among the numerous analytical homogenization models used for estimating the macroscopic elastic properties of such composite materials, common fundamental models include the Voigt and Reuss bounds, Hashin-Shtrikman (HS) bounds, and the Mori-Tanaka (MT) estimation scheme. Firstly, we conducted a comprehensive evaluation of these four analytical models.

In Figure 2-16, one shows the evolution of normalized macroscopic elastic moduli of materials with only inclusion (see Figure 2-16 (a)), only pores (see Figure 2-16 (b)) and both pores and inclusions (a representative case with an inclusion-pore ratio of 3:1 is selected, see Figure 2-16 (c)) respectively. The comparisons between the reference FFT solutions and theoretical predictions of analytical models are presented.

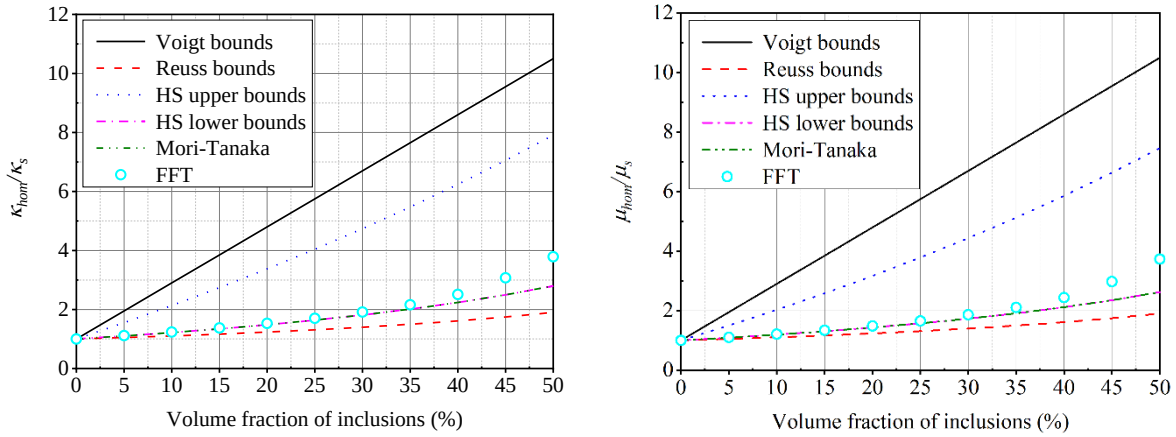

(a) Materials with only inclusion

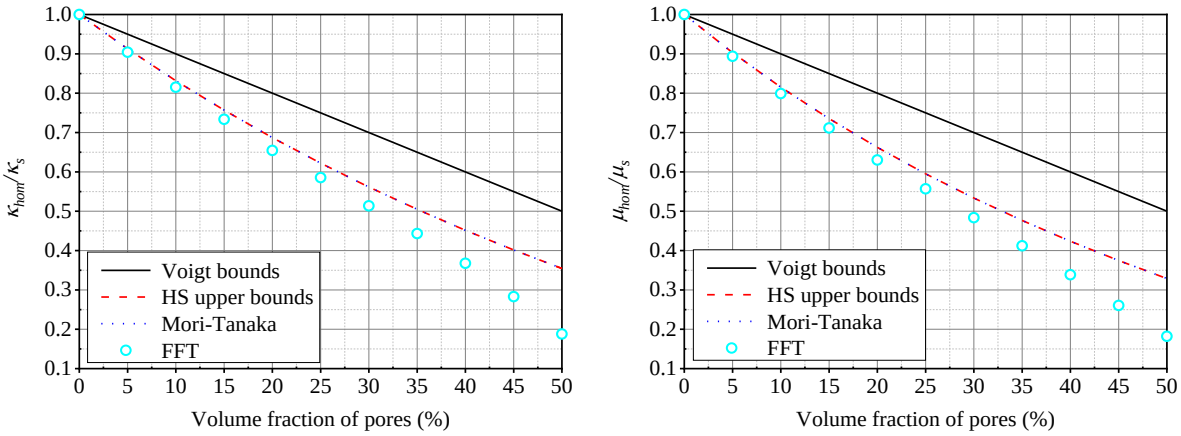

(b) Materials with only pores

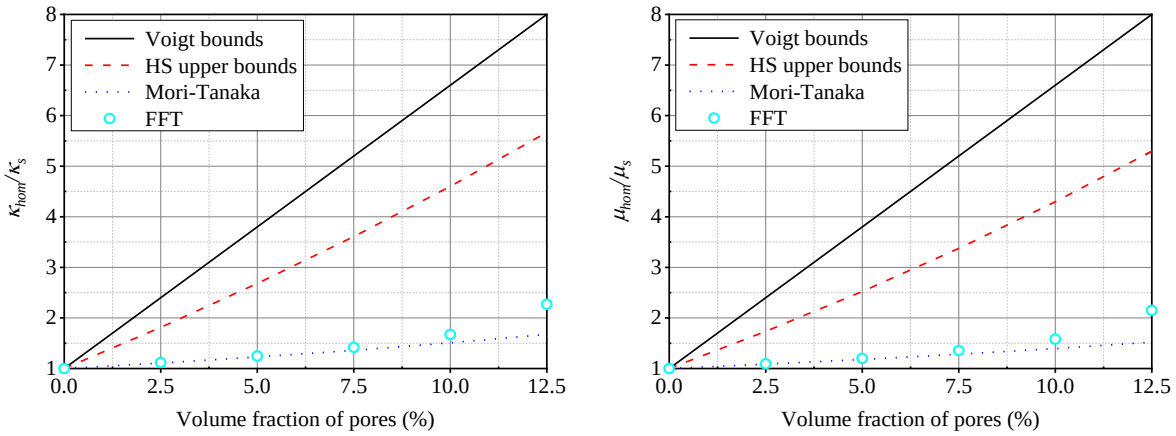

(c) Materials with both pores and inclusions

Figure 2-16 - Variation of relative elastic moduli κ_{hom}/κ_s and μ_{hom}/μ_s with inclusion volume fraction and porosity for concrete materials

LAMCUBE has investigated the influence of these parameters on the macroscopic elastic properties of heterogeneous materials by considering microstructural parameters such as porosity, inclusion volume fraction, local elastic properties of the matrix phase, and inclusions. They observed that for materials with high porosity or inclusion volume fraction, as well as for materials containing both pores and inclusions at the same scale, typical homogenization analytical models were unable to accurately predict their macroscopic elastic properties.

In light of this challenge, and with the aim of refining and enhancing these analytical predictions, a model was developed based on artificial neural networks (ANN). The structure of this model is illustrated in Figure 2-17. Following a rigorous process of training and testing using data derived from FFT simulation results, we discovered that this model exhibited exceptional levels of accuracy. Notably, the model demonstrated an exceedingly high R^2 value (greater than 0.999) and remarkably low root mean square error (RMSE) and mean absolute error (MAE) values. Importantly, the predictive capabilities of the ANN-based model have significantly enhanced the accuracy of predictions compared to analytical models (see deliverable 16-8).

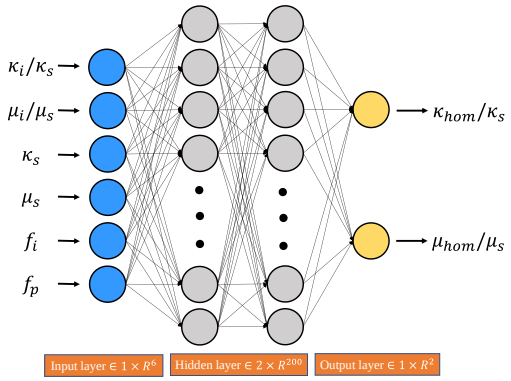

Figure 2-17 Artificial neural network structure for predicting effective elastic properties of concrete

2.2.5 Failure strength

In the past few decades, significant advancements have been made in understanding the nonlinear behaviour of heterogeneous materials. Particularly, various macroscopic strength criteria have been developed to assess the failure stresses of materials. However, establishing analytical strength criteria requires simplification of the microstructural morphology of concrete materials. For instance, attempting to derive analytical strength criteria by simultaneously considering pores, inclusions, and the interfacial transition zone (ITZ) poses significant mathematical challenges, leading to the omission of ITZ effects in research studies. Based on these analyses, LAMCUBE considered an alternative matrix configuration involving inclusions, where the matrix contains pores at different scales, and the REV of the material. Dividing the material into three scales, the matrix of the material adheres to the Drucker-Prager criterion at the microscopic scale. By utilizing an improved secant method-based three-step nonlinear homogenization approach (Cao et al. 2020; Cao et al., 2021; Maghous et al., 2009; Shen et al.,2013; Shen et al., 2020), a closed-form expression for the macroscopic strength criterion was defined.

Multi-scale models are developed for heterogeneous concrete materials to estimate their macroscopic mechanical properties in terms of micro-structural data. One crucial challenge of these models is the identification of local properties of constituent phases. To address this, LAMCUBE proposed an effective method based on ANN for the identification of micro-level parameters in concrete. The primary goal is to determine the microscale frictional coefficient and cohesion of cement particles using macroscopic values of uniaxial compression and tensile strengths as inputs. By inverting the analytical strength criterion, a comprehensive dataset is constructed, incorporating aggregates volume fraction, porosity,

macroscopic uniaxial tensile and compressive strengths as inputs, and the frictional coefficient and cohesion of cement particles as output unknowns.

An ANN model with four hidden layers, each containing 100 neurons (as depicted in Figure 2-18), is constructed and trained using this dataset. Multiple types of validation tests are performed for the ANN model. In Figure 2-19, the predicted values are plotted against the exact values to visualize their correlations. Remarkably high values of correlation coefficient R^2 are achieved.

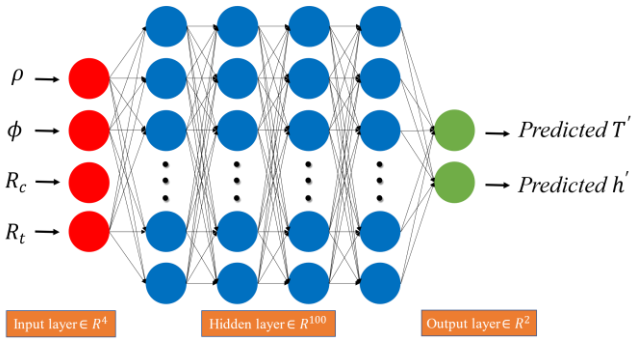

Figure 2-18 A BP neural network model to evaluate the microscopic parameter of concrete materials.

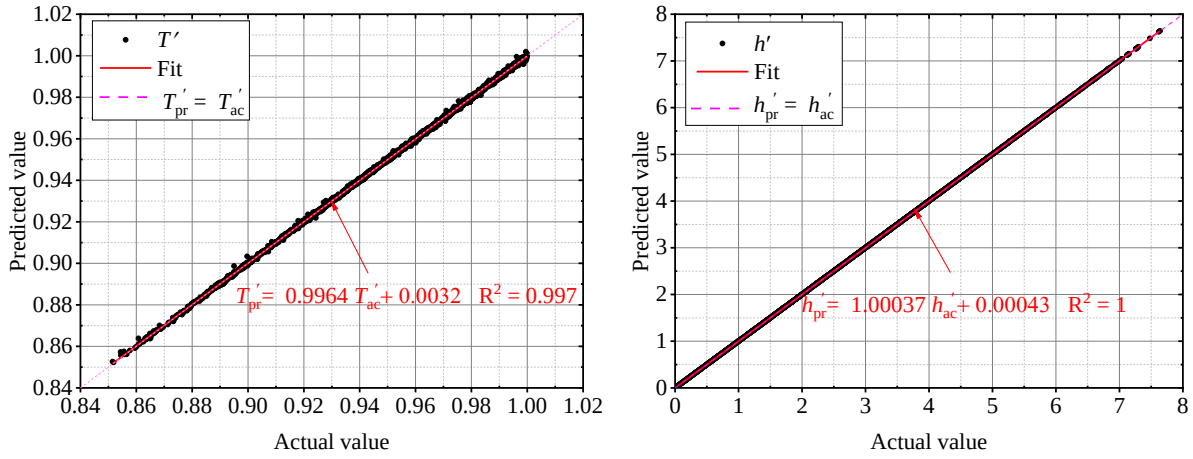

Figure 2-19 Correlation between predicted and exact values of T′ (friction coefficient) and h′ (cohesion of the cementitious matrix at microscopic scale).

These results highlight the effectiveness of the proposed ANN-based model in accurately predicting the frictional coefficient and cohesion of porous cement pastes at the microscopic scale.

3. The chemo-mechanical evolution of cementitious materials at long term in the disposal facility

This part of the report focuses on the long-term degradation of cementitious compounds, in interface with a multi-ionic environment composed by the host rock or just natural/synthetic waters with a multiscale approach. Full water saturation is considered only, the hydraulic condition prevailing at long term in a disposal facility.

3.1 From the nanoscale to the macroscale, experimental approaches and main results

3.1.1 Impact of calcareous water on the chemo-mechanical properties of concrete – transferability of laboratory studies to field scale

The results obtained in laboratory under controlled conditions need to be tested at the field scale and upscaled to the real operation conditions. In particular the concrete performance observed in lab tests need to be confirmed under the in situ conditions on industrial scale. In the framework of the IMCB (Impact of calcareous water on chemo-Mechanical Behaviour of concrete) project conducted in the MAGIC WP, IRSN in collaboration with the Helsinki University investigates the chemo-mechanical impact of calcareous water on a low-pH cementitious matrix. In particular, this study aims to estimate the potential difference in concrete performance observed in controlled conditions and on an industrial scale. To this end, one set of HCP samples was cast in the laboratory, and another set of concrete samples and massive concrete structures were casted using a large scale outside experimental platform. After the hydration period, samples were immersed in a high volume of natural calcareous ground water. Periodic characterization was performed by SEM-EDS, µ-CT, XRD and micro/nano-indentation.

Two experimental setups were used. The first system set up in December 2018 in the IRSN underground research laboratory (URL) in Tournemire (IMCB-TR) was only composed of centimetre sized samples (Figure 3-1). The second one (IMCB-ODE), started in October 2019 and located in the ODE platform of Cadarache (South of France), was focused on macroscopic scale. In both cases, the composition of the synthetic solution in the reservoir was equivalent to natural calcareous ground water from the Cernon fault in the URL of Tournemire.

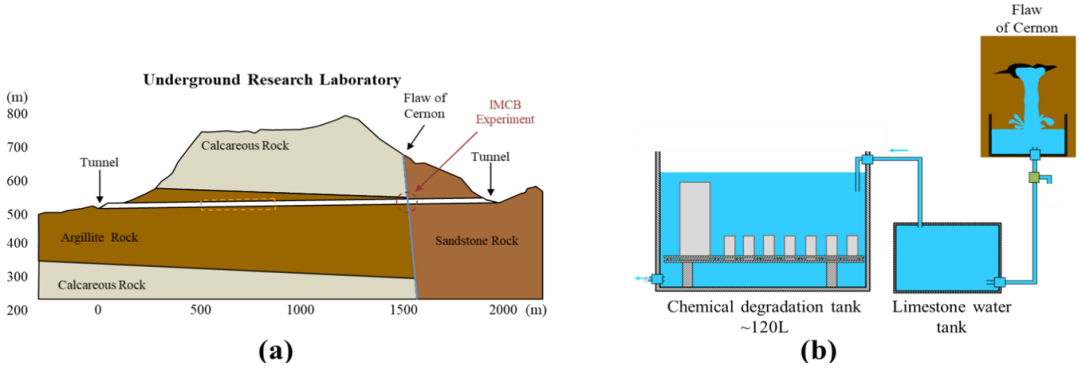

Figure 3-1 - Illustrative sketch (a) of the underground research laboratory of Tournemire and (b) of the IMCB-TR experimental setup.

The first aim of this study was to provide insights for understanding the chemo-mechanical behaviour of a low-pH cementitious matrix in contact with calcareous ground water. Results are synthetized in Figure 3-2.

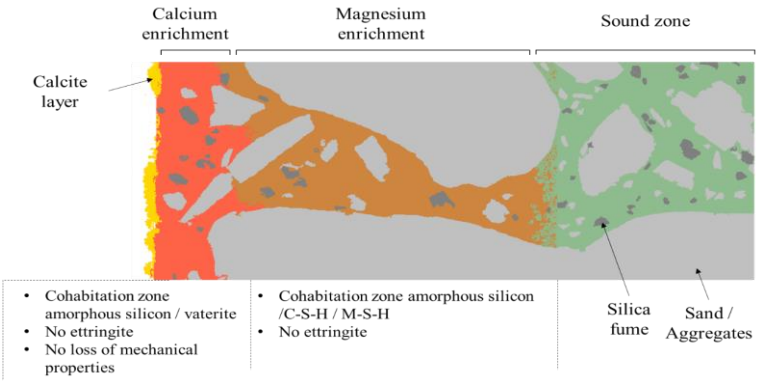

Figure 3-2 - Illustrative diagram of the degradation scenario proposed to explain the alteration of low-pH cementitious matrix in contact with calcareous water.

The experimental campaign coupled with numerical simulations reveals the following mineralogical changes:

- At the interface, a crust of calcium carbonate is visible.
- The first hundred microns are characterised by a calcium enrichment and the presence of amorphous silica. Vaterite has been identified in this domain, too. The presence of vaterite compensates for the weak elastic properties of the amorphous silica providing a high Young's modulus of the composite material (see Figure 3-3). A flaking phenomenon in this zone is anticipated, likely due to the low Young's modulus of amorphous silica.
- Magnesium enrichment is observed downstream to the previous zone. Despite the low concentration of the infiltrated solution, the model and SEM-EDS measurements show that the magnesium enrichment can, in some cases, reach 20% of the volume of the material (analyzed zone). The low mechanical properties of the magnesium phases usually observed in low-pH matrices raise the question of the durability of this zone.

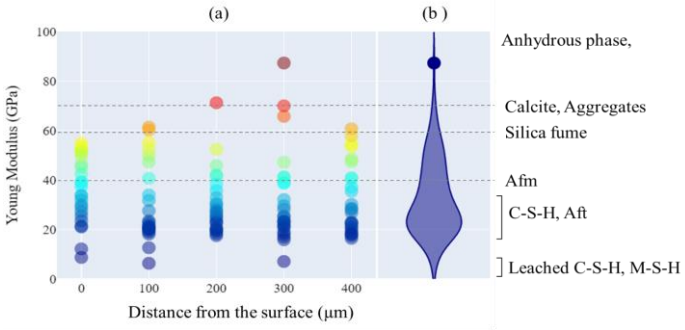

Figure 3-3 - (a) Distribution of Young's moduli measured by micro-indentation as a function of depth and (b) global violin diagram for a low-pH T3 concrete immersed for 8 months in IMCB-ODE.

The second objective of this study was to estimate the potential deviation of results between a study made in controlled laboratory conditions and another in less constrained conditions corresponding to industrial manufacturing. The manufacturing protocol seems to have a significant impact on the chemical response of the cementitious materials. A high porous zone appears at the interface in large concrete blocks cured outside and wrapped with stretch film. The evolution of transport properties in this zone has an effect on the degradation scenario. In the case of cementitious materials cured under controlled laboratory conditions, the interaction with the external solution induces the formation of a layer of calcium carbonates, which tends to close the porosity. This low porosity zone seems to have a passivation

function and slows down the leaching, so that no degradation is noticed in the cement matrix. In the highly porous zone, the formation of two large zones, one enriched in calcium at the interface and another further downstream enriched in magnesium is observed. The observed evolution of these zones raises some concerns regarding the potential flaking in the calcium carbonate zone and the low Young's modulus of the magnesium phases, which are expected to precipitate in the magnesium enrichment zone. However, the observed change seems to be limited to the highly porous zone, without impacting the integrity of the concrete structure.

As observed in the IMCB project, in contact with natural ground water, the leaching of the low-pH cement matrix may be accompanied by an enrichment in magnesium leading to the formation of brucite and/or magnesium silicate hydrates (M-S-H), the properties of which are poorly known (Dauzeres et al., 2016; Bernard et al., 2017).

The PM2SH project comprises a multi-physics study of the weathering of low calcium matrices by magnesium containing waters at the mesoscopic scale. The main aim of the study was to understand the reaction mechanisms of M-S-H formation in low-calcium cementitious matrices, and to study its influence on micro-structural and mechanical properties of concrete. Two cementitious pastes (model paste based on colloidal silica and real paste based on silica fume and slag) were exposed to solutions with different Mg concentrations (5 and 50 mmol/L).

The model cement pastes were composed by CEM I and colloidal silica, whereas the low-pH paste was produced by mixing CEM III/A with silica fume. After the manufacturing, the pastes were kept under endogenous conditions for 2 years. Then, cylindrical samples (diameter = 3 cm, thickness = 1 cm) were cut, coated with sealant on the lateral side to allow unidirectional degradation. The samples were immersed in magnesium solutions in 60 L closed tanks for 4 months. The solutions were constantly agitated and renewed every two months. At the end of the exposure time, two samples were taken, cut out and prepared for the various characterization tests.

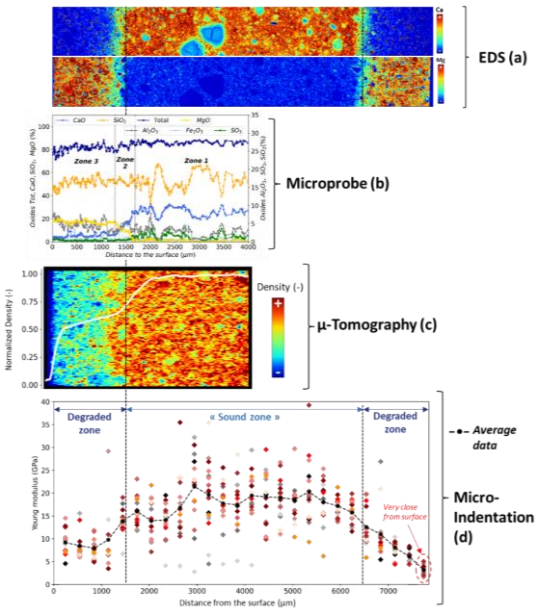

Figure 3-4 - Multi-physics characterization of a low-pH industrial cement paste after 4 months interaction with 50 mM $MgCl_2$.

In the study of the low-pH model paste, the measured mechanical properties of the degraded paste were much lower than those of T3 concrete used in the IMCB project (Figure 3-4).

The sound paste was homogeneous and composed only of C-S-H and ettringite. In contact with the $MgCl_2$ solution, at 5 mM or 50 mM, the findings were the same. The magnesium attack causes the

leaching of calcium and sulphate, dissolving the only two phases observed in XRD namely C-S-H and ettringite. The degraded zone entirely consisted of M-S-H. No other phases are available to compensate for poor microstructural and mechanical properties of M-S-H in the degraded sample, contrary to T3 concrete where the low water to cement ratio and the presence of other phases such as slag limit the impact of M-S-H formation on the microstructural and mechanical properties of the material.

In conclusion, the analysis confirms that the magnesium attack made with a magnesium-chlorine solution that is depleted in dissolved calcium and sulphate, is characterised by the dissolution of C-S-H and ettringite, as well as by the formation of M-S-H during the contact between a low-pH paste/concrete and an environment containing magnesium. **As M-S-H has much lower mechanical properties than C-S-H, the replacement of C-S-H by M-S-H does not maintain good mechanical and microstructural properties. Even if a new semi-amorphous phase is formed, the mechanical properties of the paste are significantly reduced during magnesium attack**.

3.1.2 Chemo-mechanical evolution under multi-ionic chemical attack

Artificial ageing conditions through chemical multi-ionic attack (saline water)

This work was also conducted by considering the microbial impact, discussed in the Part 4.1.

118 cubical concrete specimens have been exposed to a synthetic clay pore water solution since 2016 by COVRA at around room temperature. Buffer-like concrete was made with CEM III/B which in MAGIC is a so-called low pH cement. The porosity of buffer-like concrete made with CEM III/B was 12-13% (only capillary pores). The buffer-like concrete was expected to have a too small size of pores (see Figure 2-7) to allow microbial activity inside the concrete specimens. Later, also a buffer-like concrete specimen made with CEM III/A (a blend of OPC (35-64 wt%) and Blast Furnace Slag (36-65 wt%)) was investigated. This specimen was manufactured in 1993.

The Dutch cubical concrete samples have been submerged in synthetic clay pore water as saline as seawater (see Table 6-1 in Deliverable D16.3) since September 2016 at room temperature. This solution is envisaged to be representative for the clay rocks considered in the Netherlands to host a geological disposal facility. Magnesium is present in this pore water. Ingressing magnesium in concrete reacts with cementitious minerals to form brucite and magnesium silicate phases. These magnesium phases have been identified as non-bonding phases (Atkinson et al., 1985) and therefore are expected to have a negative impact on the strength of concrete. Sulphate is also present in this saline water. Only sulphate resistant cements had been used for the manufacturing of the Dutch samples.

The compressive strength, oxygen and carbonation fronts were also measured. ICP-OES analysis of the exposing solutions and concrete samples is to be performed in order to quantify the ingress of magnesium and egress of other species.

The following chemical analyses were performed:

- SEM/EDS/WDS to study ingress and distribution of Mg and other elements
- Elemental mapping and bulk chemistry by XRF,
- Determination of water content and phase transformations by TGA-DSC
- Mineralogical composition by powder XRD using Rietveld analyses for (semi)quantitative determination of the phase assemblage
- Raman tomography on the surface of the materials will be reported by FZJ.

A backfill and buffer-like concrete specimen was fully cracked and re-assembled and exposed to the same saline solution for about 3 years in order to investigate the self-sealing of cracks.

All concrete specimens exposed to a clay pore water solution as saline as seawater for 5 to 6 years had a higher compressive strength than measured for similar concrete specimens after 28 days hardening. The concrete specimens might still have been in a hardening stage. Some samples had been obtained from sawing casted samples. It was initially thought that this sawing has no influence on the strength.

However, after several years of exposure, the sawn samples always had a smaller strength than the only casted samples.

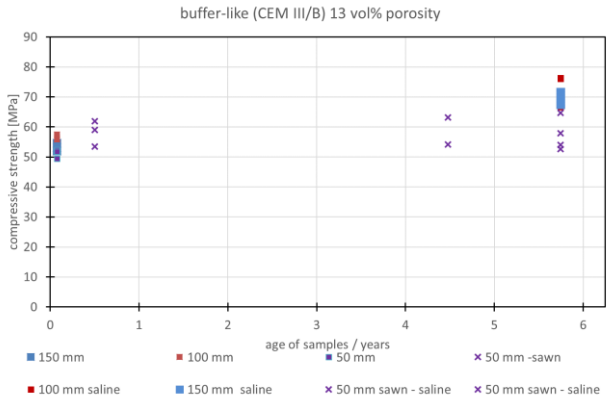

Figure 3-5 - Compressive strength evolution in function of the samples studied and the age.

Self-sealing of cracks in buffer-like concrete was observed but not for backfill concrete. The pieces of re-assembled backfill concrete could be removed by hand while this was not the case for the buffer-like specimen; the re-assembled buffer-like specimen had a compressive strength of 34 MPa. The difference in behaviour between buffer-like concrete and backfill concrete was attributed to the presence of unreacted cement as has recently also been found for Roman concrete (Seymour et al., 2023).

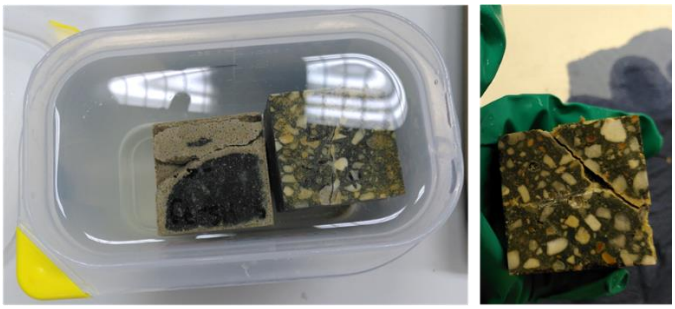

Figure 3-6 - In box: backfill concrete made with CEM III/B (left) and buffer-like concrete (right) after about 3 years of re-assembling; in gloved hand: re-assembled buffer-like concrete that appeared to have a compressive strength of 34 MPa

To summarize, in the COVRA study, ageing of mortar/concrete in contact with poorly indurated clay simulants increased compressive strengths. A comparison of mechanical strengths is provided between samples hardened for 28 days and samples exposed for 5 years or more to a clay pore water as salty as seawater. Following the saltwater immersion phase, the compressive strength of CEM III/B buffer-like samples increases by 26 to 31%, the compressive strength of CEM III/B backfill-like samples increases by 24 to 46 %, and the compressive strength of CEM I backfill-like samples (non-certified samples) increased by 40 to 47 %. The fractured surfaces of the cracked samples placed in close contact revealed a potential for self-sealing for the buffer sample, but not for the backfill sample. Regarding this increase in strength, it is not possible to separate the role of reactivity with the environment from that of hydration of the cement. However, the planned chemical analyses of FZJ, using elemental mapping (SEM/EDS) and XRD, should provide an indication about calcite formation and the degradation of CSH by carbonation, as well as the progression of Mg. These results are not yet available, but the study of the oxygen reaction front by colour contrast, and the evaluation of carbonate thicknesses, gave the first indications.

New ageing experiments under conditions representing operational disposal phase (Bukov URL)

In the experimental program of the Czech partners, the influence of three experimental environments on SURAO LPC material was tested and studied: *In-situ* air environment, *in-situ* groundwater environment and BCV bentonite suspension environment. Laboratory tests were conducted on three years old material, with an ageing of 0-18 months at the Bukov URF. Experimental boxes were placed into *in-situ* conditions and located at the Bukov URF (Underground Research Facility) at the 12th underground floor at the depth of approximately -500 m below surface. First, the air environment represents an ordinary condition of the underground environment of the former uranium mine (high humidity, 15°C). Second, interface of concrete and groundwater was set up as an open system with water continuously flowing from the source (borehole S25) into four experimental boxes. As such it simulates the underground conditions realistically and avoids spoiling the water by insufficient circulation leading to robust outgrowth of fermentative species. Third, the interface of concrete and bentonite suspension was set up into closed boxes. Bentonite suspension was prepared one week before setting up the in-situ experiment.

Analyses were carried out to identify the impact of the microbial activity on the concrete chemo-mechanical behaviour.

SURAO LPC disks were tested in terms of mineralogy, leachate chemistry, mechanical strength at different scales and microbiology (the aspect relative to the microbiology is discussed in the Part 4 of the present report) prior to the experiments and during the experiments after 6, 12 and 18 months of exposition to the respective environment. The mechanical tests on macroscale (double punch compressive test) were carried out by pressing with punches in the middle of the disc. During compression with the punch, most of the volume of the specimen was thus loaded gradually in tension, in four steps until failure. The result was also influenced by micro/macro cracks, pores, etc. In contrast, microscale testing by nanoindentation was performed on selected intact areas of the cement matrix outside the aggregate area. The results therefore did not significantly consider the influence of possible micro/macro cracks.

After first 6 months exposition to underground environment, a significant decrease in pH of LPC powder was observed (Figure 3-7). The mechanical strength was affected the least of all environments (Figure 3-8). Indeed, recent studies on biologically induced carbonate precipitation proved improved durability and impaired permeability due to secondary crack healing (Esaker et al., 2021; Kalhori and Bagherpour, 2017; Luo et al., 2018; Wang et al., 2016).

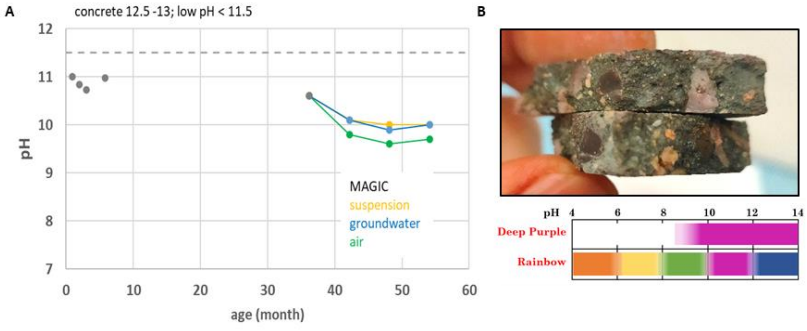

Figure 3-7 - (A) pH evolution of LPC powder in air- (green), water- (blue) and bentonite-exposed (yellow) SURAO LPC samples. (B) visualisation by rainbow indicator - cube cut edge surface exposed to air for 3 years URL Bukov at 100% RH + 2 years at CTU lab with 30-50% RH

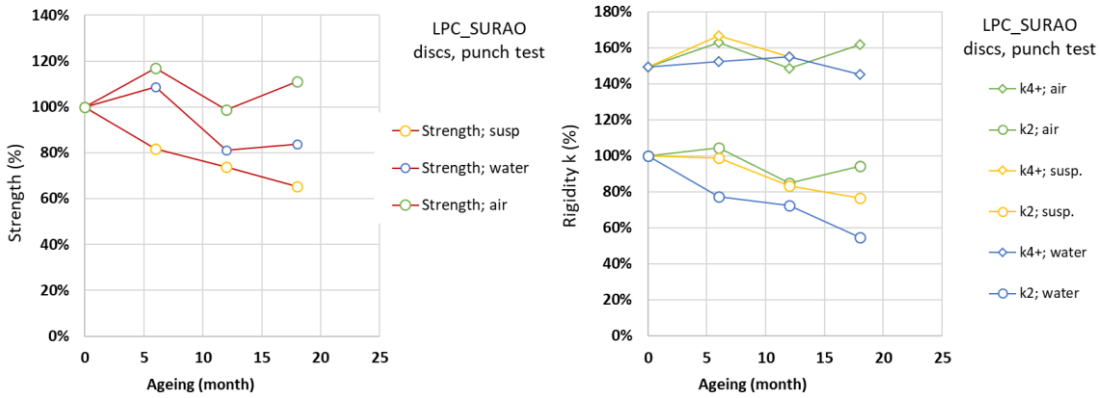

Figure 3-8 - Time evolution of mechanical parameters in all three environments (in %; strength left; rigidity k2 and k4+ right).

By using SEM and EDS element mapping, it was demonstrated that at the interface of the cement paste and bentonite the cement matrix was enriched in magnesium. This feature was unique for this surrounding and magnesium gradually penetrated the cement matrix depending on time of exposure (Figure 3-10). The concentration of magnesium ions in bentonite pore water and groundwater was 0.695 mol/L and < 0.0027 mol/L, respectively. The pH of the low-alkali concrete was around 10, which corresponds to the conditions that lead to magnesium attack (Dewitte et al., 2022). In turn, a significant change (decrease) in strength is observed for the suspension environment. A relatively large area of the sample (surface zone - approx. 1.5-2 mm) with higher pH was observed when using a rainbow pH indicator**Erreur ! Source du renvoi introuvable.**. Finally, lower mechanical strength has been proven by the decreasing number of LPC samples from each set that resisted the stresses in each step of the mechanical test.

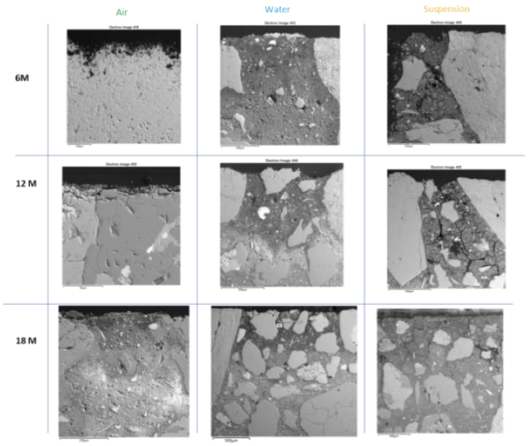

Figure 3-9: Relative crack penetration and surface changes of air-, water- and bentonite-exposed LPC samples after 6, 12 and 18 months.

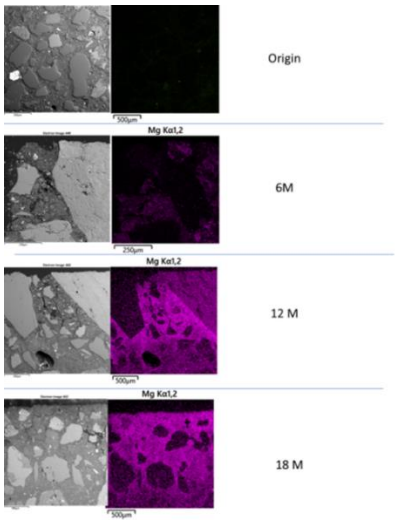

Figure 3-10: Scanning electron micrograph showing the penetration of magnesium into the cement matrix after 6, 12 and 18 months.

Prior to testing, LPC specimens were cleaned of bentonite suspension residues on the surface. A rainbow indicator was used to determine pH and visualize its changes in the cross-section of the (broken) samples (Figure 3-11). The degraded thickness is consistent with the results in Figure 3-10.

Figure 3-11 pH determination of LPC_SURAO by rainbow indicator (T3 – 18 months aged samples; broken discs after punch tests).

To summarize the main results: The degree of surface degradation of the samples was found to be the lowest in air environments, followed by water environments, with the highest degradation observed in bentonite suspensions.. The decreasing number of stress-resistant samples in each series at each stage of the mechanical test (bentonite < water < air) correlates with crack formation and decreasing mechanical strength in each environment and time. Primarily in the experimental environment of a bentonite suspension, an accelerated degradation by magnesium ions was observed. The results are in agreement with destabilization of the C-S-H component to M-S-H, which occurs at the interface of the cement paste deprived of portlandite and the Mg rich bentonite suspension. The nanoindentation results showed a slight improvement in mechanical resistance over time, independent of the environment (see deliverable D16-4). This can be explained by the rehydration of the sample after exposing the material during sample preparation from larger cubes (drilling, cutting). However, the resistance is slightly lower in the peripheral regions of the samples. This may be due to microcracks at the surface caused by sample preparation or microcracks/increased porosity caused by development/interaction with the environment.

3.1.3 Chemo-mechanical evolution of concrete samples exposed to clayey rock

Long term evolution of concrete in contact with the Opalinus clay

The PSI/Empa team has worked with mortar and concrete specimens of different types stemming from the CI (Cement-clay Interface) experimental campaign at the Mont Terri Underground Research Laboratory (URL) after several years of interaction.

In the PSI/Empa study, the mortars/concretes have, in increasing order, an average compressive strength of 24 MPa (LAC concrete), 36 MPa (OPC concrete), 40 MPa (ESDRED mortar) and 80 MPa (ESDRED concrete and OPC mortar) (Figure 3-12). Concerning non-destructive tests, the E^{dyn} data scatter due to the material heterogeneity was larger than that due to the measurement repeatability level, while the two data scatter types were on average similar for α_L. The correlation between dynamic and quasi-static Young's modulus values indicates that the dynamic values are 10 to 40 % higher than the quasi-static ones. Only the LAC specimens exhibited a clear and coherent spatial dependence of the mechanical properties on the specimen distance from the OPA interface. This difference is consistent with the presence of cracks and debonded ITZs in the cores at 0 mm, but not in the cores at 50 mm distance.

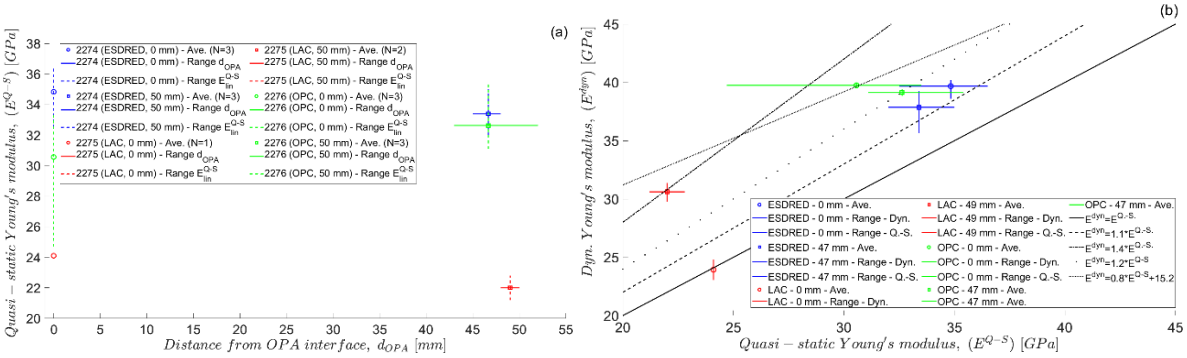

Figure 3-12 - (a): Quasi-static, compressive Young's modulus values (E^{Q-S}, vertical axis) of the three concrete specimen ensembles (2274, 2275 and 2276), as a function of the specimen surface distance (d_{OPA}, horizontal axis) from the interface with the Opalinus Claystone (OPA). (b): correlation between E^{dyn} and E^{Q-S} values (markers), with some indicative theoretical models (lines) provided for reference.

A qualitative inspection by X-ray tomograms of the cored specimens allowed two essential observations. First, the LAC concrete cores were the only ones to exhibit evidence of resolvable (i.e., above 60 µm in size) damage features, mainly macroscopic cracks and disbanded Interfacial Transition Zones (ITZs), see Figure 3-13 for an example, while the ESDRED and OPC cores appeared completely undamaged above this length scale. The presence of these two damage features agrees well with the observation of lower E^{dyn}, E^{Q-S} and f_c values for the LAC concrete than for the two other concrete types. It is not possible for the team either to exclude or to confirm that the sampling by coring induced such cracks. However, even in the case the coring did induce the observed cracks, their occurrence in the LAC concrete specimens and not in those of the two other concrete types still suggests that the former material was more degraded than the other two, given that the same exact workflow was followed for the coring and the three cast concrete volumes were subjected to exactly the same boundary conditions.

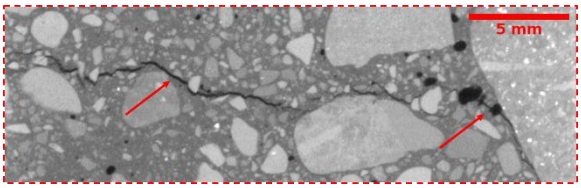

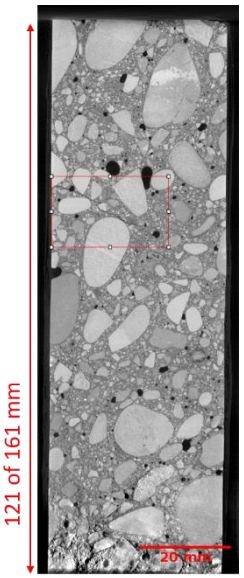

Figure 3-13 - X-ray tomogram of one LAC concrete specimen (2276-A6), showcasing the presence of damage. The right inset shows a cross-section from the tomogram along the core's longitudinal direction. Notice that the tomogram covered 121 mm of the total core's length (161 mm). The region highlighted by the red rectangle is shown in the left inset as a zoom-in, to better highlight the presence of a mesoscopic scale crack (left arrow) running through half of the core's horizontal size. Such crack is interconnected with a disbonded Interfacial Transition Zone of one aggregate (right arrow).

The eventual gradient with the distance from the OPA interface could not yet be correlated with differences in tomographic features between specimens at the interface and about 50 mm distance. The mentioned future voxel value distribution analysis could further support such a validation. Second, both the ESDRED and OPC mortar cores showed no resolvable (i.e., above 44 µm in size) signs of damage and the ESDRED exhibited a significantly larger air void content, not yet quantified at the time of this report but to be performed before MAGIC's end.

Thus, overall, X-ray tomography could provide information that supports the interpretation of the results obtained from the mechanical characterizations, with clear evidence of severe damage at a length scale above 60 µm only in the LAC concrete specimens.

Long term evolution of an OPC concrete in contact with the Boom clay

A Boom Clay-OPC concrete interface was sampled by SCK-CEN at the HADES underground research facility in Mol, Belgium. In the study, the autoradiography porosity map shows that the porosity of OPC concrete increases in the first 2 mm from the interface after 14 years of interaction in contact with Boom Clay (Hades URF) (Figure 3-14). This figure illustrates autoradiography porosity maps of the interface along with various quantitative data, including metrics for total connected porosities and porosity profile histograms. The autoradiography porosity map offers insights into the distribution of porosity across a 4 × 8 cm surface. On the concrete side, the recorded porosity levels are influenced by the volume fraction of aggregates present within the probed regions. Specifically, the orange rectangular area represents the porosity arising from the intermingling of cement binder and small aggregates, which is approximately 20 %. Meanwhile, at the interface, regions with higher porosity readings are observed within the cement binder, with an average porosity of 35 % (indicated by the red rectangle) extending to the first 2 millimeters.

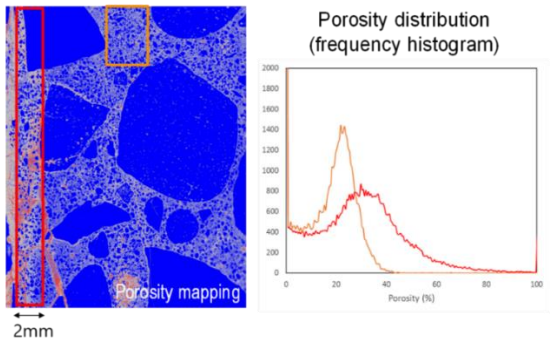

Figure 3-14 - Autoradiography porosity map of the concrete-Boom Clay interface - Frequency histograms obtained from the rectangles plotted on the autoradiography.

The water sorptivity coefficient is then 3 times higher for altered concrete (at the interface) than for sound concrete. The cumulative water absorption data reveals an initial rapid absorption phase, followed by a subsequent slower absorption phase. A significant enrichment in Mg is observed in the concrete in contact with the clay, spanning a thickness of 500 µm (Figure 3-15).

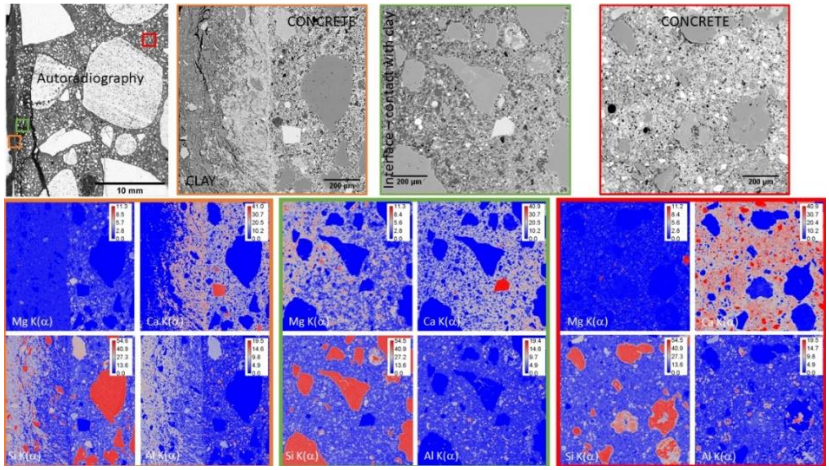

Figure 3-15 - Localization of the mapped area on the autoradiograph: The green, orange, and red outlines on the maps correspond to their positions on the autoradiography, and at the bottom, BSE images and quantitative chemical maps are presented. Atomic weight % is used for calibration, ensuring a consistent scale for the analyzed elements across all maps.

The mapping reveals the leaching of Ca in the OPC concrete at the interface and the increase in Mg concentration is inversely correlated with calcium concentration (mineralogical mapping). According to Darcy's law in conjunction with Lucas-Washburn's equation, the increase in water sorptivity can be attributed directly to changes in capillary porosity and mean pore radius.

SCK-CEN has built mineral maps based on the chemical analyses. Figure 3-16 depicts a map of the concrete near the interface in an area where porosity is increasing. This mineral map clearly identifies the aggregates, which are consistent with those found in the "reference state" concrete. Notably, a prominent collection of pixels extends between the C-A-S-H and clay chemical compositions. After segregating the aggregates and residual fly ash (FA), the remaining pixels, representing the hydrates (components of the hydraulic binder), were plotted on either the M^{+}-4Si-R^{2+} or Si-Ca-AlFeMg diagrams. In the Si-Ca-AlFeMg diagram, we can differentiate various clusters of pixels by imposing limits on the calcium and magnesium content. The two ends of this trend correspond to (i) pixels with the highest calcium content (Ca > 30 wt%), situated close to the C-A-S-H composition, and (ii) pixels with the highest magnesium content (Mg > 12 wt%), forming a tightly clustered group associated with the M-S-H, zeolites, and clay stoichiometry. These specific pixels appear as light blue grains with dimensions less

than 50 µm on the mineral map. This elongated cluster of pixels signifies a chemical transformation that is dependent on the distance from the interface. Calcium and magnesium concentrations exhibit an inverse relationship, with an increase in magnesium observed in the concrete in contact with clay, resulting in a decrease in calcium concentration. This relationship varies with increasing distance from the interface.

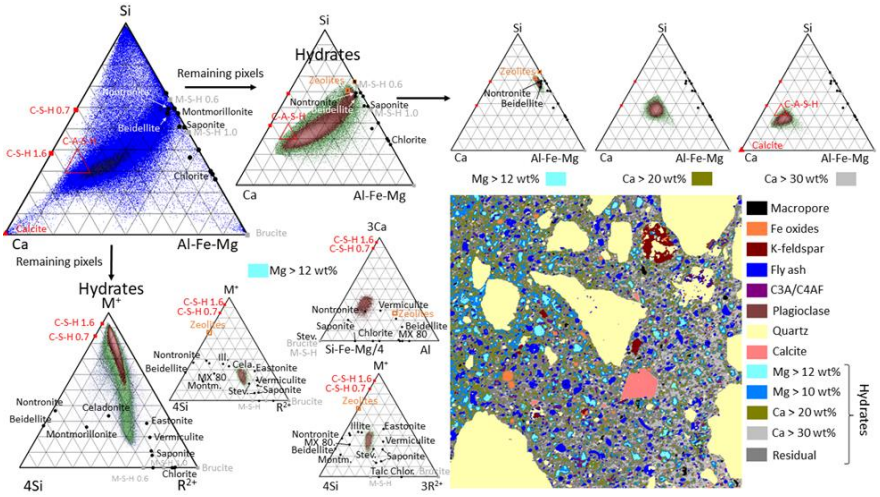

Figure 3-16 - Mineral maps of the concrete adjacent to Boom Clay, featuring Si-Ca-AlFeMg ternary plots that encompass all the pixels within the map. Various segmentation steps were employed to distinguish the hydrates, with labels such as Stev. (stevensite), Ill. (illite), MX 80 (smectite MX80), Chlor. (chlorite), and Montm. (montmorillonite) corresponding to different mineral phases.

3.2 The modelling at small scale

3.2.1 Development of a Lattice Boltzmann (LB)-based simulator for the pore scale modelling of the paste microstructure evolution

Due to strong differences in chemical composition, cement is typically not in equilibrium with the host rocks. Therefore, pore water exchange between these materials leads to dissolution-precipitation processes and mineralogical changes. These, essentially pore scale processes, affect the mechanical properties and eventually the integrity of the cement paste, thus of the whole concrete. For the sake of computational efficiency, the large-scale, long-term simulations of the cement paste's chemo-mechanical evolutions are typically modelled using a continuum approach. Ideally such models should rely on parameters upscaled from pore-level simulations.

Cementitious materials are hierarchical porous media with characteristic microstructure features controlling transport phenomena and reactivity at different scales. Pore size distribution in cement ranges from few nanometres ("gel" pores) to few millimetres (air voids) (Gong, Zhang, Sicat, & Ueda, 2014; R. A. Patel et al., 2018). The complexity is compounded by various chemical processes such as carbonation (Dauzères et al., 2022; Huang et al., 2018; Phung et al., 2016; von Greve-Dierfeld et al., 2021), interaction with other materials (for example host clay for radioactive waste repositories (Savage & Cloet, 2018) or aggressive species ingression such as sulphates (Dauzéres, 2016; Schmidt, Lothenbach, Romer, Neuenschwander, & Scrivener, 2009). These interactions lead to non-linear changes in the paste's porosity and chemical composition (Barbara Lothenbach & Winnefeld, 2006; Mäder et al., 2018), occurring across different spatial and temporal scales. In particular, small changes in the pore connectivity and preferential transport pathways can result in substantial alteration of macroscopic transport properties, such as permeability and diffusivity. To simulate such processes accurately, a multi-scale approach operating on both the continuum and the pore-scale is required (Churakov & Prasianakis, 2018).

The aims in modelling of the PSI/Empa contribution in the WP-MAGIC was the:

- Development of a Lattice Boltzmann (LB)-based simulator for the pore scale modelling of the paste microstructure evolution.
- Acceleration of pore scale modelling numerical simulations with ML/AI methods and development of surrogate models for microstructure evolution.
- Application of numerical and analytical approaches to assess mechanical properties of cement paste and mortar based on 3D pore scale microstructure and microstructure evolution modelling.
- Validation of the model by experimental data (presented in Part 3.1) and parameter upscaling.

Such modelling activities are intrinsically multidisciplinary and benefit from collaboration with project partners from SCK CEN and CNRS, who have strong expertise in microstructure-based mechanical homogenisation studies based on numerical and analytical approaches, respectively, whereas the PSI team is particularly advanced in pore scale reactive transport simulations and small scale sample characterisation.

Development of numerical modelling tools

The LB method is based on the solution of the kinetic Boltzmann equation, which, at the macroscopic limit, corresponds to the Navier-Stokes equations (Lallemand & Luo, 2000; Qian, d'Humières, & Lallemand, 1992). The lattice can then simulate complex interfacial fluid-solid interactions by adapting its nodes to quasi-solid/liquid states (Prasianakis et al., 2018; Sukop & Thorne, 2006). The discrete LB equations are particularly suitable for parallel numerical algorithms, due to the locality of the LB operator. In most practical implementations of the LB equations, the communication and exchange of information is only required between the immediate neighbouring nodes. This allows for (a) simple implementation of complex boundary geometries, essential for simulating porous materials and (b) efficient parallelization of the algorithm for use in high performance computing facilities (Prasianakis et al., 2018). The parallel algorithm efficiency makes it ideal for use with massively parallel architectures such as graphics processing units (GPUs) as well as in hybrid CPU/GPU supercomputers (Kuznik, Obrecht, Rusaouen, & Roux, 2010; Safi, Prasianakis, & Turek, 2017). Their structural efficiency for parallel data allows to achieve speedups up to several orders of magnitude compared to computation on an equivalent conventional CPU processor (Kuznik et al., 2010). Furthermore, the small amount of exchangeable data between computing nodes means that LB algorithms can be very efficient on interconnected GPU networks.

However, the LB model describes only the mass transport in fluid and the fluid-solid interface evolution. The chemical equilibria calculations need to be implemented and coupled via separate thermodynamic modelling routines. Geochemical speciation solvers provide the quantities of chemical speciation and phase stability in the system under the assumption of local equilibrium. These calculations can be done using the Law of Mass Action (LMA) (as in PhreeqC (Parkhurst, 1995)) or Gibbs Energy Minimization (GEM) (as in GEMS-Selektor (Kulik et al., 2013)). Because of the complex nature of computations related to thermodynamic equilibrium and geochemical speciation, the calculations become a computational bottleneck in reactive transport modelling. Large computational demands arise from the multitude of species involved and the necessity to carry out chemical calculations at each mesh point for every time step. Consequently, the integration of the LB and geochemical solvers results in a poorly balanced code, with most of its computational resources spent in the thermodynamic modelling routines (Prasianakis et al., 2020). Moreover, it is worth noting that the time scales for chemical reactions and mass transport mechanics differ significantly.

The LB reactive transport algorithm used in MAGIC is implemented in two codes: (a) a CPU-based Python-Fortran code, coupled with PhreeqC (R. A. Patel, Churakov, & Prasianakis, 2021; R. A. Patel et al., 2014) for small scale 2D/3D domains, with full coupling between the LB and the thermodynamics

calculation and (b) a GPU-based CUDA/C++ code (Safi et al., 2017) coupled with a pre-trained (through GEMS-Selektor thermodynamics calculations) artificial neural network (ANN) used as a surrogate model. The latter code can be used for large-scale 3D domains described by more than 1 billion computational grid points, where performing chemical calculations via typical thermodynamic modelling routines becomes computationally unfeasible.

Feedforward type ANNs are used for the pore-level simulations. This is one of the simplest but most efficient network types, suitable for solving complex regression problems. The ANNs used in this study were obtained by a supervised learning approach in order to encode the thermodynamic equilibrium depending on the composition of the solution, with the data that GEMS provides. A mean squared error loss function is used for training such ANNs. The right balance between the size of the network and its resulting accuracy was pursued. For that, several networks were tested, by varying the number of neurons per hidden layer, the number of hidden layers and the activation functions of the neurons. Moreover, several training algorithms were tested. It is noted that a common issue in this type of networks is the element mass conservation between input and output of the networks, which can be an issue if not properly resolved. The architecture of the ANN and its typical performance against a native geochemical solver is shown in Figure 3-17. The ANN takes the total Ca and Si concentration expressed at $(Ca(OH)_2)_{aq}$ and $(SiO_2)_{aq}$, provided by the LB code as input. The output consists of multiple phases including solids such as jennite and tobermorite in accordance with the CSHQ model (Kulik, 2011). The ANN training is done using the state-of-the-art backpropagation algorithm (Rumelhart et al., 1986).

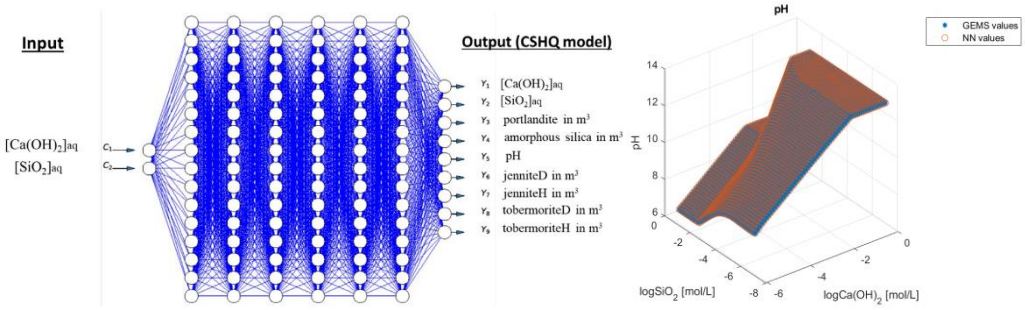

Figure 3-17 - (left) A neural network model used for reactive transport simulations of leaching and C-S-H re-precipitation. The inputs are the species' concentrations in solution and the output is the thermodynamic equilibrium of the C-S-H phases and the resulting aqueous species. (right) Graphical representation of the comparison of the neural network values (NN values, e.g. pH, red circles) vs the geochemical solver values (GEMS, blue stars). The two manifolds practically overlap.

Numerical modelling results

Numerical simulations of the microstructure evolution were performed for different scenarios assuming CH dissolution and a more complex scenario with CH dissolution coupled with C-S-H dissolution re-crystallisations. Simulations have been conducted with the GPU-based CUDA/C++ code (Safi et al., 2017) coupled to ANN for geochemical calculations. The cubic domain of 100 μm^3 volume used for the simulations was produced by the HYMOSTRUC code (van Breugel, 1995) and discretised with particle spacing of 1 µm. The microstructure was provided by SCK CEN and was based on a 60-day hydrated Ordinary Portland Cement and is similar to (Ravi A. Patel et al., 2021; R. A. Patel et al., 2014; Varzina et al., 2020). The portlandite dissolution was implemented in the LB code through an equation based on the transition state theory (Lasaga, 1984), which was implemented as a source term in the LB equation. The necessary physical constants for the reaction were identified from experimental results (Galan, et al., 2015; Johannsen & Rademacher, 1999). Figure 3-18 shows a comparison between the domain state at the beginning of the simulation and after 1.5 million LB steps or 2136.75 s (1 LB time step = 0.0014245s). At this point, approximately 68.7% of the portlandite has been dissolved.

Additional simulations have been conducted to investigate the sensitivity of the dissolution to the mineral surface reactivity. This is aimed at the evaluation of the effect of microbial activity on the evolution of the paste microstructure. Microbial activity is expected to modify the porosity through increased precipitation of secondary mineral phases, followed by an alteration and dissolution of cement hydrates. Further details on the LB portlandite dissolution simulations, including a detailed description of the model and the effects of reactivity, can be found in the Deliverable 16.7. The same report also contains the details about the investigation of the temporal and spatial evolution of both the chemical composition and the paste's microstructure and their effects on the mechanical properties of a paste and a concrete, as part of a synergistic collaboration (PSI, SCK-CEN, LAMCUBE).

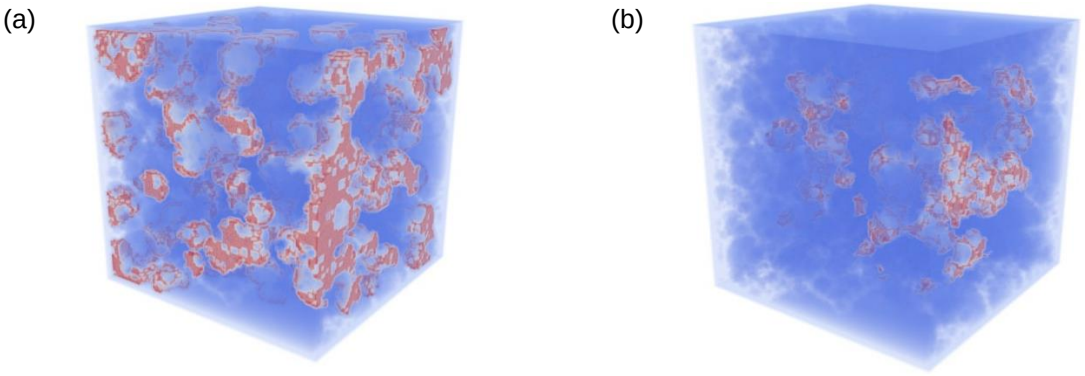

Figure 3-18 - Ca leaching LB simulations in a 100 μm^3 domain, considering the dissolution of portlandite. The left column shows the initial state, while the right shows the state after 1.5 million LB steps. Red nodes signify dissolving portlandite, which are in contact with the solution, while white nodes are inactive portlandite surrounded by solid matrix, light blue nodes indicate distribution of C-S-H and aggregates and dark blue is water.

At the next model complexity level, both CH and C-S-H dissolution are considered simultaneously. The dissolution of C-S-H nodes (both high and low density) release Ca similar to CH dissolution. In addition, the C-S-H's releases Si, whose diffusion is also tracked in the model. Figure 3-19 shows a comparison between the domain state at the beginning of the simulation and after 4 million LB steps or 5698 s. At this point, all of the portlandite has been dissolved, in addition to 33% of C-S-H both high and low density. To account for the changes in the Ca:Si ratio of the pore water solution, a recrystallisation of C-S-H solid solution with variable composition is implemented. To better understand the behaviour of such a complex system, the modelling is performed for boundary conditions with different Ca and Si concentrations, particularly under conditions pertaining to the OPA interface. Such models are particularly important for simulating the processes at cement-clay interfaces, as the clay may be a Ca and Si source. Precipitation is a more complex phenomenon than dissolution, since the precipitation rate depends on the pore size and the available mineral surfaces, which can serve as the templates for heterogeneous nucleation and precipitation. To model such phenomena, which involve several species, it is crucial to consider the chemical speciation.

(a) (b)

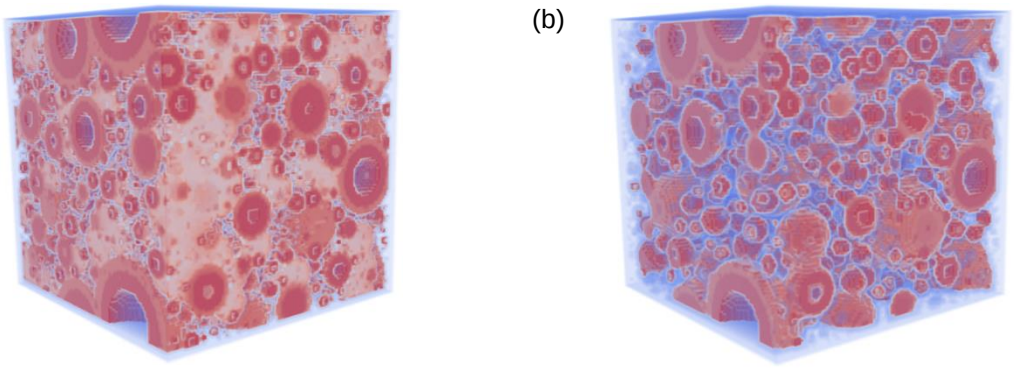

Figure 3-19 - Ca leaching LB simulations, considering the dissolution of CH and C-S-H phases. The left column shows the initial state, while the right shows the state after 4 million LB steps. Red nodes signify dissolving high density C-S-H, orange nodes dissolving low density C-S-H, light orange nodes are dissolving portlandite, light blue domains indicate distribution of C-S-H and aggregates and dark blue is water.

In the course of this project, a multiphase LB code for the reactive transport simulation was coupled with a surrogate model to compute chemical equilibria in the cement paste. This code was applied for the analysis of the temporal evolution of cement hydrates, under leaching and carbonation, in 3D and by using a realistic representation of mineral phases and of boundary conditions. Such analysis not only provides access to the spatial evolution of the microstructure but also sets temporal constraints on the evolution scenario. Obtained microstructures can be used for the numerical homogenisation of mechanical properties and enable the estimation of a temporal scale for mechanical degradation of the cement paste performance. Interestingly, the spatial evolution of the microstructure and of the mechanical properties, as obtained by these time dependent simulations, are comparable with the results obtained for a much more simplified model using a stochastic description of dissolution/precipitation phenomena without rigorous time constraints. The principles of numerical homogenization developed for the paste are also applicable for mortar and concrete. The analysis includes a homogenized cement paste, an interfacial transition zone (ITZ), air voids and aggregates.

Significant progress has been achieved in applying ML and AI approaches to the acceleration of numerical simulations in reactive transport modelling and upscaling the mechanical properties of the cementitious systems. With surrogate models achieving several orders of computational speedup when replacing native geochemical solvers, time resolved 3D reactive transport simulations of the microstructure evolution become possible. Finally, a successful step by step upscaling of mechanical properties from the paste to the concrete scale was shown.

In particular, the evolved geometry can be used for retrieving correlations between parameters such as porosity, diffusivity and the local chemical composition. These correlations can then be applied at the macro-scale, for example for finite element method-based simulations, to track phenomena happening within a single cell. Since the time evolution is calculated, such correlations may also be time-dependent or related to the dissolution degree. For example, the porosity increase, with regards to the dissolution of a percentage of the solid nodes or the diffusion rate for certain pores, can be tracked.

In addition, the evolution of the chemical composition itself can be used for upscaling. The evolved geometry has different amounts of CH, C-S-H and unhydrated phases with a different porosity. These percentages can be extrapolated to larger volumes, which can then be used as REV for macroscale codes. The upscaled REV can have different mechanical properties (Young's modulus, compressive and tensile strength, etc.) reflecting the microscale phenomena.

The data can be useful for different environmental conditions, which can be reflected at different boundary conditions in the pore scale simulations. For example, different Ca and Si concentrations

at the boundary can reflect the interactions with different clays. Moreover, changing the reaction rate can model conditions with different pH or temperatures.

3.2.2 Development of a chemo-mechanical model of combined dissolution precipitation processes in cement under microbial-chemical-mechanical attacks at the pore scale with spatial resolution of 1 µm

The goal of the study of SCK CEN was to develop and improve the Chemo-Mechanical understanding of the evolution of cementitious materials at the microscale, in particular, leaching and carbonation. To achieve this goal, SCK CEN and PSI aimed at developing a chemo-mechanical model of combined dissolution precipitation processes in cement under microbial-chemical-mechanical attacks at the pore scale with spatial resolution of 1 µm. The existing model should be extended from an existing state of the art Lattice-Boltzmann based pore scale reactive transport model to simulate the chemical evolution based on a given boundary condition and material microstructure and composition.

One of the main challenges in the high-resolution modelling is the computationally expensive speciation simulation. The improvement of the model should be done on the one hand by simplifying the chemical description and taking into account most relevant chemical and microbial processes either by considering simplified system chemistry or using neural networks for geochemical calculations. The last approach is technically very promising but requires extensive training of the network on the large datasets for specific chemical formulations of the cement system and the chemical and microbial attack.

The calculated evolution of microstructure should then be used to estimate the changes in mechanical properties of the cementitious materials and to evaluate the main parameters controlling their mechanical properties. The formation of the secondary mineral phases or their dissolution is captured by the micro-scale Lattice-Boltzmann models used by PSI and SCK CEN.

The obtained microstructure at a given point in time is transferred to the FEM structural model, where each phase gets assigned its own mechanical parameters. By comparing different degradation states, the effects of combined microbial - chemical attack on the mechanical behaviour of cement pastes can be analysed. The results of the micromechanical model were the elastic properties of the representative volume element obtained via a standard numerical homogenization scheme.

Predictions from the microscale model could be compared against micromechanical tests carried out on macroscale experiment. This work provided direct information to those partners who are looking for chemo-mechanical cement paste data in order to upscale transport and mechanical properties for use in macroscale simulations.

The implemented experimental approach and modelling

As mentioned above, the approach to achieve the goal of better understanding of the leaching and carbonation process and its influence on chemo-mechanical properties is by LB modelling. Cement paste microstructure consists of different mineral phases and a complex network of pores between the solid phases. The porosity has a multiscale character with specific features manifesting at nano and micro-meter scales and even at mm scale in case of fractures. Hardened cement paste consists of numerous solid phases, most important of which are portlandite (CH), calcium-silicate-hydrates (C-S-H), and aluminium containing phases such as AFm and AFt. Mineralogical and consequently microstructural changes occur in cementitious systems due to chemical evolution towards stable mineral fluid equilibria in the cement paste itself or as result of chemical equilibration with the environment. The mineralogical composition and microstructural transport properties determine the chemical stability of the solid, the mobility of species, and the overall fluid flow through the system. Accurate description of chemical interaction in cement systems is a prerequisite for the prediction of long-term performance and assessment of mechanical properties of cementitious materials. In practical applications, chemical changes manifest as hydration and degradation, which are occurring at the same time. Even the

prediction of the mineralogical and microstructural changes during hydration alone is a challenging task. In cementitious materials, the rate of chemical evolution is often controlled by ion transport. This is because cementitious materials are characterized by fine pores, with the majority below the scale of a few micrometers. Moreover, cementitious materials also have heterogeneous distribution of solid phases. Similar to pore sizes, also the sizes of solid phases are mostly below the scale of a few micrometers. Hence, to obtain representative properties of the materials and provide reliable process descriptions, studies have to be done at least on the spatial scale of micrometers. Cement paste microstructure is described by a complex network of pores and interconnected solid phases. Each transition between phases or minerals requires an interface with mostly a very sharp transition of physical, chemical and mechanical properties. The numerical description of such systems requires numerical approaches that can cope with many boundaries, sharp transitions and are computationally cheap. Based on experimental data, numerous macroscopic models have been developed to describe the mechanical behaviour of concrete. However, in general, these models do not establish explicit connections between macroscopic properties and microstructural parameters. To overcome this limitation, micro-mechanical approaches have been developed to estimate the macroscopic mechanical properties of concrete composites by considering microstructural parameters and constituent properties as the basis.

Within the MAGIC project, the project partners at SCK CEN, CHRS-LAM3 and PSI jointly investigated the effect of the leaching on the mechanical degradation of cement using 3D lattice Boltzmann simulations and numerical simulations of mechanical properties of cement paste. Several studies conducted in MAGIC WP aim at establishing connections between microstructural parameters, material composition characteristics, and macroscopic mechanical properties, enabling accurate predictions of concrete performance. This approach significantly improves the predictive power and accuracy of the models, while also efficiently completing complex mechanical modelling within a condensed temporal framework.

Because of the wide range of length scales involved, it is practically impossible to include and analyze all phases with one large scale single experiment or numerical model. Previous work on the scaling of strength across hierarchically structured composite materials in the presence of defects with distinct morphology and origin within the microstructure has been studied on the level of the hardened cement paste. In this work the cement paste stiffness and its evolution due to chemical changes has been studied separately in three levels, starting from pure hardened cement paste without any defects or inclusions, and then adding the inclusions.

The approach of several scale levels has been also adopted by Drugan & Willis (1996). They derived a variational formulation for a micromechanics-based, explicit nonlocal constitutive equation relating the ensemble averages of stress and strain for a class of random linear elastic composite materials. They report that the minimum representative volume element (RVE) size for the usual macroscopically homogeneous “effective modulus” constitutive models is at most twice the reinforcement diameter (or inclusion) to achieve a maximum error of 5% of the constant “overall” modulus term. For an error below 1% the size is 4.5 times the reinforcement diameter.

Based on these findings this work builds further on the upscaling of mechanical properties up to the concrete scale. The principles of numerical homogenization of concrete include homogenized cement paste, interfacial transition zone (ITZ), air voids and aggregates. In this study, only aggregates and homogenized cement paste matrix are considered. Future refinements will incorporate air voids for estimating the elastic properties. ITZ may become important for estimating strength properties, which will not be addressed with numerical homogenization.

Numerical simulation results

According to the goal of the project, the elastic properties of sound, leached and carbonated cement pastes and concretes used for the experimental studies in WP MAGIC were estimated. The initial composition of the cement mix is provided by the HYMOSTRUC model. In this study, the microstructural state is sought at 100 days, when the material is expected to reach close to maximum degree of hydration. For the sake of simplicity, only major phases are considered in the microstructure for estimating the mechanical properties. AFt and AFm phases are in trace quantities and hence ignored. The resultant volume fractions are re-normalized to 100%. The resulting microstructural arrangement is shown in Figure 3-20.

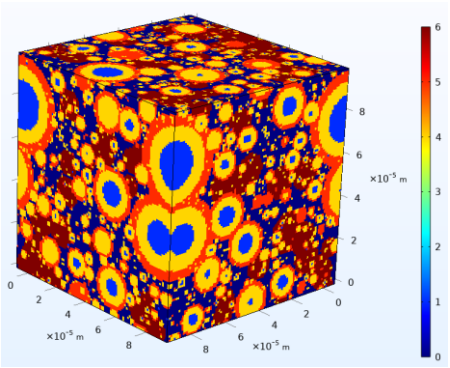

Figure 3-20 - Synthetically generated microstructure based on HYMOSTRUC model. 0: water filled micropore; 1: Unhydrated clinkers; 4: HD C-S-H; 5: LD C-S-H; 6: CH

The link between mechanical properties and leaching is given in terms of % of leached portlandite. This information is obtained on the basis of the pore scale model. The example of microstructure at respectively 25% and 50% leached portlandite is shown in Figure 3-21.

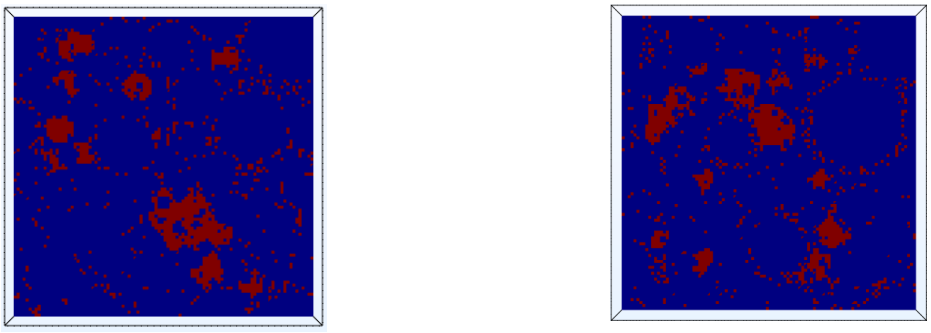

25% leached CH *50% leached CH*

Figure 3-21 - Leached microstructure. Portlandite (CH) is denoted by red colour.

These results have been homogenised to an effective Young's modulus of cement paste at 0%, 25%, 50%, 75% and fully leached sample. The decrease in the elastic modulus with increase in leaching degree as shown in Figure 3-22 is consistent with experimental observations previously acquired in parallel.

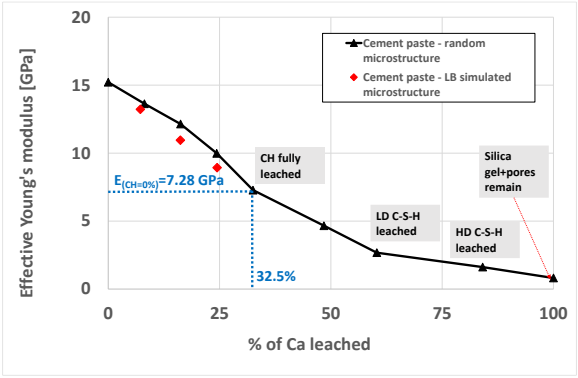

Figure 3-22 - Young's modulus of cement paste as a function of mass % of Ca leached.

The effective moduli obtained on the basis of LB simulations are in good correspondence with the randomly generated and numerically leached microstructure. This reveals that for the elastic modulus, the spatial distribution of leached zones is not that sensitive, at least at the microstructural scale. In other words, mere knowledge of volume fractions of different phases suffices to reasonably estimate the effective modulus of the material. This also explains why analytical homogenization techniques are generally successful in estimating the effective properties such as elastic modulus, diffusivity and conductivity, where RVE exists.

The initial scale is the scale of cement paste. Typical size is around 100 μm to assure REV considering the large solid phases. Considering the REV size from (Drugan & Willis, 1996) and rounding it up, we used a factor of 5 for each consecutive scale. This results in the range of spatial levels, each being 5 times larger than the previous one. Beginning from the paste scale of 100 μm, the next level has a size of 500 μm with a maximum particle size of 100 μm, the next one 2.5 mm with a maximum particle size of 500 μm. Another level is 12.5 mm and the final one is a bit larger than 62.5 mm to be able to accommodate the largest aggregates of size 19 mm (this results in a domain size of 95×95×95 mm^3).

Spherical aggregates are generated numerically to reproduce the sieve curve distribution. Spheres are randomly distributed in a 3D domain. A truncated normal distribution of aggregate sizes is used to interpolate between each sieve value. The process of particle generation and placement stops when the required volume fraction of aggregates, V_{agg} is reached.

Particle generation starts at the largest sizes of the sieve curve (i.e. between 16 mm and 19 mm in this study). The particles are generated one by one. Each aggregate particle is assigned to the appropriate spatial scale level (see Figure 3-23).

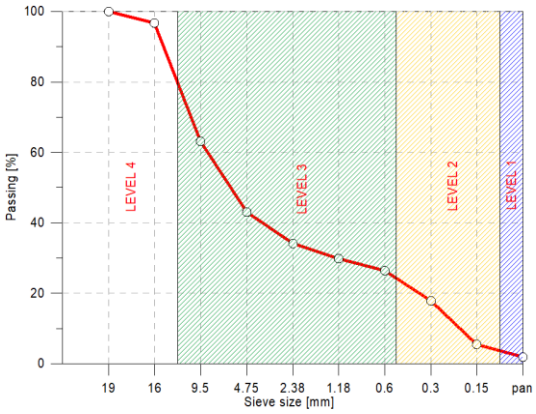

Figure 3-23 - Sieve curve and spatial levels.

The level 4 is the “concrete” level. When the particle is assigned to level 3, it is assumed, that the same particle will be in each of the virtual smaller cubes in a larger domain. By summation of all aggregate volumes, we can reconstruct the sieve curve, which is shown in Figure 3-24.

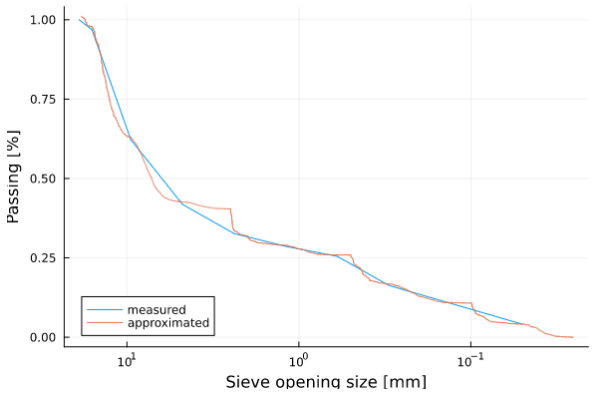

Figure 3-24 - Comparison between measured and numerically generated sieve curve.

Figure 3-25 shows the effective Young’s modulus of leached concrete as a function of mass % of Ca leached. The model shows that the effective modulus reduces by approximately 30%, 60% and 70% when CH, LD C-S-H and HD C-S-H are fully leached, respectively. This is a significant loss of effective modulus. Although direct comparison of the results is difficult due to a lack of literature data, at least, the trend can be compared based on analytical homogenization on similar cement carried out by Heukamp (2003) on mortar. They report 16% and 80% reduction in the effective modulus when CH and C-S-H are fully leached, though within the same order of magnitude, deviates from this study because the material used here is a concrete.

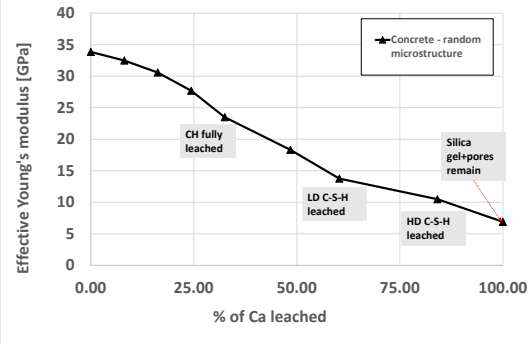

Figure 3-25 - Young’s modulus of concrete as a function of mass % of Ca leached.

To summarize, chemo-mechanical models based on first principles are very scarce. The chemical evolution of materials has been modelled at the cement paste scale because cement paste is the reactive part of a concrete. The cement paste evolution has been set by the indicator that describes the state of the evolution. In the case of leaching, this indicator was expressed in terms of % of calcium leached. Two approaches of the microstructure leaching were tested; random leaching, where the leaching is not done in the physical way, but as a probability that depends on the vicinity of the solid node to the liquid one. Another way is through the simulation of physical processes using the lattice Boltzmann method. For each selected state of material leaching, numerical homogenisation has been performed in order to obtain elastic properties (Young’s modulus). Upscaling to concrete has been done by numerical implementation. A model has been developed that reproduces the actual sieve curve of the experimental concrete. The upscaling of mechanical properties has been done step-by-step for specific parts of the sieve curve. Finally, the mechanical properties of concrete were obtained that agree well with the experimentally measured values.

From the two approaches of leaching, we have observed similar results related to the mechanical properties. This explains why analytical homogenization techniques are generally successful in estimating the effective properties such as elastic modulus, diffusivity and conductivity, where RVE exists.

3.2.3 Introduction to a chemo-hydro-mechanical model capable of handling fracture propagation in porous media

The investigations of UFZ revolves around the utilization of a fully coupled chemo-hydro-mechanical (CHM) variational phase field model. This model is designed for simulating fracture initiation and propagation, considering chemical reactions in cementitious systems. The integration of three key subprocesses– *reactive transport*, *fluid flow in porous media*, and *mechanical deformation of fractured porous media*– is achieved using a variational phase-field approach in a staggered manner.

The staggered approach enables us to skip subprocesses (such as running a chemo-mechanical benchmark by excluding fracture propagation) when unnecessary and conduct benchmarks for each pair of subprocesses to verify the implementation through classical benchmarks. Additionally, recognizing the computational challenges associated with fully coupled models, our code is fully parallelized to optimize efficiency and address the high computational cost involved.

Notably, this numerical model was implemented within the OpenGeoSys research software platform (www.opengeosys.org) as detailed by Bilke et al. (2019).

The implementing and modelling approach used in the MAGIC WP is described in detail in the deliverable D16-8.

Results of numerical simulations

To ensure the correctness of our implementation, we have established a series of benchmarks to assess the coupling between different processes:

- Hydro-Mechanical coupling (consolidation benchmark)
- Hydro-Phase Field (fluid flow in fracture benchmark)
- Reactive transport
- Evaluating the impact of changes in porosity on mechanical deformation (degradation)
- Investigating the effect of changes in effective diffusion in the presence of fractures and changes in porosity

In the consolidation benchmark (Wang, 2000), our goal is to validate the hydro-mechanical code by applying a load to a soil sample. Therefore, we skipped the reactive transport process and phase field. As excess pore pressure dissipates through drainage, effective stress increases, causing soil particles to compact and resulting in greater soil settlement. We compare our results with the analytical solution proposed in the literature at various time steps (Figure 3-26 and equations 1,2,3).

(a)

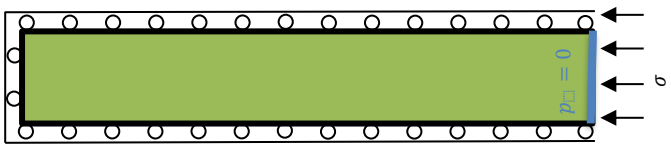

(b) (c)

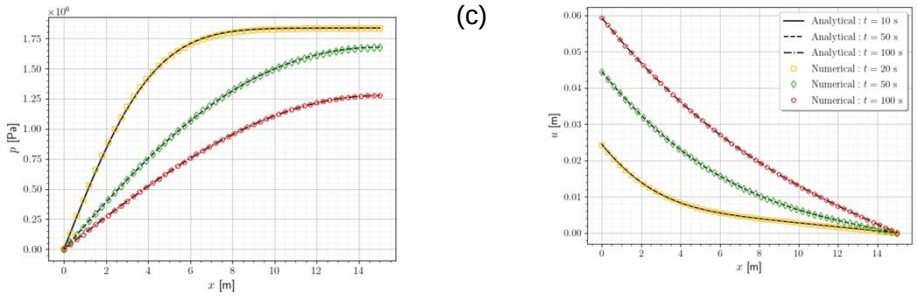

Figure 3-26 - (a) Schematic view of consolidation benchmark (reactive transport and phase field are skipped). Comparison of numerical and analytical solutions for (b) pressure and (c) displacement along the sample at different times.

$$p(x,t) = \frac{4d\sigma_x}{\pi}\sum_{m=0}^{\infty}\left[\frac{1}{(2m+1)}exp\left(\frac{(2m+1)^2\pi^2}{4L^2}ct\right)\sin\left(\frac{(2m+1)\pi}{2L}x\right)\right] \quad 1$$

$$u(x,t) = c_m d\sigma_x\left[L - x - \frac{8L}{\pi^2}\sum_{m=0}^{\infty}\left[\frac{1}{(2m+1)}exp\left(\frac{(2m+1)^2\pi^2}{4L^2}ct\right)\cos\left(\frac{(2m+1)\pi}{2L}x\right)\right]\right] + b\sigma_x(L-x) \quad 2$$

Hydro-Phase Field (fluid flow in fracture benchmark)

This benchmark aims to validate fluid flow within a fracture (Yang, 2018) by assessing the hydro-phase field implementation in the code. Therefore, we skipped the reactive transport and mechanical deformation processes. The sample contains a pre-existing crack, and our goal is to determine the pressure distribution along this fracture. The obtained results are then compared with analytical solutions (Figure 3-27).

$$\frac{p(x,t)}{p_0} = 1 + \frac{4}{\pi}\sum_{m=0}^{\infty}\left[exp\left(-(2m+1)^2\left(\frac{t_D}{4}\pi^2\right)\cos\left(\frac{(2m+1)\pi}{2}\zeta\right)\frac{(-1)^{m+1}}{2m+1}\right)\right] \quad 3$$

(a)

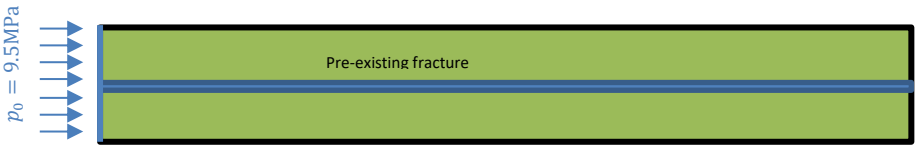

(b)

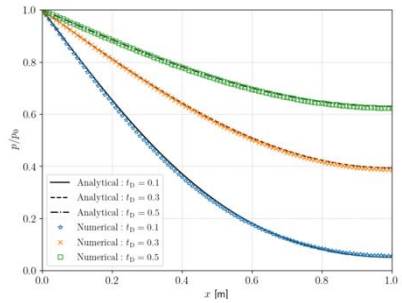

Figure 3-27 - (a) Schematic view of consolidation benchmark (reactive transport and mechanical deformation are skipped). (b) Comparison of numerical and analytical solutions for pressure along the fracture at different times.

Reactive transport

This benchmark investigates the dissolution of calcite due to changes in the porosity and permeability of a layered column containing calcite exposed to sulphuric acid, inspired by Renchao Lu (Lu et al., 2022). The experimental setup comprises a porous column with three distinct layers, where only the middle layer consists of calcite (Figure 3-28). The calcite particles within this interlayer undergo dissolution reactions, as represented by the chemical equations:

$$CaCO_3(s) + H^+ \rightleftharpoons Ca^{2+} + HCO_3^-$$

$$HCO_3^- + H^+ \rightleftharpoons H_2CO_3^*$$

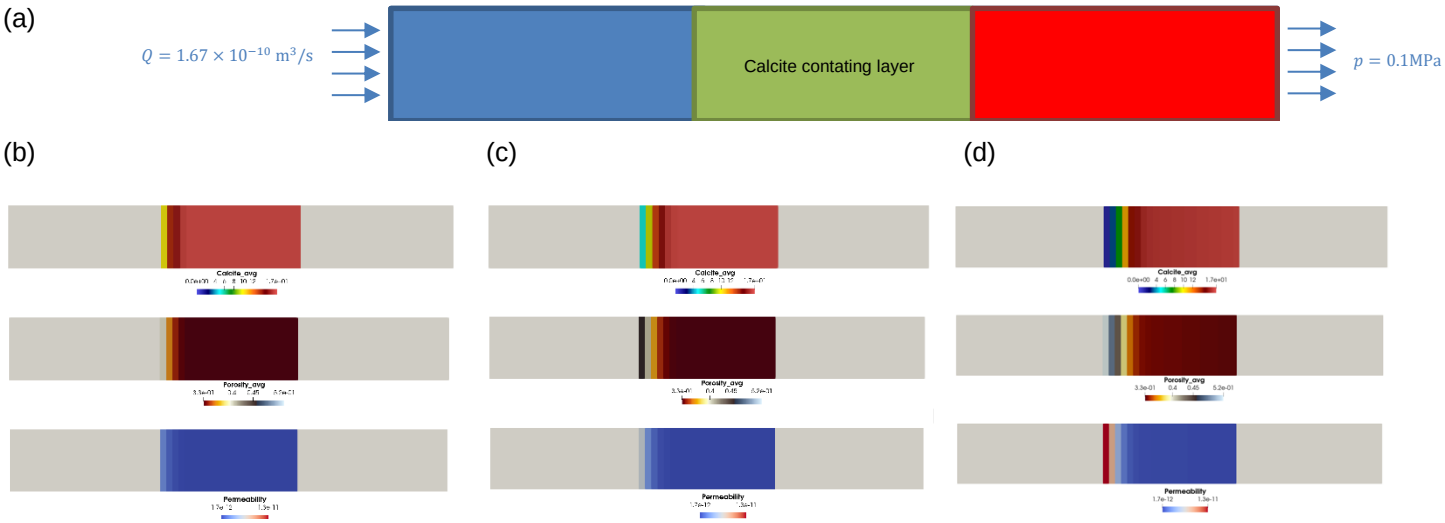

Figure 3-28 - (a) Schematic view of reactive transport for dissolution at the interlayer (the mechanical deformation in fractured porous media is skipped). (b), (c), and (d) depict profiles of calcite, porosity, and permeability at different times.

Evaluating the impact of changes in porosity on mechanical deformation (degradation)

In this study, UFZ aimed to examine alterations in the compression behaviour of a sample following dissolution and investigate the associated chemo-mechanical effects (Figure 3-29). Our experimental approach involved subjecting an intact specimen containing calcite to compression loads while concurrently initiating calcite dissolution based on specified reactions detailed previously.

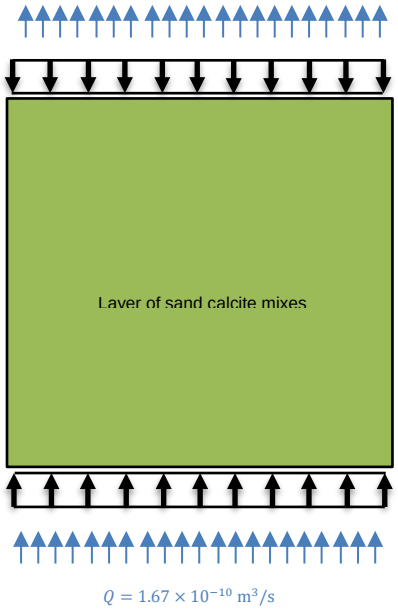

(a)

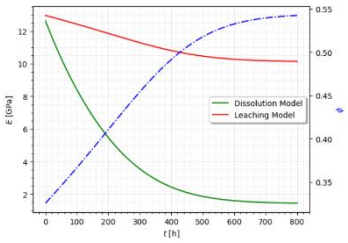

(b)

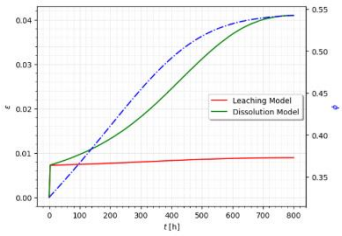

(c)

(d)

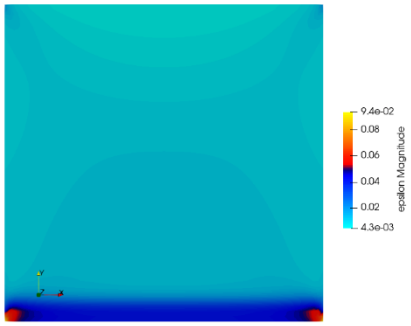

(f)

Figure 3-29 - (a) Schematic view of the chemo-mechanical benchmark. (b) Young's modulus and (c) strain at different times for leaching and dissolution models at the observation point near the bottom edge. Strain profiles for (d) leaching model and (f) dissolution models after 800 hours.

Investigating the effect of changes in effective diffusion in the presence of fractures and changes in porosity

In this benchmark, a saturated sample with fractured edges containing calcite is subjected to a tensile load, leading to calcite dissolution through the injection of sulphuric acid. The main objective of this benchmark is to demonstrate the influence of fractures and variations in porosity on reactive transport processes (Figure 3-30).

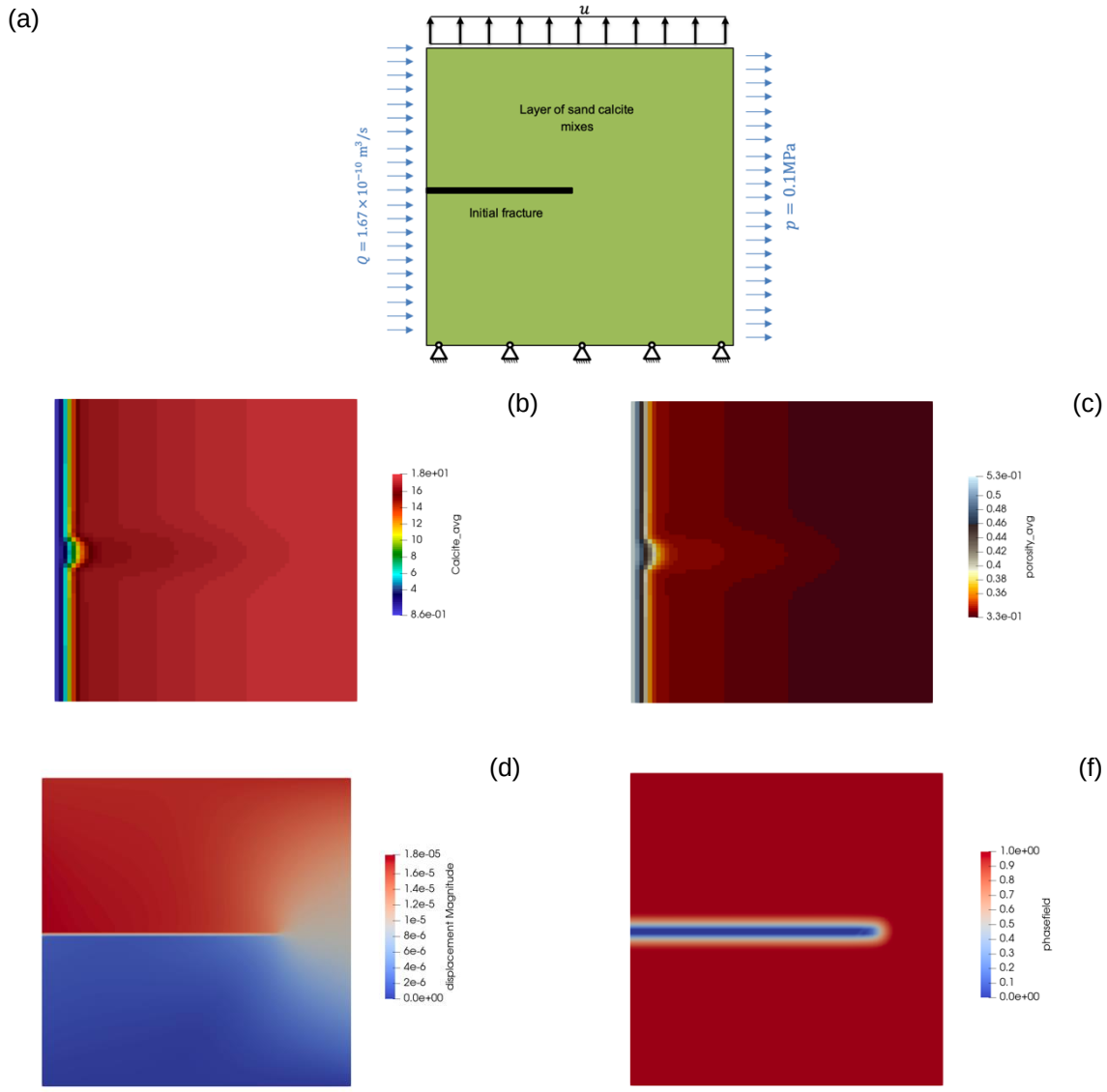

Figure 3-30 - (a) Schematic view of the fracture propagation benchmark under the dissolution of calcite. Profiles of (b) calcite, (c) porosity, (d) displacement, and (f) phase field after fracture propagation due to tensile load.

To summarize, the work of UFZ makes a substantial step forward in chemo-mechanical modelling with the introduction of a fully coupled model that systematically investigates the influence of dissolution on mechanical deformation. This model not only accounts for mechanical aspects but also adeptly manages both fracture initiation and propagation. Through this research, UFZ aim to offer valuable insights into the complex processes associated with dissolution, with a specific focus on highlighting the interplay between chemical reactions and mechanical behaviour.

4. Microbial activity evaluation and potential impact on the concrete chemo-mechanical evolution

This part discusses the effect of microbial activity on the degradation of cementitious material and the precipitation of mineral phases as well as its impact on the concrete chemo-mechanical behaviour. Changes in chemical, hydraulic and mechanical properties are monitored for sterilised samples and samples exposed to micro-organisms. The conditions studied are, for a part, the same as in the part 2 and 3, i.e. the effect of percolation or contact with water (multi-ionic chemical attack) or slurry representative of the deep geological disposal environment. One part also concerns the chemo-mechanical stability of concrete in consideration of the microbial activity under aerobic and anaerobic conditions.

4.1 Microbial impact in artificial ageing conditions

Artificial ageing conditions due to salt water and microbial attack on old samples

The objective in a study of the Duch concept performed by SCK CEN together with COVRA and FZJ, is to identify the anaerobic and aerobic microbial influence on the chemo-mechanical behaviour of concrete and self-sealing of concrete. The backfill concrete was expected to have sufficient large pores for microbial activity inside the concrete specimen. The backfill samples made with Ordinary Portland Cement (OPC, CEM I) were envisaged to be exposed to an aerobic environment for this microbial activity. An anaerobic environment was expected for backfill samples made with OPC (20-34 wt%) blended with Blast Furnace Slag (BFS) (66-80 wt%) i.e. CEM III/B. BFS has traces of iron sulphides by which the concrete pore water is reducing after manufacturing. Carbon steel embedded in grouts made with cements blended with BFS have been shown to achieve instantaneously passive corrosion while it may take some time to achieve passive corrosion for carbon steel embedded in grouts made without BFS (Atkins et al., 1991). In total, there were 3 series of backfill samples: one series made with CEM I and two series made with CEM III/B. The porosity was determined for one backfill series made with CEM III/B: 20-21% capillary pores and 24-25% total porosity.

As mentioned in Part 2.1.1 about carbonation, buffer-like concrete was made with CEM III/B. The porosity for buffer-like concrete made with CEM III/B was 12-13% (only capillary pores). The buffer-like concrete was expected to have a too small size of pores to allow microbial activity inside the concrete specimen. Indeed The range in diameters of microbes is between 0.2 µm and 2 µm. Manufactured concrete can also have pores with a maximum in diameter till 50 nm. A maximum in 100 nm (0.1 µm) is not uncommon for concrete by which it can also be assumed that the potential microbial activity is limited due to space restriction. Later, also a buffer-like concrete specimen made with CEM III/A (a blend of OPC (35-64 wt%) and Blast Furnace Slag (36-65 wt%)) was investigated. This specimen was manufactured in 1993. Cubical samples with an edge of 5 cm were submerged in synthetic clay pore water in 1.5 l boxes.

Included in this part are only the results concerning the microbial activity, the results concerning the chemical and mechanical evolutions of concrete being described in parts 2 (for unsaturated conditions) and 3 (for saturated conditions).

A microbial community was present in the water and also on the concrete cubes (Figure 4-1).

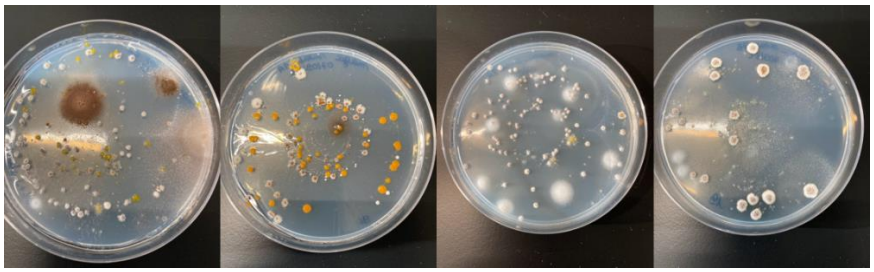

Figure 4-1 - Example of different colonies from the water samples grown on R2A agar plates in aerobic conditions.

To obtain proper abiotic controls, samples were irradiated prior to the test, which was shown to not negatively affect the mechanical strength of the concrete cubes. After 1.5 year, the number of viable cells on the concrete cubes increased, putatively indicating that the microbial community could form a biofilm on the concrete. In addition, we also tried to explicate the origin of the microbial community by studying the water from large boxes with concrete samples (water to which certified[2] concrete samples made with CEM III/B were exposed and water to which not-certified concrete samples were exposed made with CEM I & CEM III/B), which was taken to prepare the samples used during this project, tap water and sand to prepare the concrete cubes. The water in the small boxes is fundamentally the same as the water taken from the large boxes with certified or not-certified specimens. However, the microbial community seems to be more abundant and active in the small boxes. This suggests the presence of a factor that enhances the microbial community in the smaller containers. 16S rRNA amplicon sequencing demonstrated a very diverse microbial community in the samples, which is different from the one in the sand used for the concrete samples (Figure 4-2).

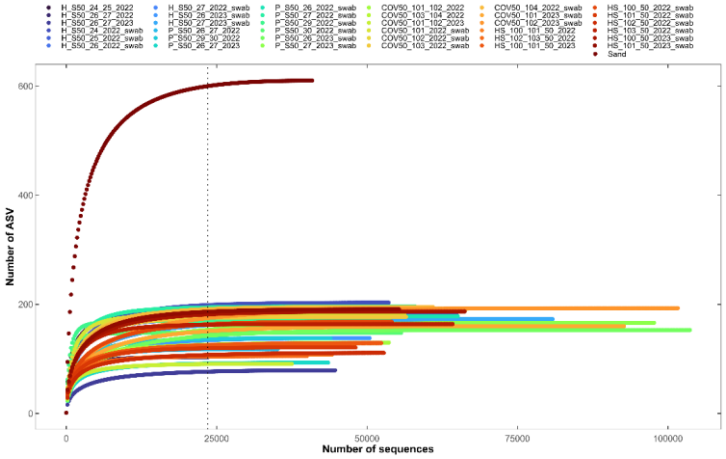

Figure 4-2 - Rarefaction curves for the16S rRNA gene amplicon sequencing data showing for each sample the number of OTUs in function of the number of reads. The dashed line represents the number of subsampled reads.

Differences are observed between the certified and non-certified samples, but more research is needed to explain the observed differences. In this study the key results are:

[2] Certified concrete has achieved the requested strength after 28 days hardening and the samples have a sufficient small range in density and strength to obtain a moisture storage capacity of the manufactured concrete. Not-certified concrete if not all samples have achieved the requested strength, the range in density and strength is to large obtain a moisture storage capacity from water retention curves.

- In all samples an active microbial community was present and viable cells were detected and isolated from all water samples and concrete cubes. Sterilization of the water and concrete specimens was needed in order to obtain sterile environment. This sterilization was performed with gamma-radiation till a dose of 57.6 kGy (dose rate 6.4 kGy per hour) had no impact on the mechanical strength of concrete.
- One sample (COV50_101_102; buffer-like concrete made with CEM III/B) was also positive for Sulphate Reduce Bacteria (SRB).
- The number of viable cells on the concrete cubes increased in all 4 samples during the 1.5 years.
- While the total number of microbial cells in the small boxes was comparable to that in the large boxes from which the samples were derived, microbial activity was on average at least 5 times higher in the smaller boxes.
- 16S rRNA gene amplicon sequencing indicated the presence of a diverse bacterial community in all samples.
- The microbial community evolved during the 1.5 years incubation and differences in the relative abundance of specific genera were observed both in the water and on the concrete cubes.
- The microbial community in samples originating from certified specimens (all made with CEM III/B) were different compared to those originating from not-certified specimens made with CEM I and CEM III/B.

Artificial ageing to mimic the Czech disposal conditions with microbial attack

As for the previous study, the Czech group results about the chemical and mechanical properties are discussed in Parts 2 and 3.

Regarding the Czech experiments, it seems it is mainly the water (at different conditions of exposure: air humidity, continuous water flow or water suspending clay) that determines the fate of exposed LPC samples. The metabolic activity of microorganisms is above all driven by and dependent on the presence of water. Here we showed that the environmental microbial load designated the colonization of the LPC "nude" samples and was represented by mixed microbial communities with dominant heterotrophic species in all three environments – air, water, and bentonite.

The fastest growth of biofilm detected by molecular-genetics methods was detected in water-exposed samples, followed by air-exposed samples. Samples exposed to bentonite could not adopt similar features (Figure 4-3). It was probably the close **contact with bentonite suspension** and insufficient space around the samples that hindered to evolve a rich biofilm.

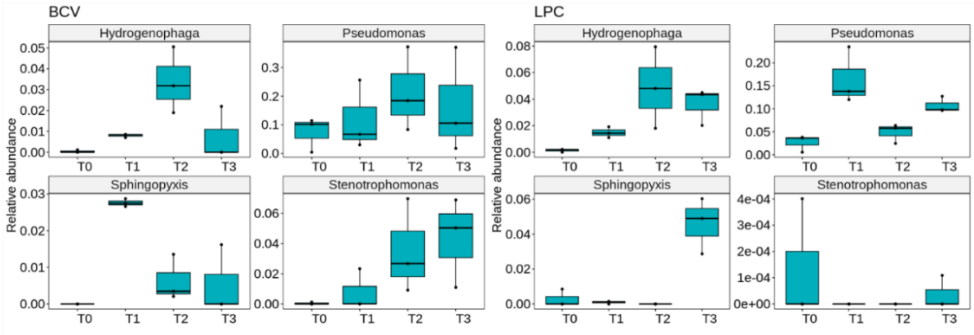

Figure 4-3 - Periodic changes of chosen microbes detected in bentonite (BCV) and in the concrete exposed to the bentonite suspension (LPC).

However, samples in contact with bentonite were the least durable samples indicating that other than biotic factors control the durability of LPC (in contact with bentonite) such as the cation exchange between Mg type bentonite and LPC. The deteriorative effect is relatively strong with microfracture propagation rate of approx. 1 mm per year. Moreover, the cracks formed on the surface layer were not healed despite the proved existence of urease-positive clones in LPC samples. We suggest this might be a result of an insufficient number of nucleation sites due to slow biofilm formation and low availability of water that is taken by bentonite.

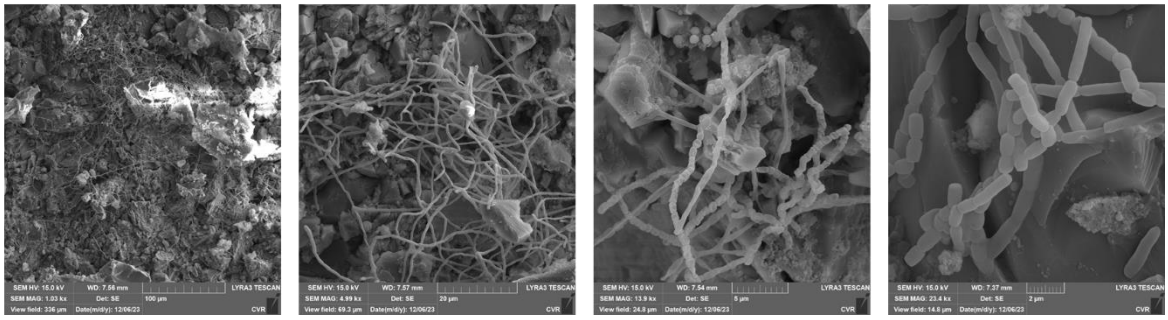

Figure 4-4 - SEM analysis of the biofilm after 1.5 years of exposure under water.

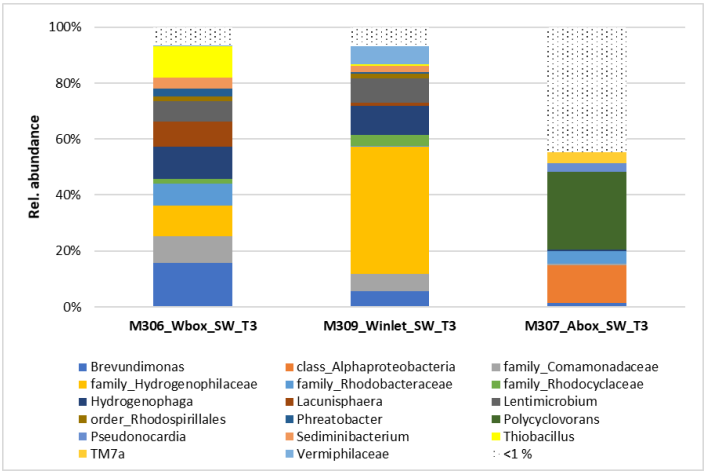

Figure 4-5 - Relative abundance of present microbial communities in the biofilm of water box (1.5-years exposure), the biofilm formed around the inlet tube, and the biofilm of the containers exposed to underground air, respectively.

In **water environment** a different scenario was observed. Rapid and robust colonization of LPC samples in the water first by sulphur-oxidizing bacteria and by heterotrophic bacteria is most probably the reason for both LPC matrix deterioration in the first step and calcium precipitation in the second step resulting in healing of formerly cracked samples (Figure 4-4 and Figure 4-5).

Fast growth of bacteria on the sample surface probably enables to form enough nucleation sites for calcium precipitation under these circumstances (water environment, higher pH, certain bacterial diversity) and calcium being leached out from the cementitious matrix due to contact with the acidic biofilm. This effect was observed only in 6-months-old samples, whereas in 12- and 18-months-old samples the relative crack penetration was low. However, the rigidity of the surface layer in water-exposed samples declined rapidly in time and corresponded to fast outgrowth of surface biofilm. Similarly, the *de novo* crystallization of cristobalite in water-exposed samples after 1.5 years is also most probably microbially induced confirming the important role of bacteria in mineralization but also their potential to change concrete composition and structure.

Air-exposed samples are not in direct contact with water; however, the growth of the biofilm is fast and vigorous and colonize better the interior of the samples (Figure 4-6).

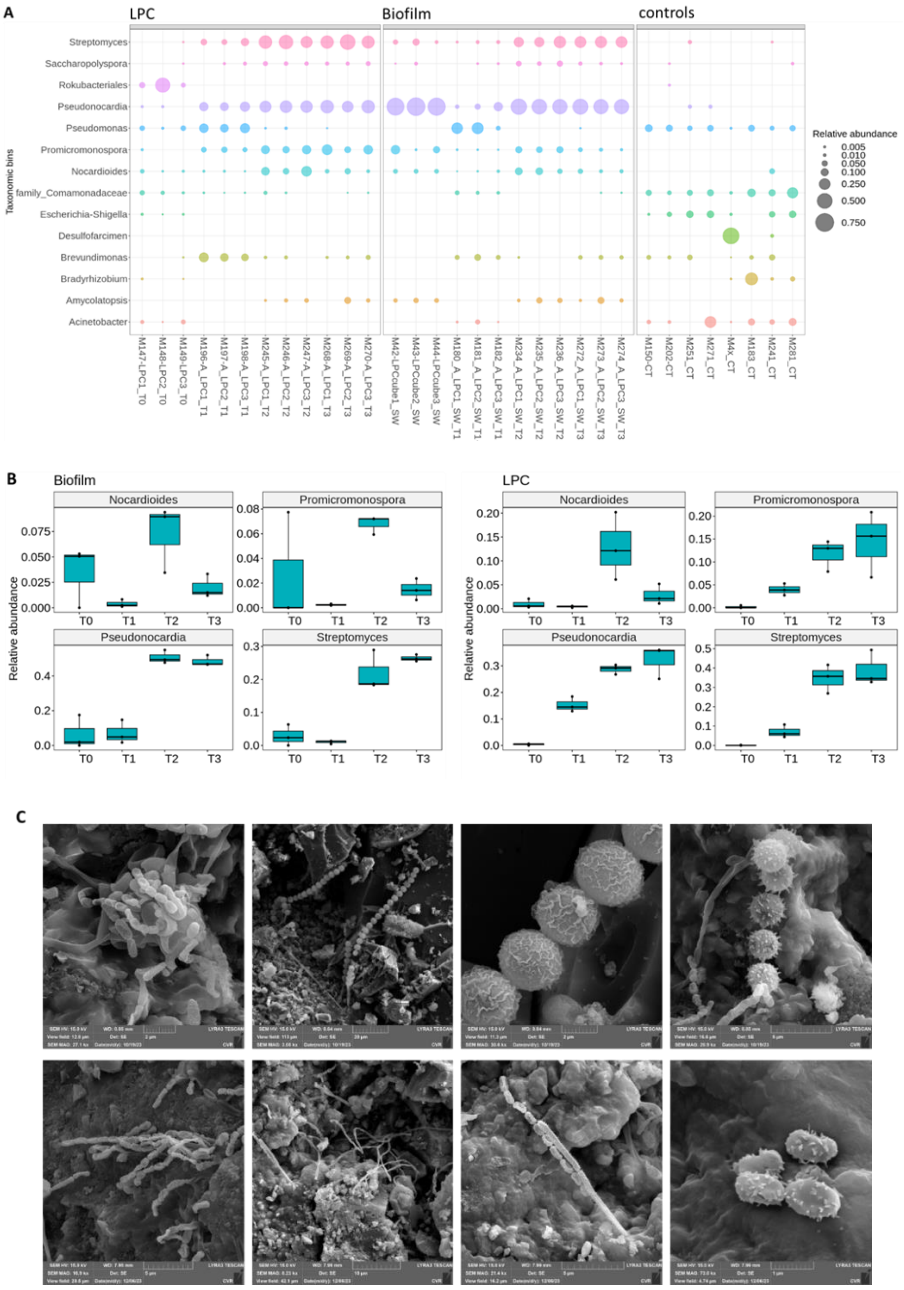

Figure 4-6 - A) Relative abundance (more than >1%) of bacterial genera on surface and interior of SURAO LPC samples exposed to underground air ventilation for 6, 12 and 18 months. B) Periodic changes of chosen microbes detected in and on the concrete exposed to the underground air ventilation. C) Surface SEM analysis of 1 (up) and 1,5-years-old (bottom) samples indicating genus Streptomyces and chains of fungal spores.

Local production of acidic metabolites most probably caused dissolution of calcium from concrete samples and formation of calcium rich layer composed of gypsum and vaterite. The explanation of calcium sulphate precipitation without detection of sulphur-oxidizing species and sulphate present in the surrounding environment is rather speculative suggesting sulphide oxidation as a driving force for primary matter production as observed in early colonizers. This effect would be attributed to the first

stage of colonization of such samples that is in accord of our *de novo* drilled and cut samples. Moreover, the microbially-induced local precipitation of gypsum and vaterite might lead to strengthening of the exposed material despite lowering surface pH likely to reduce partially the concrete strength.

The natural microbial activity coupled with the multi-ionic attack conduct to a degraded/interacted surface significantly affected the total volume of the specimen in comparison to the reference sample stored at relatively dry (laboratory) conditions. Scanning Electron Microscope (**SEM**) analysis of the samples revealed distinct structural changes on the surfaces over time, varying according to the environment. In an air environment, a thin layer of organic products on the surface was observed. In a water environment, there was a penetration of the degradation area into the cement matrix, characterized by a decrease in the amount of calcium and oxygen, indicative of a disruption in the Calcium-Silicate-Hydrate bond. In a bentonite suspension environment, the cement matrix showed an enrichment of magnesium and an increase in crack propagation.

In the case of a water environment, as mentioned in Part 3, the main degradation mechanism is a combination of leaching and carbonation in the second phase due to the absence of portlandite. During degradation, there was a decrease in the amount of oxygen and calcium in the cement matrix forming degradation areas reaching a penetration of over 1 mm (see D16-4). Carbonation degradation without leaching was observed in the air environment, penetrating to a depth of 87 µm, but only after 18 months. The degree of surface degradation of the samples was found to be the lowest in air environments, followed by water environments, with the highest degradation observed in bentonite suspensions.

Microorganisms were detected on the sample surfaces in both water and air environments from the beginning of the exposure period. After 12 months of exposure in the water environment, metabolic products in the form of elemental sulphur (S) were found on the sample surfaces.

Phase composition by XRD showed the presence of gypsum only in air environment. After 18 months, a new phase, indicative of a high-temperature cristobalite phase, was observed on the surface but only in the water environment. This new phase suggests the presence of microbial activity.

Microscale testing by **nanoindentation** is performed on selected intact areas of the cement matrix outside the aggregate area. The results therefore do not significantly take into account the influence of possible micro/macro cracks. The nanoindentation results show a slight improvement in mechanical resistance over time, independent of the environment (see D16-4). This can be explained by the rehydration of the sample after exposing the material during sample preparation from larger cubes (drilling, cutting). However, the resistance is slightly lower in the peripheral regions of the samples. This may be due to microcracks at the surface caused by sample preparation or microcracks/increased porosity caused by development/interaction with the environment.

The **punch test** presented previously in Figure 3-8, is carried out by pressing with punches in the middle of the disc. During compression with the punch, most of the volume of the specimen is thus loaded gradually in tension, in four steps until failure. The result is also influenced by micro/macro cracks, pores, etc.

From the evolution of the load branch directives (rigidity - k2, k4-1, k4-2, k4+), it is possible to infer the increase of plastic deformation at the beginning of the test (decrease of k2 and k4-1 for different periods and environments) while K4-2 and k4+ remain similar or slightly improve (compare to slight improvement of nanoindentation results). This effect is most visible for the aqueous environment, then for the suspension. In both cases, a persistent decrease (0-1.5y) is evident. This is probably due to the evolution of the micro/macrocracks in the sample. The cracks may be essentially unfilled (i.e., with zero mechanical resistance in tension) or filled with secondary fill partly maintaining mechanical resistance. The consequence of crack development and filling should be changes in strength. A significant change (decrease) in strength is observed for the suspension environment. The SEM analysis shows a significant range of unfilled cracks (depth to approx. 1.3 mm from the surface). The pH using the indicator

shows a relatively large area of the sample (surface zone - approx. 1.5-2 mm) with a higher pH for the suspension samples. A similar but lesser effect is observed for the water environment samples (decrease in strength, SEM, pH). Also, the decreasing number of samples from each set that resisted the stresses in each step of the mechanical test (suspension < water < air) correlates with the crack formation and the decrease in mechanical resistance in each environment and time.

Exposure of SURAO LPC samples to different environments showed distinct behaviour in terms of loss of the mechanical strength that can be caused by local pH changes due to cation exchange or **biofilm** outgrowth.

To summarize, we can conclude from these experiments that microbial presence can be either deteriorative or protective depending on the extent of water and local pH changes in environment where heterotrophic microorganisms dominate. Microbial assisted changes seem important in air and water environment while C-S-H to M-S-H chemical conversion is main driving force of negative effects on the contact with bentonite suspension.

4.2 Interaction between low-pH cementitious material and microbes in low-carbon source groundwater

This project conducted by UNIMAN focuses on the colonization of cement by alkaliphilic microorganisms and their impact on the structural properties of the material during geological disposal. The aim was to quantify the impact of microbial colonization, linked to the metabolism of GDF-relevant electron donors and acceptors, on the chemo-mechanical evolution of low-pH cement.

The main objectives of the project are:

- Assess the extent of the impact of microbial metabolism of porewater electron donors and acceptors on the structure and properties of cement in long-term GDF-relevant experiments.
- Develop and apply 3D X-ray CT and 2D-3D image correlation techniques to monitor in situ changes in new experiments designed from knowledge obtained in 1, using appropriate microbial inocula from these experiments.
- Generate data for modelling by other MAGIC partners and further explore possibilities of collaboration, e.g., on the impact of microbial processes on local swelling or other changes in microstructure, and the impacts of these processes on material properties.

4.2.1 The implemented experimental approach and modelling

To fulfil the requisites of low-pH cement, small tablets were cast using a CEBAMA reference mix, containing a pore solution with a pH of around 9. These cement tablets were incubated in a synthetic groundwater, based on the geochemical composition of water extracted from the Oxford clay formation in the East Lincolnshire area. Microcosms were set up in triplicates with different treatments, and Harpur hill sediments, rich in alkaliphilic bacteria, were added. Batches of 30 mL groundwater with 5 g sediment from the Harpur Hill high pH GDF analogue site, were dispensed into 50 mL capacity serum bottles. 20 mM of nitrate was supplemented to each of the bottles as an electron acceptor. In one of the sets, 15 mg/L yeast extract was incorporated to represent the low levels of organics typical of deep groundwater, while hydrogen was purged every 15 days, serving as the electron donor in the system. The other set contained no added carbon, which served as negative control. Concurrently, positive control microcosms containing 15 mM sodium lactate as both an electron donor and carbon source were set up. Parallel experiments devoid of nitrate were also conducted as controls for all three sets. The microcosm treatments were autoclaved at 120°C for 20 minutes to ensure the sterilization of the system before adding the inoculum. To observe changes over a long time, they were incubated for 6 months at 20°C.

At 15-day intervals, 1 mL aliquots were extracted from each setup for subsequent analyses, including IC (ion chromatography) and ICP-OES (inductively coupled plasma optical emission spectrometry), pH determination, and 16S rRNA gene analysis. One cement tablet from each setup was also taken out after one, two, three, and six months. The cement tablets from different induction periods and treatments were compared using SEM for 2D imaging and µ-XCT for 3D imaging analysis.

4.2.2 Main results

The work of UNIMAN showed that lactate in the high carbon source system with added nitrate (GLN) was degraded to acetate with a pH drop from 10 to 9.0 in 6 months. This was accompanied by a decrease in the concentration of nitrate, which was reduced to nitrite (Figure 4-7).

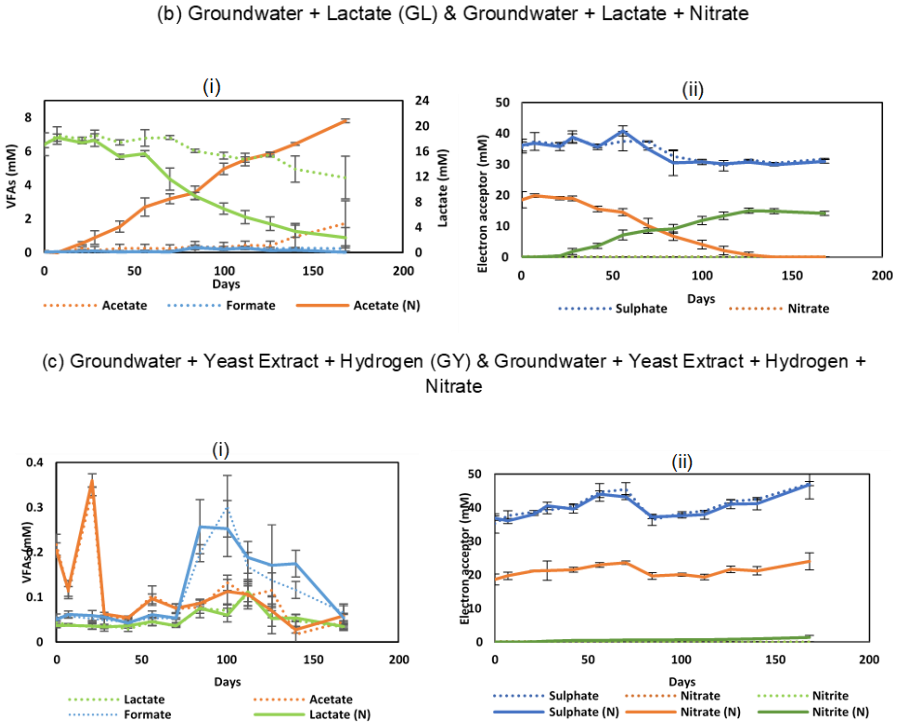

Figure 4-7 - VFAs concentration and electron acceptor (sulphate, nitrate, nitrite) concentration for (ai & aii) Groundwater & Groundwater + Nitrate (GN), (bi & bii) Groundwater + Lactate (GL) & Groundwater + Lactate + Nitrate (GLN), (ci & cii) Groundwater + Yeast extract (GY) & Groundwater + Yeast extract + Nitrate (GYN) treatment of microcosm. For GL & GLN system, two axes represent lactate, which decomposes in acetate. The dotted line (….) represents no-nitrate, and the solid line (------) represents the nitrate system.

Multi-technique analyses provided evidence that microbial carbon metabolism underpinned the reaction between carbonate and Ca^{2+}(aq) to form calcite and aragonite precipitates, which contributed to crack sealing. Pore size distribution and pore counts for this system also decreased significantly (Figure 4-8). In comparison, for the low carbon system with nitrate (GYN), there were very minor changes in measured VFAs and nitrate values, suggesting minimal nitrate reduction by the microbes. Interestingly, there was an increase in the calcium, magnesium, and sodium concentrations, which might be leached from the cement surface over time. However, 2D-3D images showed no significant change in pore size distribution or pore counts over 6 months in the low-carbon GYN system (in contrast to the GLN experiments).

a) Groundwater + Lactate (GL)

b) Groundwater + Lactate + Nitrate (GLN)

c) Groundwater + Yeast extract (GY)

d) Groundwater + Yeast extract + Nitrate (GYN)

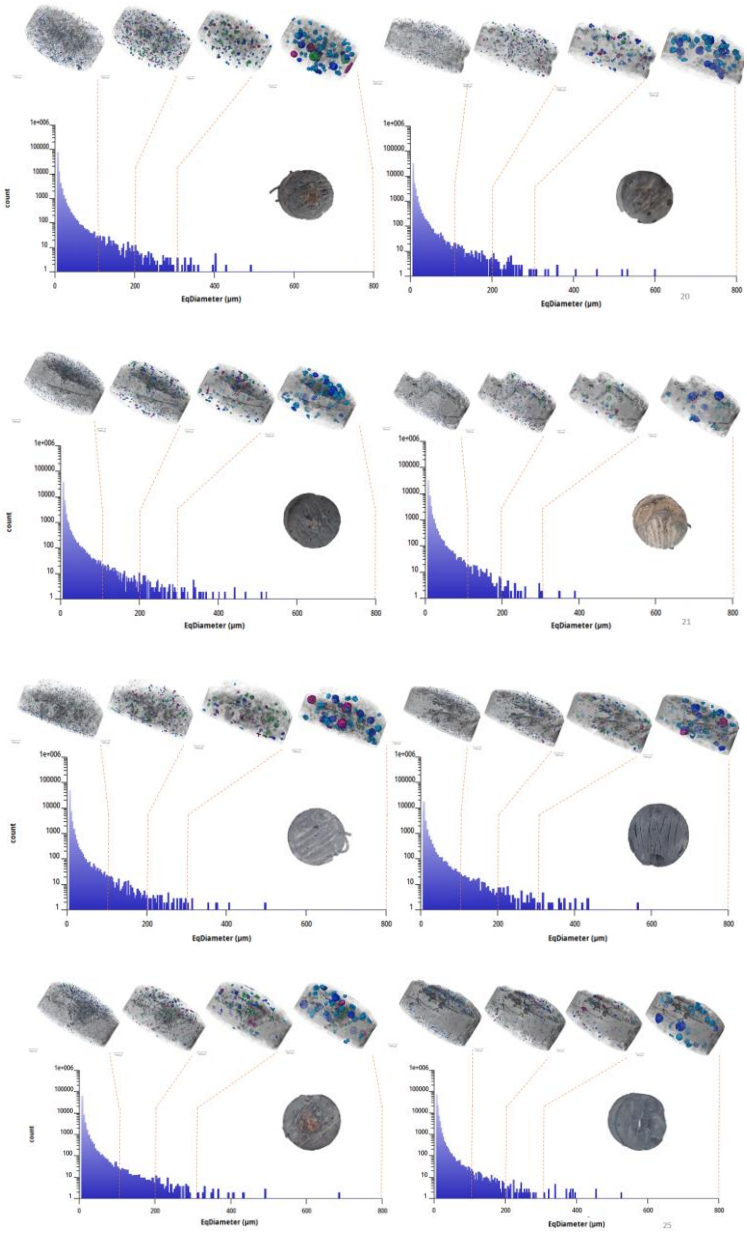

Figure 4-8 - 1- and 6-month 3D XCT image and semi-log graph of pore diameter v/s count for (a) groundwater + Lactate (GL), (b) Groundwater + Lactate + Nitrate (GLN), (c) groundwater + Yeast extract (GY), and (d) Groundwater + Yeast extract + Nitrate (GYN)

Overall, this work provides evidence that bio-mineralization of calcite was prominent in the higher carbon GLN experiments, but very little microbial activity was observed in the lower carbon GYN system. There was no sign of biodegradation of cement for both systems. Microbial community analysis by 16S rRNA gene sequencing is ongoing to give a more holistic analysis of the system, highlighting key organisms and processes that may have promoted biomineralization in the higher carbon experiments. Additional tests are planned to identify impacts on the structure of the cement, including quantifying changes in water absorption capabilities in the treated samples by high-resolution XCT scanning. Future work could include follow-up longer-term studies using appropriate groundwaters, ideally in situ, dissected using the cross-disciplinary approach used in this study to discuss cement-microbe interactions.

In the context of a geological disposal facility (GDF), the pH of the cement and surroundings is anticipated to decrease with time. Starting with low-pH cement as material ensures that the environment would be analogous and relevant to the aging concrete. Over time groundwaters will saturate the cement barriers and other cementitious structures in the GDF, and these groundwaters may deliver trace nutrients and carbon, which the dormant microbes could use to grow in the alkaline environment of cement structures.

Using relevant electron donor, electron acceptor, microbial inoculum, and groundwater recipes in this project, our data suggest microbial degradation of low pH cement under GDF-relevant conditions is not expected over the time periods studied. Furthermore, under conditions where microbial activities were accelerated by the addition of higher levels of electron donor (lactate) and acceptor (nitrate), biomineralisation of carbonate minerals is feasible, potentially leading to crack-healing and cement repair.

4.3 Microbially induced alteration of cement phases with natural waters

The scope of this study was the microbial impact on the chemo-mechanical evolution of CEM I and/or low-pH hardened cement paste exposed to calcareous solution in batch experiments. These experiments are analogous to the abiotic experiments performed by IRSN in the Tournemire site (results exposed in 3.1), an underground research laboratory in argillite in the southeast of France to support the expertise on geological disposal of radioactive waste.

4.3.1 The experimental approach

These batch experiments were carried out with microorganisms, which are present in the natural calcareous waters. To stimulate microbial activity a suitable carbon source was added for appropriate/selected experiments. The microbial diversity in the calcareous waters was identified and monitored by culture-independent methods. The dissolution of the cementitious phases was monitored by performing ICP-MS and IC analyses in regular intervals (all geochemical data are given in deliverable D16-4). Surface topography evolution and surface rate quantification were performed using a combination of surface-sensitive methods, including µCT. In addition, the incubated cementitious materials were analysed regarding their mineralogical composition (SEM/EDS) by IRSN.

4.3.2 Main results

Geochemical evolution

The pH of the natural groundwater from Cernon (n=2) was 7.80±0.28, containing 7.4±0.39 mg/l of sulphate, 1.5±0.45 mg/l of nitrate, 4.7 mg/l of total nitrogen (TN), 4.9±0.84 mg/l of total organic carbon (TOC), and 41.2±5.72 mg/l of total inorganic carbon (TIC). This indicates that there are electron acceptors for anaerobic microorganisms (nitrate and sulphate) and for aerobic microorganisms (oxygen) available together with electron donors (TOC and TIC) as carbon source. On the other hand, Ca, Mg, Na and Si accounted for the most abundant elements (>1000 µg/L) in the fresh groundwater. Other minor elements, including K, Zn, Fe, Ni, Cu and U were also quantified via ICP-MS.

During the 3 months of incubation, we observed that the content of TN and nitrate in each collected water samples under both conditions were largely decreased to undetectable level with IC comparing to fresh natural groundwater, whereas the sulphate concentration in each collected water showed the opposite trend. Moreover, the TOC content in microcosms with 2 mM of lactate in the collected water samples ranged from 38.5 to 80.1 mg/l. However, the TOC content in microcosms without additional lactate was 2 to 5 times greater than that in fresh natural groundwater. The increase of TOC content in these microcosms may resulted from the dissolution of carbon from cement samples into water or from the microbial activities stimulated by addition of lactate. The evolution of TIC content in both incubations

was consistent, decreasing until 41 days of incubation and afterwards increasing to 44.3±0.64 mg/l and 48.9±0.57 mg/l in microcosms without lactate and with additional lactate, respectively.

Changes in the elemental composition in collected water samples were also observed (data not shown). The concentration of Ca and Mg in the fresh natural groundwater samples were 81250±7141.8 µg/L and 17600±1697.1 µg/L, respectively. Their concentration greatly decreased in water samples collected after 20 days of incubation but gradually increased afterwards. Conversely, the concentration of K largely increased to 5950±2192.0 µg/l and 13200±989.9 µg/l in microcosms without lactate and with additional lactate, respectively, after 20 days of incubation and decreased afterwards. Similar observations were made for Si contents. The concentration of Ba in freshly collected groundwater was 4.0±0.65 µg/L and gradually increased in waters of microcosms under both conditions. The concentration of Na also gradually increased due to the addition of 2 mM of sodium lactate.

Microbial diversity analysis of water and cement samples

The microbial diversity of fresh natural groundwater collected in 2022 and 2023 showed different dominant bacterial genera (relative abundance > 10%). Pseudomonas and Rhodoferax are the major genera in groundwater collected in 2022, whereas in groundwater collected in 2023, Hydrogenophaga, Alkanindiges and Rhodoferax are predominant. Overall, up to 240 and 85 genera were identified in groundwater communities from 2022 and 2023, respectively. This indicated that the microbial communities of natural groundwater are highly diverse but various at different times.

Water samples were collected from microcosms (number 2 & 3 with natural groundwater, and number 6 & 7 with groundwater plus additional lactate) on the 20th and 41st days of incubation, together with fresh natural groundwater to compare microbial community changes. The biomass recovered from cement samples (incubated for 86 days in both conditions) was also subjected to microbial diversity analysis. Proteobacteria was the most abundant phylum in all microbial communities from water samples and cement surfaces, followed by Bacteroidota, Patescibacteria and Cyanobacteria in certain water communities.

Moreover, we observed that the gammaproteobacterial Pseudomonas largely enriched (up to 53.8%) in water communities incubated for 20 days under both conditions, except for the water from one microcosm with additional lactate (W7_20d), which was dominated by a unidentified gammaproteobacterial genus (see details about sampling code in latest MAGIC deliverable D16-4, Figure 4-9A). However, microbial communities in water samples from 41 days incubation under both conditions were dominated by Alphaproteobacteria with relative abundance >50% except for one microcosm with natural groundwater (W2_41d) (Figure 4-9B). Furthermore, the alphaproteobacterial Azospirillum, Magnetospirillum and Caulobacter were the most abundant taxa across all samples with various relative abundance (Figure 4-9B). On the other hand, gammaproteobacterial Dechloromonas was the major genus in a microcosm with natural groundwater (W2_41d), whereas in microbial communities from water samples with additional lactate, an unidentified gammaproteobacterial genus represented the majority (Figure 4-9A). Interestingly, gammaproteobacterial Pseudomonas dominated all microbial communities of the surface of cement samples despite the difference of the groundwater conditions (Figure 4-9A). However, variances were also observed in microcosms under the same conditions. For example, in the microcosms (number 2 & 3) incubated with natural groundwater, the abundance of Acinetobacter on one of the cement surfaces (C2_86d) reached 51.6% but its abundance in another cement sample (W3_86d) was <1% (Figure 4-9A). A similar observation was made for alphaproteobacterial Sphingobium on one of the cement surfaces (C3_86d) (Figure 4-9B).

Altogether, we observed a pattern of dominant bacterial genera in the microbial communities of the water samples and cement surface based on different incubation times but the conditions of groundwater appeared to have minor effects on the microbial communities.

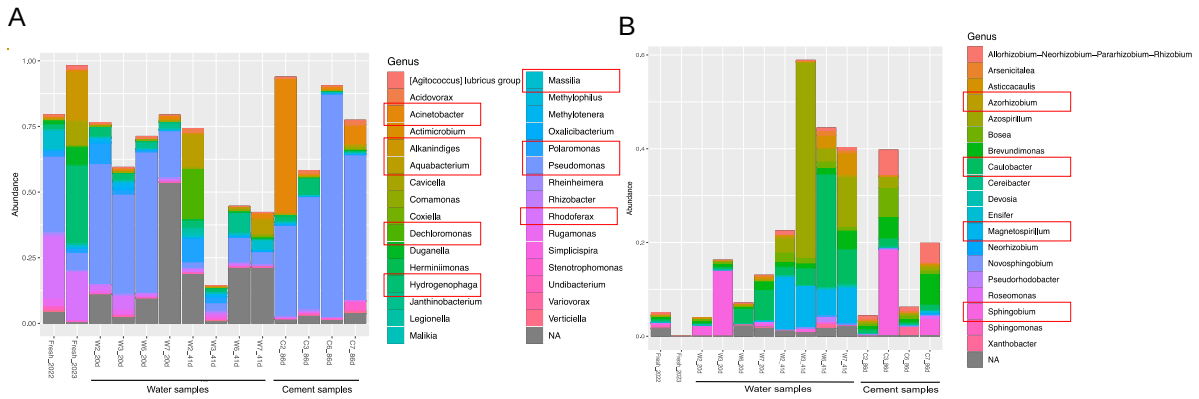

Figure 4-9 - Microbial diversity of fresh natural groundwater collected in 2022 and 2023 (Fresh), water samples from 20 and 41 days of incubation with natural groundwater (W2 & W3), and with groundwater and additional lactate (W6 & W7), and surface of cement samples incubated with natural groundwater (C2 & C3), and with groundwater and additional lactate (C6 & C7) for 86 days at genus level of Gammaproteobacteria (A) and genus level of Alphaproteobacteria (B). The red boxes highlight the dominant or common microbial taxa in all communities.

Microbial colonization on cement surface

By using SEM, bacterial shape-like aggregation associated with extracellular polymeric substances (EPS)-like structure were observed on the surface of a cement sample that was incubated in microcosms with additional lactate for 3 months. Instead of an EPS-like structure, we observed irregular spikey shapes of precipitation on the surface of the cement sample incubated with natural groundwater for 3 months (Figure 4-10).

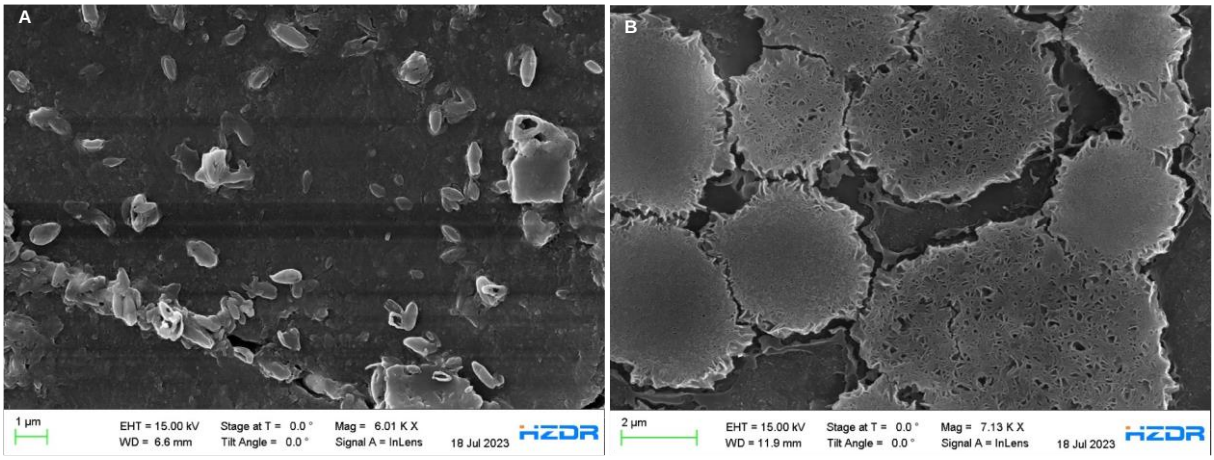

Figure 4-10 - Scanning electron microscopic images of surface structures from cement samples incubated with groundwater supplied with 2 mM of lactate (A) and natural groundwater (B) for 3 months.

Analysis of the cement surface

Previous work was conducted on industrial low-pH concrete and cement paste immersed in solution (Neji et al., 2023), reporting that when the porosity is low, a layer of calcium carbonate precipitates at the interface, limiting the degradation mechanisms. Here, our EDS-SEM analysis showed a calcite layer on the surface of each sample incubated in different conditions of groundwater (Figure 4-11). Moreover,

no gradient degradation was observed, suggesting a clogging effect due to calcite precipitation that limits the leaching of species from the sample.

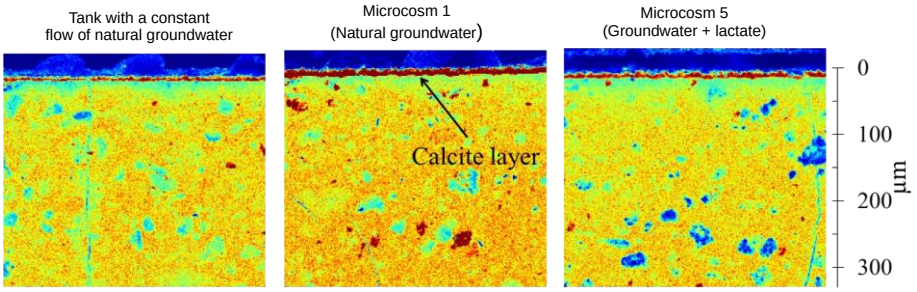

Figure 4-11 - EDS mapping for calcium content of low-pH cement samples incubated in a tank with constant flow of natural groundwater, in a microcosm with 300 mL of natural groundwater, and in a microcosm with 300 mL of groundwater supplied with 2 mM of Na-lactate. The rainbow colormap denotes the high content (red) and low content (blue) of calcium.

The XRD analysis further confirmed the calcite precipitation on all the cement surfaces based on the diffractogram. The low sulphate content in all groundwater solutions suggests that the dissolution of ettringite (initially present in the sound material) can be used as a marker of degradation. In all cases, at a depth of 80 µm below the surface, ettringite is already observable, validating the barrier role of the calcite layer.

In the experiments of HZDR supported by IRSN, low-pH cement samples were incubated under different conditions, mainly focusing on microbial impact of Cernon groundwater (calcareous water) on cement degradation or calcite precipitation. Despite the highly diverse microbial communities of natural groundwater (up to 240 genera), Pseudomonas species were the main microorganisms recovered from the biomass of cement surfaces. This suggests that they can colonize on the surface of low-pH cement as Pseudomonas are known for biofilm formation on material surface by secreting EPS-based matrix. This is congruent with the SEM images of cement samples extracted from microcosm with additional lactate. Although Pseudomonas was also identified on the cement surface from the microcosms with natural groundwater, a similar EPS-like structure was not observed. This may be due to lower microbial biomass not stimulated by exogenous lactate because the TOC content in the water of these microcosms was relatively low. On the other hand, the large decrease of calcium concentration in calcareous groundwater may have resulted from calcite deposited on the cement surface supported by SEM-EDS and XRD analyses. The calcite layer precipitated on the surface may serve as a barrier to prevent cement degradation by attack solution such as calcareous groundwater. Although stimulation of microbial growth was attempted by addition of lactate, no impact on cement degradation for the 3 months' incubation period was observed. The entire setup will be continued for up to 9 months and other analyses, including µ-CT (for cement porosity) and SEM-EDX (for composition of precipitation on cement surface) will be performed.

5. First steps in the chemo-mechanical modelling of base cases

Three partners modelled base cases in the MAGIC WP (see D16-9 for details): LMDC, LEI and CSIC. Their objective was to perform a simulation of long-term ageing of a base case study (wall of OPC concrete) representing a tunnel of radioactive waste embedded in a saturated clayey rock (Bure host rock) at 500 m depth (example of the French disposal facility case).

- The French laboratory LMDC Toulouse used the Cast3M finite element code in which a thermo-hydro-chemical model coupled to a poro-mechanical model was implemented.
- The Spanish National Research Council (CSIC) developed a model of the chemo-mechanical evolution of cementitious materials in disposal environments, by using an upscaling method from nano to micro to REV.
- The Lithuanian Energy Institute (LEI) modelled the chemo-mechanical processes at the safety structure scale with Computer codes COMSOL Multiphysics, Phreeqc and iCP (interface for COMSOL-Phreeqc).

5.1 Three modelling approaches

The primary goal of CSIC's contribution is to enhance comprehension regarding the coupled HCM effects of cement-based materials, aiming to evaluate the long-term containment of HLW. The specific objectives include investigating the coupled HCM response of concrete under repository conditions, developing a novel HCM model for concrete and conducting numerical simulations of the HCM behaviour over the long-term time scale. The code CheProf (CHEmical PROcesses Object-oriented with Fortran 2003) calculates reactive transport in a one-dimensional domain discretized by finite elements. It is developed by the Hydrogeology Research Group (GHS) from the Department of Civil Engineering at the Technical University of Catalonia (UPC). The code serves the dual functionality of reading and writing input files using Phreeqc simulations and a defined database. The input data is structured in ChemSys and LocalChem files, where "ChemSys" contains all chemical equations of state, such as mass action laws, kinetic rate laws, definition of components, phase constraints and activity models, while "LocalChem" refers to chemical state variables, such as temperature, concentrations of all species and volume fractions of phases.

The mechanical and hydraulic rock properties were based on measured laboratory results reported by Kim et al. (2018). Moreover, the concrete properties were based on reported data by Olivella et al. (2021). For the weakened concrete in the concrete-rock interface of the “altered model”, an increased porosity value of 25% and 30% decreased Young’s modulus were imposed by CSIC. Due to limited time and computational resources the simulations were run till 25 years.

For HMC process modelling, LEI used the iCP (interface for COMSOL Multiphysics and Phreeqc software). iCP is an interface developed by Amphos21 (Spain) to couple two standalone simulation programs: the general-purpose Finite Element platform COMSOL Multiphysics and the geochemical code Phreeqc (Nardi et al, 2014). The main goal of the interface is to take advantages and capabilities of mentioned codes, providing a numerical platform that can efficiently simulate a wide number of multiphysics problems coupled with geochemistry. iCP is written in Java and uses the IPhreeqcC ++ dynamic library and the COMSOL Java-API. The geochemical reactions are solved in parallel by balancing the computational load over multiple threads.

LEI research was focused on HMC model development to consider the impact of chemical interactions on mechanical properties of the concrete under disposal conditions. The constrains for concrete behaviour under repository conditions are time and scale dependent. Different physical processes might dominate during relevant repository phases (ventilation, resaturation, etc.) and contribute to subsequent phase. LEI analysed coupled HMC processes in the safety structure scale. Following the system description in the Base Case (Ibrahim et al, 2023), concrete behaviour was analysed under varying conditions. Direct modelling of reactive transport in line with HM related processes in porous media was

performed in two-dimensional space. Modelling such a complex system is a highly computational resources demanding task. Due to limited time and computational resources the simulations were run till 10,000 years.

The LMDC studied the durability of long-term storage structures under chemo-mechanical degradation. The THCM model developed by LMDC aims to enhance its adaptability to a range of mineralogies while improving its numerical performance compared to traditional geochemical models by utilizing model reduction techniques based on limiting the number of variables. These simplifications comply with a chemical context of calcium leaching coupled with carbonation in saturated and un-saturated conditions at variables temperatures. It is adaptable to different types of cements. This model was applied to predict the mechanical behaviour of the Base Case of the project. The THCM model developed in LMDC couples' calcium leaching and cement paste carbonation. The THC model is characterized by a model reduction approach that considers only two primary state variables to manage chemistry (CO_2 in the liquid phase, Ca^{2+} in the liquid phase) associated with Wl (water quantity) and T (temperature), thus forming four coupled conservation equations. The assumptions of this reduction are based on physical considerations. Several evolution laws have been developed to describe both the thermodynamic equilibrium of the cement hydrates with the pore solution, considering the variety of cement mineralogy, the effect of temperature and the progressive dissolution of the hydrates. The equations of this model have been implemented in the Cast3M finite element code. The model is used to predict variations in porosity, degree of saturation, quantity of residual hydrates, depth of carbonation and calcium leaching. This model can be adapted to consider different structures and different types of cement, and it can be used to make predictions over long periods at a reasonable numerical cost compared with conventional geochemical codes. A homogenization scheme based on the Mori-Tanaka method is adopted to account for the effects of the two types of chemical degradations on mechanical properties: hydrate dissolution, which decreases the Young's modulus, and carbonation, which leads to calcite formation and increases the Young's modulus. The THC model was coupled with the poro-mechanical model of LMDC (FLUENDO3D) in order to evaluate the creep behaviour of the tunnel subjected to the lithostatic pressure. The simulations were run till 1 million years.

The three participants to this base case study assumed that the disposal facility was located at 500-m depth. As mechanical boundary conditions, a lithostatic load of 12 MPa was placed on the top boundary of the model. Displacements perpendicular to both vertical and horizontal boundaries were restricted. As flux boundary conditions, a liquid pressure of 5 MPa was applied at the bottom boundary, while no-flux conditions were imposed on the remaining borders. The flux boundary condition depended on the stage of modelling. During the steady-state stage there are no flux conditions; after the excavation, the system allowed flux at the external 1.30 m radius circle by prescribing atmospheric pressure on it; and after the construction of the concrete support, this condition was set at the inner 1.00-m radius circle.

For CSIC's model, twenty-three species in solution and five solid phases have been considered in the calculations, for LEI also, while for LMDC the reduction of the model limited the number of diffusing species to calcium and carbon dioxides, all the other species staying reactive but static, what limits the number of diffusion equations to be solved, and then the computational cost. The time gained by LMDC for the chemical module was used to increase the realism of the mechanical behaviour, considering among other, long-term creep of degraded concrete.

The Figure 5-1 illustrates the geometries and meshing used for the THMC modelling for the different partners.

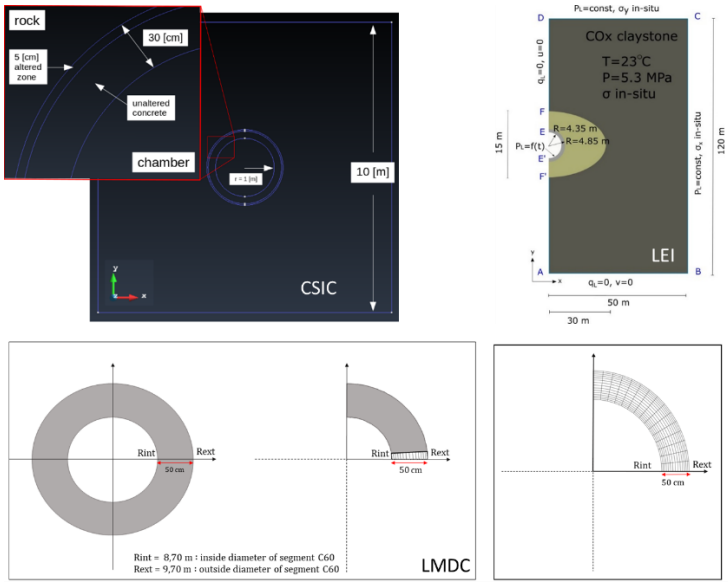

Figure 5-1 – Illustration of geometries and meshing used in the Base Case modelling by partners.

5.2 Results

Because the three teams have addressed the base case study differently, they were able to describe more or less accurately the THMC problem, and due to their more or less computation costs, were able to simulate shorter or longer durations of tunnel ageing. As CSIC was the most complete model in terms of chemistry, and the more expensive in terms of computation despite a linear HM module and a constant temperature, it reached only the 25 first years of the tunnel aging. As LEI used a lighter chemical module, and a linear HM model, it reached 10,000 years; and finally, the LMDC, with its model reduction technique was able to simulate the tunnel until one million years, and to consider the creep of the chemically degraded concrete. So, to illustrate both the ability of the models and the main results, the highlights below start with the 25 first years computed by CSIC, continues with the results of LEI until 10,000 years, and finishes with the LMDC until one million years.

5.2.1 25 first years of ageing

According to CSIC, illustrated in Figure 5-2, the leaching of calcium from concrete to the host rock leads to a degradation of C-S-H (Ca/Si 1.6) which are converted in C-S-H (Ca/Si 1.2) until 8 mm depth, while portlandite is removed from the cement paste until 26 mm depth. This leaching leads to a variation of Young's modulus which slowly affects the mechanical behaviour of the tunnel. To consider this coupling CSIC affects a reduced Young's modulus at the extrados of the tunnel (pink zone in Figure 5-3), it performed also a non-altered calculus to quantify the effect of the chemical alteration on the mechanical behaviour of the tunnel.

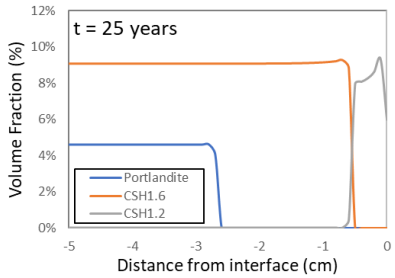

Figure 5-2 - Chemical degradation of the extrados of the tunnel at 25 years (simulations from CSIC).

According to CSIC a displacement of 2 mm can be observed at 25 years in the vertical direction within the support structure. In the horizontal direction, the displacements observed have a magnitude of 0.8 mm. Similar values were observed in both “base” and “altered” models. In relation with the variation of porosity of the concrete structure due to the hydro-mechanical effect, it was observed that this parameter remained invariable during the evaluated period of 25 years.

With the calculated liquid pressure and the stresses result data, the mean effective stress and the deviatoric stress have been calculated to plot the stress path of each analysed point and compare differences between “base” and “altered” models. Figure 5-3 presents the stress paths within the concrete support structure.

In the vertical direction within the concrete structure, it was observed that the state of stress was under compression during the 25-year period of simulation and the stress path at point A is below the failure limit in both “base” and “altered” models (Figure 5-3). As long as it is analysed closer to the inner area of the lining, the failure limit was exceeded and the stress state changed. Point B reached failure after 2 years, while point C reached it after 6 months. On the horizontal direction, all support structure points were in a compression stress state and remained below the failure limit during the whole evaluated period. The stress paths observed in points A and D revealed that an altered zone may affect the concrete integrity as a result of lower stress values for a softer material.

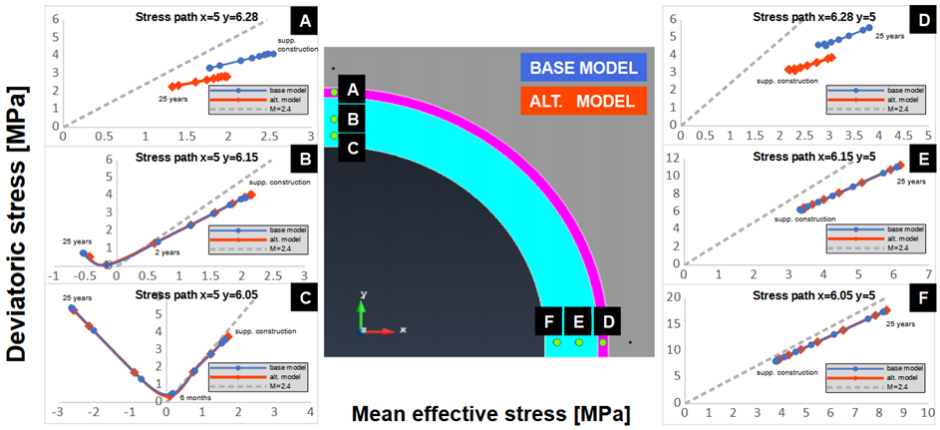

Figure 5-3: Stress path of concrete in the analysed points (Simulations at 25 years, performed by CSIC).

5.2.2 10 000 first years of ageing

LEI results showed that with the assumed material hydraulic properties and water retention properties, the EDZ, surrounding disposal tunnel, became unsaturated during the ventilation phase (till 100 years). The extent of unsaturated conditions increased gradually approximately up to EDZ outer boundary. Once the ventilation was terminated, the EDZ started to re-saturate (Figure 5-4).

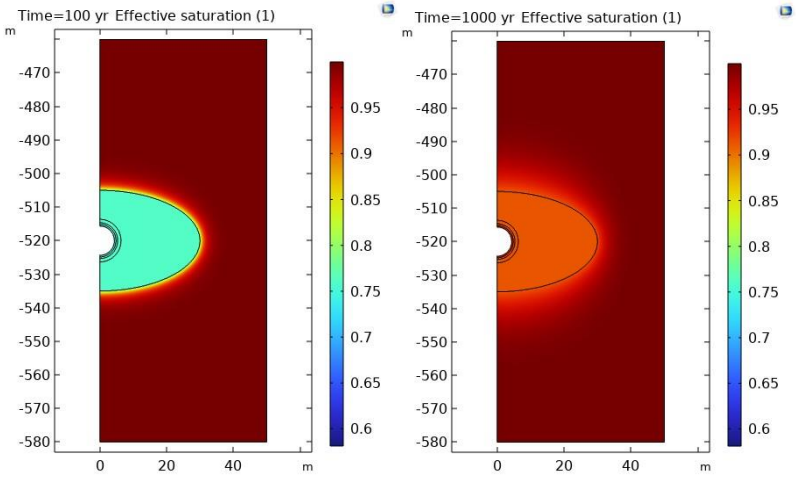

a) b)

Figure 5-4 - Porewater flow conditions (effective saturation) around the tunnel at different times after excavation: a) 100 years, b) 1000 years (Simulations between 100 and 1000 years performed by LEI).

When the EDZ was re-saturated again (after ventilation stopped), the pH did not return to initial pH value of COx porewater (~7) at the concrete-EDZ interface. Simulation results indicated that the higher pH zone was not restricted to concrete only, it propagated into the EDZ (Figure 5-5). Once the system become re-saturated again and without imposed regional groundwater flow, the transport is diffusion dominated. This is indicated by a symmetrical pH distribution from the liner. The pH distribution is related to the distribution of Na, K, Cl concentrations in the pore water. Modelling results showed that Na and K are slowly transported from the liner into the EDZ.

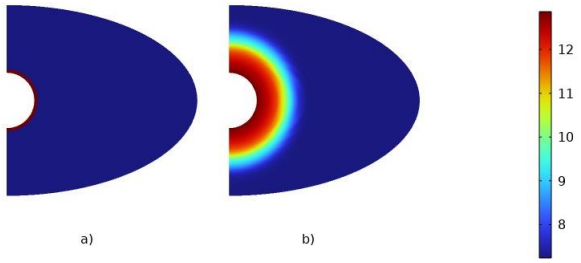

Figure 5-5 - pH distribution around the tunnel at different times: a) at 0 yr, b) at 10,000 yr (LEI results).

Relating the mechanical properties of concrete (elasticity modulus) to the calcium concentration in the solid skeleton, the changes of Young's modulus would be expected to be of limited extent (<20 cm from the external liner boundary) (Figure 5-6). Concrete weakening in terms of decreasing elasticity modulus was observed within ~5 cm of the liner outer part by the end of the simulation (10,000 yr).

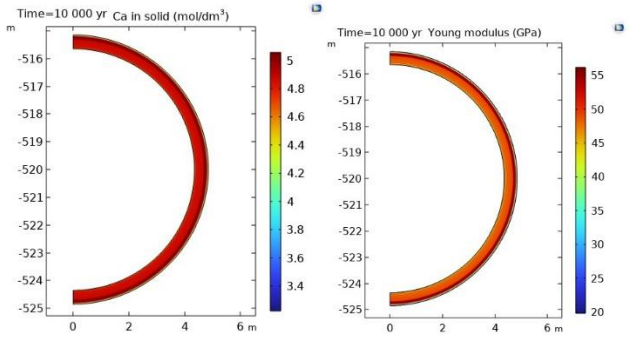

Figure 5-6 - The concentration of calcium in the solid skeleton and Young's modulus.

5.2.3 One million years of ageing

At LMDC Toulouse, the chemo-mechanical simulation was performed for one million years. The tunnel undergoes atmospheric carbonation on the intrados and decalcification coupled with liquid carbonation on the extrados due to contact with water from the saturated geological environment. After calculating the volumes of the phases resulting from the thermo-hydro-chemical model, an elastic homogenization for mechanical properties was applied based on the Mori-Tanaka scheme. Once the elastic properties are calculated based on the chemical state of the tunnel, the poro-mechanical model is applied to the tunnel, imposing lithostatic load on the extrados to evaluate tunnel creep. The dependence of elastic properties on the chemical state is calculated using a homogenization scheme which takes into account the precipitation of calcite, the dissolution of cement hydrates and the evolution of concrete porosity. Once the elastic parameters are homogenized, another nonlinear homogenization scheme provides the prediction of the shear resistance in relation to the mineralogical state. Knowing the elasticity and strength parameters, a nonlinear macroscopic creep model using these homogenized parameters predicts the strain rate as a function of loading. The creep model is coupled to a damage model and a plastic model to consider the irreversible damage induced by loading on degraded concrete. The distribution of calcite precipitation and remaining calcium in the solids after dissolution of hydrates are represented in Figure 5-7. The effect of leaching on the outer edge of the tunnel leads to a reduction of the concrete Young's modulus over the half of the wall due to hydrates dissolution (E in Figure 5-8 a)). A slight increase in the Young's modulus is observed on the tunnel side exposed to carbonation due to calcite precipitation. After one million years under 4 MPa radial pressure on the concrete, there is a radial displacement of 3 cm due to the creep of non-altered and degraded concrete (Figure 5-8 b)). Of course the pressure will not be constant in reality, it will depend on the creep speed of the host rock which must be characterized precisely for a more realistic long-term prediction of the interaction between the tunnel and the rock..

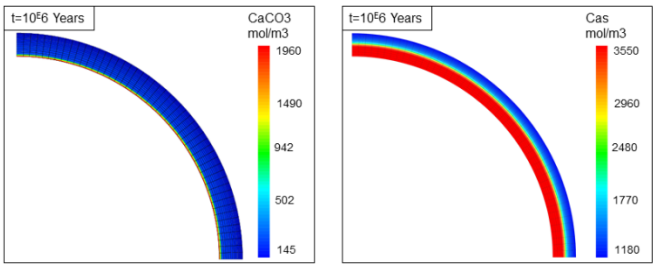

Figure 5-7 - Distribution of calcite and remaining solid calcium after 1 million years of chemical degradation (LMDC results)

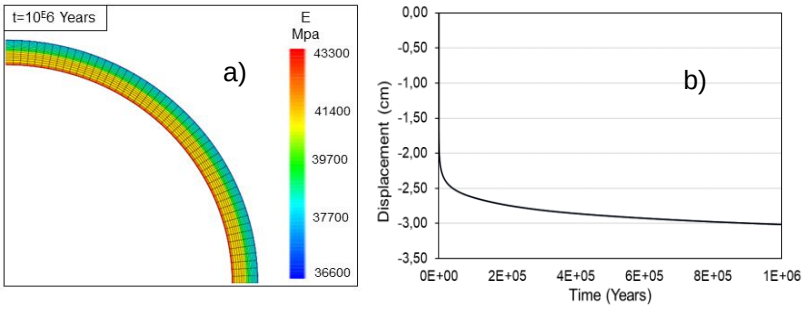

Figure 5-8 - a) Fields of elastic Young's modulus after 1 million years of chemical degradation, b) Radial displacement (convergence) of the tunnel intrados over time (LMDC results)

5.3 Synthesis of Base Case modelling

According to CSIC and based on modelling results under isothermal conditions during the first 25 years, the concrete mineral dissolution and precipitation in the analysed system were identified as slow processes. According to LEI, reactive transport modelling results with the assumed cement hydration model and relevant disposal conditions showed that the higher pH front was not limited to the concrete-EDZ interface but propagated into the EDZ within the analysed time period (10,000 yr). The pH value typical for clay rock porewater (~7) did not return on the concrete-EDZ interface during the analysed time period. Within the modelled time period, a decrease in pH value (to pH~11 and lower) in the concrete region was not observed and the corrosion of the reinforcement would not be expected. Material weakening in terms of decreasing Young's modulus was limited and modelled within ~5 cm of the liner outer part by the end of simulation of LEI, corresponding to 10,000 years. LMDC performed its simulation of the tunnel until one million years, the creep of degraded concrete leads to a radius reduction of the gallery of 3 cm, this reduction mitigates the host-rock pressure, but the concrete host rock interaction assessed by this type of modelling is based on a simplified behaviour law of the host rock which could underestimate the radial pressure at long term.

At the end of the exercise, the three laboratories implicated in the base case study at structural scale were able to consider the chemo-mechanical interactions inside the concrete structure, but the exercise shows that it is now necessary to have a reliable modelling of degraded concrete / host rock poro-mechanical interaction at very long term. Calculations are still in progress.

6. Synthesis of the added-value of MAGIC in the understanding of concrete structures aging in the geological disposal context

6.1 New knowledge acquired about the chemo-mechanical evolution of concrete during the operating period

The research developed in the field of unsaturated conditions (which includes the operating period and also the first decades after closure of a geological disposal facility), is focusing on the carbonation of cementitious materials and partly on the chemical and mechanical consequences associated to the rebar corrosion.

Effect of accelerated carbonation

At small scale, CEA developed an experimental program dedicated to provide the data and information that were necessary for the simulations of the cracking of the cement paste (C_3S and C-S-H pastes). The carbonation rate of the C_3S paste is much lower than that of the C-S-H paste, due to the protective presence of portlandite. The presence of portlandite in the cementitious materials is a key with respect to carbonation intensity. This explains why low-pH concretes are more susceptible to carbonation than Portland cement-based concretes. The results specifically acquired in MAGIC provide a clearer picture of the effect of carbonation on water retention in cementitious materials. The release of free water during carbonation is an important point - that remains unfortunately unaccounted for - as the amount of water affects not only CO_2 transport (and therefore the carbonation rate) but also deformation (and therefore potentially cracking). This is considered in the modelling part of this report.

Concerning modelling, Mines Paris Tech have simulated damage evolution in CAST3M. This approach allows to predict/assess crack openings which would then be fed back in HYTEC through the double-porosity approach available in HYTEC. A poromechanical calculation was implemented with CAST3M, thanks to the HYTEC computation of pore pressure and mineralogical compositions. This development has several advantages, which overcome the past limitations of chemo-mechanical coupling approaches from the literature:

- It is based on a physical approach: the damage and internal stresses are parametrized using the processes (carbonation and drying shrinkage, external loading) responsible for the generation of cracks;
- A dual porosity approache was used to model fractured porous media which does not require the use of upscaled behaviour laws (diffusion, …);
- The fact that the coupling from CAST3M towards HYTEC is performed considering dual porosity allows for a two-way physical coupling which greatly simplifies the mass balance and geochemical problems;
- The approach allows to simulate the closure of previously existing cracks (from mineral precipitation or stress evolution);
- Its physical roots make it, theoretically, applicable to other cement pathologies;
- It can be adapted to other reactive transport or mechanical simulators, even though HYTEC presents all the features relevant for the coupling (water production by the dissolution of cement hydrates, water evaporation and the subsequent drying).

Comparison with experimental data yielded satisfactory results and provided an explanation for the disturbance front. Since HYTEC provides a complete THC description, this coupling constitutes a first fully coupled THMC approach, with a high potential for use in other contexts.

In the case of CEM I concrete studied by several partners at macroscale, for a fully carbonated state obtained by accelerated carbonation, the mechanical properties tend to increase the material's mechanical properties (+ 10 % modulus of elasticity and + 25 % compressive strength). For an

intermediate level of carbonation (50%), the effect on mechanical properties is not significant compared with sound concrete. These results can be explained by pore filling by calcite formation, and, when the material is partially carbonated, by a phenomenon of differential carbonation shrinkage that can act as a confining pressure. Knowing that, at the end of the operating phase, the carbonation of the tunnel segment concrete should be limited to one or a few centimeters, the impact on structural mechanical behaviour should therefore be limited. The results obtained in triaxial compression (Pc = 3 MPa) show that whatever the level of carbonation, the strength increases by around 55% compared with the uniaxial case.

A complementary work on the same materials was conducted by LAMCUBE to obtain a better understanding of carbonation effects with a focus on the microstructure evolution from the microscale to the mesoscale. Comparisons between sound and carbonated samples are performed. It is found that there is no clear difference of the deformation mechanism. However, as the carbonation process induces additional material heterogeneities, the strain distributions of carbonated samples exhibit a higher heterogeneity.

Effect of accelerated carbonation on reinforced concrete

The LMDC pull-out tests study showed failure by concrete splitting for samples whose steel-concrete interface (SCI) had previously been mechanically damaged by a bending test led on prisms and characterized by two residual crack widths w1 (≈ 200-300 µm) and w2 (≈ 400 µm), whatever the level of damage. The differences between maximum shear stress depending on the level of SCI damage are low. On the other hand, failure occurred by rebar slip in case of material defect presence at the SCI, i.e. top bar effect, with a strong decrease of the maximum shear stress value. After a phase of 70 days of accelerated atmospheric carbonation, the maximum shear stress increased slightly more in the case of pull-out samples resulting from w1 crack opening prisms, than in the case of a w2. This trend appeared to be due to differences in residual crack width and thus variability of damage at the SCI, given that carbonation is not detected at this interface. The maximum shear stress decreased for the samples with top bar effect.

6.2 New knowledge acquired about the chemo-mechanical evolution of concrete during the long term period

The research concerning the cementitious materials aging was conducted from the nanoscale to the macroscale by considering the effect of chemical changes on the microstructure and consequences on the transport properties and mechanical behaviour.

At microscale, investigations were done on different aspects of the chemo-mechanical characterization of cement pastes' microstructure and the link on the diffusion properties. Mortar specimens, were exposed to Opalinus Clay pore solution, undergo diffusion and degradation experiments at 40°C. A newly designed reaction cell was employed for diffusion experiment and accelerated degradation experiment. The collaborative efforts of Empa and PSI have successfully laid the groundwork for in-depth investigations into cement paste microstructure evolution. The available HTO breakthrough curves can be now used for the validation of transport models.

The chemo-mechanical impact of calcareous water containing magnesium on the low-pH cementitious matrix was also investigated by in situ and lab experiments. IRSN in collaboration with the Helsinki University confirms that the magnesium attack is characterised by the dissolution of C-S-H and ettringite, as well as by the formation of M-S-H during the contact between a low-pH paste/concrete and an environment containing magnesium. As M-S-H has much lower microstructural and mechanical properties than C-S-H, the replacement of C-S-H by M-S-H does not maintain good mechanical and microstructural properties. Even if a new semi-amorphous phase is formed, the mechanical properties of the paste are significantly reduced during magnesium attack.

At meso-macroscale, the evolution of Portland cement was tested under multi-ionic chemical attack. In the COVRA study, ageing of mortar/concrete (CEM I and CEM III/B) in contact with poorly indurated clay simulants increased compressive strengths. A comparison of mechanical strengths is provided between samples hardened for 28 days and samples exposed for 5 years or more to a clay pore water salty as seawater, despite ingress of magnesium. The increase in compressive strength is between 24% and 47% depending on the material. The fractured surfaces of the cracked samples placed in close contact revealed a potential for self-sealing for the buffer sample, but not for the backfill sample. By the end of the project, the SEM/EDS and XRD analyses at FZJ should provide an assessment of the chemical changes and thus explain the mechanical evolution of the materials. Performing compression tests at intermediate time intervals would have provided an indication of whether the changes in compressive strength were exclusively increasing.

The chemo mechanical evolution of low-pH cementitious materials was also tested at macroscale. In the Czech team study, after 18 months' exposure (air, groundwater, bentonite suspension), a reduction in low pH concrete rigidity and mechanical strength was observed by punching tests, especially in the case of immersion in groundwater and exposure to bentonite. The reduction in strength and rigidity is around 20 to 40%. The samples show microcracks in the first few millimeters of the surface exposed to the bentonite. This is attributed, as for the study conducted by IRSN at microscale, to Mg ingress visualised by EDS elemental mapping. However, the influence of sulphates from the bentonite slurry and the impact of drilling and cutting operations cannot be excluded. New Ca mineral phases appear on surfaces of samples exposed to air. According to XRD measurements, these are gypsum and vaterite. Whatever the type of exposure, nanoindentation show an increase in modulus of elasticity of the cementitious matrix according to time, probably caused by hydration. Modulus of elasticity measured by nanoindentation is systematically lower closer to surface. SEM shows carbonation of ~100 µm deep in air and carbonation/leaching of ~1 mm in water. In the LMDC study, after a first phase of accelerated atmospheric carbonation, the reinforced concrete prisms which provide pull-out test samples were stored under COx water with humidification-drying cycles to investigate coupled effects of corrosion and state of steel-concrete interface on steel corrosion onset and steel-concrete bond behaviour. This work is still in progress.

Two teams focused on concrete ageing in contact with clay rocks. Among the mortar/concrete (OPC and blended cement) of the CI experiment from Mont Terri, only the LAC specimens (close to low-pH concrete) exhibited a clear and coherent spatial dependence of the mechanical properties on the specimen distance from the OPA interface. This difference is consistent with the presence of cracks and debonded ITZs in the cores at 0 mm, but not in the cores at 50 mm distance. Quantitative analysis of the measurements by X-ray tomography and microstructural characterization by SEM/EDS should provide a better explanation of the mechanical variations. In the SCK CEN study, the autoradiography porosity map shows that the porosity of OPC concrete increases in the first 2 mm from the interface after 14 years of interaction in contact with Boom Clay (Hades URF) due to Ca-leaching dominating over carbonation. The water sorptivity coefficient is then 3 times higher for altered concrete (at the interface) than for sound concrete, with an initial rapid absorption phase, followed by a subsequent slower absorption phase. In addition, a significant enrichment in Mg, as in the Czech group and IRSN studies, is observed in the concrete in contact with the clay, spanning a thickness of 500 µm.

A part of the work dedicated to the concrete aging under saturated conditions, especially the batch/percolation experiments to mimic 1/ the Belgian disposal conditions (SCK CEN) and 2/ a saline solution from the Konrad mine (GRS) are still in progress.

6.3 New knowledge about the impact of microbial activity on concrete aging

Multi-ionic chemical attack and microbial attack

The collaborative study by COVRA, SCK CEN and FZJ on the Dutch concept revealed a diverse microbial community in both water and concrete cubes, which is different than the community in the sand used to prepare the concrete cubes. The microbial community evolved in 1.5 years and more viable cells were observed on the concrete cubes suggesting the possibility of biofilm formation. The microbial community is present just by working with concrete. Sterilization was performed with a dose rate of 6.4 kGy per hour. This dose rate is about 1000 times larger than the dose rate of the concrete buffer interfacing the carbon steel overpack. The impact of such high radiation doses for the strength of grout (backfill) as well buffer-like concrete was measured to be negligible.

There seems to be a different microbial community present in the certified samples compared to that present in the non-certified samples but the major factor explicating these differences is not yet clear. Putatively, the superplasticizer used in the certified conditions could be an explaining factor. Furthermore, the experiments showed that gamma irradiation did not adversely affect the mechanical strength. Currently, the descriptive nature of the microbial results hampers a conclusive assessment of their impact on mechanical strength.

Experiments related to the Czech concept demonstrated that mainly water and the way how the samples are exposed to different sources of water (air humidity, continuous water flow or water suspending clay) determines the fate of low-pH concrete. In addition, metabolic activity of microorganisms is primarily driven by and dependent on the presence of water. Depending on the extent of water and local pH changes, microbial activity can be either deteriorative or protective. However, microbial-induced effects are not always as important as chemically induced changes. In air and water environments, microbiology seems to be the main driver whereas in bentonite, the chemical conversion of C-S-H to M-S-H is the most important parameter that induces negative effects.

Microbial effects in natural waters and low-carbon groundwater

In the experiments that applied a mechanistic approach, no effects on concrete samples were detected in most cases. The collaborative work of HZDR and IRSN, showed no effects of biodegradation on cement samples incubated with Cernon groundwater after 3 months, even if the microbial community was stimulated with lactate. Putatively, this time period is too short to induce some measurable effects. The results of the nine months incubation period are still pending. In addition, the decrease of calcium concentration in calcareous groundwater may resulted in calcium deposit on the cement surface, which may serve as a barrier to prevent cement degradation. Also, no effects of biodegradation on cement were observed in nitrate reducing conditions in experiments performed by UNIMAN. Nevertheless, different microbiologically induced processes were observed in high- versus low-carbon environments. Formation of calcite and aragonite precipitates were observed in high-carbon environments, which contributed to crack sealing and also pore size and pore counts decreased.

The period of the experiments carried out by SURAO/CTU/UJV/CVREZ and TUL was considerably longer compared to that of HZDR/IRSN and UNIMAN, which could explain why microbial-induced effects were observed or not.

To summarize, as part of the MAGIC WP, no evidence of accelerated degradation due to the microbial activity was highlighted.

6.4 The progress in model development at the microscale and upscaling approach

In the course of the project, a multiphase LB code for the reactive transport simulation was coupled with a surrogate model of chemical equilibria in cement paste. This code was applied for the analysis of the temporal evolution of cement phases under leaching and carbonation in 3D using a realistic representation of mineral phases and boundary conditions. Such analysis not only provide access to the spatial evolution of the microstructure but also set temporal constraints on the evolution scenario.

The obtained microstructures used for the numerical homogenisation of mechanical properties enable to estimate the temporal scale of mechanical degradation of cement paste performance. Interestingly the spatial evolution of the microstructure and the mechanical properties by time dependent simulations are comparable with the results obtained by a much more simplified model using a stochastic description of dissolution/precipitation phenomena without rigorous time constraints. The principles of numerical homogenization developed for cement paste are applicable for mortar and concrete. The analysis includes homogenized cement paste, interfacial transition zone (ITZ), air voids and aggregates.

A pore-scale reactive transport mode for describing the coupled processes of flow, multi-component transport, microbially induced calcite precipitation, and evolution of the solid surface was developed and validated using published experimental data and ready to be used for the interpretation of the experimental results of biofilm growth to be obtained in the project. The numerical experiments focus on fluid flow through a 2D channel with a rough surface. The numerical results show that heterogeneous calcite precipitation causes a generally decreased surface roughness under advection-dominated and transport-limited conditions. Moreover, the results of power spectral density analysis demonstrate that microbially induced calcite precipitation affects surface topography both through general changes in surface roughness over the entire spatial frequency range (trend of fractal dimension change) and via local modifications in surface topography in the micron wavelength spatial frequency range. Sensitivity studies clearly show that uniform and non-uniform types of precipitation can be caused by different flow rates. Such different types of precipitation lead to different surface shapes. Quantitative insights into the evolution of surface height under different flow and reaction conditions provide a comprehensive understanding of surface evolution by microbially induced calcite precipitation at the pore scale. This has implications for enhanced predictability of contaminant transport in the subsurface with microbial activities at the core scale and beyond. This pore-scale study presents insights into the microscopic physicochemical processes of biofilm-mineral-fluid interaction and its impact on surface topography and solute transport. Overall, the generalizable approach presented in this study contributes to improve the predictability of contaminant transport at the pore scale.

Significant progress has been achieved in the application of ML and AI approaches for acceleration of numerical simulation in reactive transport modelling and upscaling the mechanical properties of the cementitious systems. With the several orders of computational speedup for surrogate models replacing native geochemical solvers, time resolved 3D reactive transport simulations of the microstructure evolution become possible. Further, an ANN-based model has been developed during MAGIC to complete and improve the analytical models for elastic moduli of cement pastes. The results provided by the ANN model are in line with those obtained from the FFT-based direct simulations.

Finally, a successful step by step upscaling of mechanical properties form cement paste to concrete scale was demonstrated.

6.5 The progress in the chemo-mechanical modelling of the base case

The choice of the base case is the result of a collaborative work between the modelers and experimenters working together during the first year of the MAGIC WP, to determine the most representative case of the different context. The case of an OPC concrete wall in contact with a clayey rock was decided, exposed to the clay pore solution with resaturation over the face in contact with the host rock with a natural loading due to the rock convergence and exposed to the carbonation on the other face.

According to CSIC and based on modelling results under isothermal conditions during the first 25 years, the concrete mineral dissolution and precipitation in the analysed system were identified as slow processes. According to LEI, reactive transport modelling results with the assumed cement hydration model and relevant disposal conditions showed that a higher pH front was not limited to concrete-EDZ

interface but propagated into the EDZ within analysed time period (10,000 yr). A pH value typical for clay rock porewater (~7) did not return on the concrete-EDZ interface during analysed time period. Within the modelled time period, the decrease in pH value (to pH~11 and lower) in the concrete region was not observed and the corrosion of the reinforcement would not be expected. Material weakening in terms of decreasing Young's modulus was limited and modelled within ~5 cm of the liner outer part by the end of simulation of LEI, corresponding to 10,000 years. LMDC performed its simulation of the tunnel until one million years; the creep of degraded concrete leads to a radius reduction of the gallery of 3 cm. This reduction mitigates the host-rock pressure, but the concrete host rock interaction assessed by this type of modelling is based on a simplified behaviour law of the host rock, which could underestimate the radial pressure at long term.

At the end of the exercise, the three laboratories involved in the base case study at structural scale were able to consider the chemo-mechanical interaction inside the concrete structure, but the exercise shows that it is now necessary to have a reliable model of degraded concrete / host rock poro-mechanical interaction at very long term.

7. References

Angst U.M., Elsener B., Larsen C.K., Vennesland Ø, Chloride induced reinforcement corrosion: electrochemical monitoring of initiation stage and chloride threshold values, Corros. Sci. 53 (2011) 1451–1464.

Armand, G., Leveau, F., Nussbaum, C. et al. Geometry and Properties of the Excavation-Induced Fractures at the Meuse/Haute-Marne URL Drifts. Rock Mech Rock Eng 47, 21–41 (2014). https://doi.org/10.1007/s00603-012-0339-6.

Atkins, M., Beckley, N., Carson, S., Cowie, J., Glasser, F.P., Kindness, A., Macphee, D., Pointer, C., Rahman, A., Jappy, J.G., Evans, P.A., McHugh, G., Natingley, N.J., and Wilding, C., (1991). Medium-active waste form characterization: the performance of cementbased systems Task 3 Characterization of radioactive waste forms A series of final reports (1985-1989) No 1, Nuclear Science and technology EUR 13452, 164 p

Atkinson A. (1985) Th e time dependence of pH within a repository for radioactive waste disposal. AERE Rept. R-1l 777, Harwell, England

Bel, J.J., Wickham, S.M. and Gens, R.M. 2006. Development of the Supercontainer Design for Deep Geological Disposal of High-Level Heat Emitting Radioactive Waste in Belgium. MRS Online Proceedings Library.

Bernard E., Lothenbach B., Le Goff F., Pochard I., Dauzères A. (2017) Effect of magnesium on calcium silicate hydrate (C-S-H). Cement and Concrete Research 97: 61–72.

Bilke, Lars and Flemisch, Bernd and Kalbacher, Thomas and Kolditz, Olaf and Helmig, Rainer and Nagel, Thomas (2019): Development of Open-Source Porous Media Simulators: Principles and Experiences. Transport in Porous Media, vol. 130, p. 337-361, Springer, DOI:10.1007/s11242-019-01310-1 Wang, 2000

Bisschop, J. and Van Mier, J. (2002). Drying shrinkage microcracking in cement-based materials. Heron, 47 (3), 2002.

Cao Y., Shen W., Shao J.-F. and Wang W. (2020) A novel FFT-based phase field model for damage and cracking behavior of heterogeneous materials. International Journal of Plasticity 133:102786.

Castel, Arnaud & Vidal, Thierry & Viriyametanont, K & Francois, Raoul. (2006). Effect of reinforcing bar orientation and location on bond with self-consolidating concrete. ACI STRUCTURAL JOURNAL. 103. 559-567.

Castel A., François R., Modeling of steel and concrete strains between primary cracks for the prediction of cover controlled cracking in RC beams, Engineering Structures, Vol. 33, Issue 12, December 2011, 3668-3675

Cheng YC, Zhang YW, Jiao YB, Yang JS (2016), Quantitative analysis of concrete property under effects of crack, freeze-thaw and carbonation, Construction and Building Materials 129(2016), 106-115

Churakov, S.V. and Prasianakis, N.I. (2018) Review of the current status and challenges for a holistic process-based description of mass transport and mineral reactivity in porous media. American Journal of Science 318, 921–948.

Dauzères A., G. Achiedo, D. Nied, E. Bernard, S. Alahrache, B. Lothenbach, Magnesium perturbation in low-pH concretes placed in clayey environment—solid characterizations and modeling, Cement and Concrete Research. 79 (2016) 137–150. https://doi.org/10.1016/j.cemconres.2015.09.002.

Dauzères A., Helson O., Churakov S., Montoya V., Zghondi J., Neeft E., Shao J., Cherkouk A., Mijnendonckx K., Sellier A., Deissmann G., Arnold T., Lacarrière L., Griffa M., VIDAL T., Neji M., Bourbon X., Ibrahim L., Seigneur N., Poyet S., Bary B., Linard Y., Le Duc T., Hlavackova V., Pasteau A., Jantschik K., Middelhoff M., Perko J., Tri Phung Q., Seetharam S., Shan W., Singh A., Lloyd J., Vilarrasa V. (2022): Initial State of the Art on the chemo-mechanical evolution of cementitious materials in disposal conditions.

Dehoux, A., Bouchelaghem, F., Berthaud, Y., Micromechanical and microstructural investigation of steel corrosion layers of variable age developed under impressed current method, atmospheric or saline conditions, Corrosion Science, Volume 97, 2015, Pages 49-61, ISSN 0010-938X, https://doi.org/10.1016/j.corsci.2015.04.016.

Deissmann, G., Ait Mouheb, N., Martin, C., Turrero, M. J., Torres, E., Kursten, B., Weetjens, E., Jacques, D., Cuevas, J., Samper, J., Montenegro, L., Leivo, M., Somervouri, M., Carpen, L. (2021). Experiments and numerical model studies interfaces. Final version as of 12.05.2021 of deliverable D2.5. HORIZON 2020 project EURAD, EC Grant agreement no, 847593.

Dewitte C., Bertron A., Neji M., Lacarrière L., Dauzères A., Chemical and Microstructural Properties of Designed Cohesive M-S-H Pastes, (2022) Materials, 15 (2), art. no. 547, DOI: 10.3390/ma15020547

Drugan, W.J., Willis, J.R., A micromechanics-based nonlocal constitutive equation and estimates of representative volume element size for elastic composites, Journal of the Mechanics and Physics of Solids, Volume 44, Issue 4, 1996, Pages 497-524, ISSN 0022-5096, https://doi.org/10.1016/0022-5096(96)00007-5.

Esaker, M., Hamza, O., Elliott, D., Monitoring the bio-self-healing performance of cement mortar incubated within soil and water using electrical resistivity, Construction and Building Materials, Volume 393, 2023, 132109, ISSN 0950-0618, https://doi.org/10.1016/j.conbuildmat.2023.132109.

Galan I. et al. (2015) Assessment of the protective effect of carbonation on portlandite crystals. Cement and Concrete Research 74: 68-77.

Gong, F., Wang, Y., Zhang, D., Ueda, T., Mesoscale Simulation of Deformation for Mortar and Concrete under Cyclic Freezing and Thawing Stress, Journal of Advanced Concrete Technology, 2015, Volume 13, Issue 6, Pages 291-304, Released on J-STAGE June 16, 2015, Online ISSN 1347-3913, https://doi.org/10.3151/jact.13.291; Kalhori, H., Bagherpour, R., 2017. Application of carbonate precipitating bacteria for improving properties and repairing cracks of shotcrete. Construction and Building Materials 148, 249–260. https://doi.org/10.1016/j.conbuildmat.2017.05.074

Kangni-Foli, E. (2019). Apport de matériaux cimentaires modèles à la description des cinétiques de carbonatation de bétons bas-pH: conséquences sur la microstructure le transport de gaz et les déformations. PhD thesis, Paris Sciences et Lettres.

Kangni-Foli, E., Poyet, S., Le Bescop, P., Charpentier, T., Bernachy-Barbé, F., Dauzères, A., L'Hôpital, E., and de Lacaillerie, J.-B. d. (2021). Carbonation of model cement pastes: The mineralogical origin of microstructural changes and shrinkage. Cement and Concrete Research, 144:106446.

Kuznik, J., Obrecht, C., Rusaouen, G., Roux, J.J., LBM based flow simulation using GPU computing processor, Computers & Mathematics with Applications, Volume 59, Issue 7, 2010, Pages 2380-2392, ISSN 0898-1221, https://doi.org/10.1016/j.camwa.2009.08.052.

Heukamp F. H., Chemomechanics of Calcium Leaching of Cement-Based Materials at Different Scales: The Role of CH-Dissolution and C-S-H-Degradation on Strength and Durability Performance of Materials and Structures, Ph.D. thesis, Massachusetts Institute of Technology, U.S.A. (2003).

Huang, Y., Shao, H., Wieland, E., Kolditz, O., and Kosakowski, G. (2018). A new approach to coupled two-phase reactive transport simulation for long-term degradation of concrete. Construction and Building Materials, 190:805–829.

Huang, Y., Shao, H, Wieland, 3., Kolditz, O., Kosakowski, G., Two-phase transport in a cemented waste package considering spatio-temporal evolution of chemical condition, Materials Degradation (2021) 5:4 ; https://doi.org/10.1038/s41529-021-00150

Ibrahim, L.; Lacarriere, L.; Sellier, A. (2023). EURAD Report of Base case definition. Dissemination level: XX. 06/12/2023.

Jackson, M.D., Mulcahy, S.R., Chen, H., Li, Y., Li, Q., Cappelletti, P., and Wenk, H.-R., (2017). Philipsite and Al-tobermite mineral cements produced through low-temperature water-rock reactions in Roman marine concrete, American Mineralogist, v. 102, no. 7, p. 1435-1450.

Johannsen K. and Rademacher S. (1999) Modelling the Kinetics of Calcium Hydroxide Dissolution in Water. Acta hydrochimica et hydrobiologica 27(2): 72-78.

Kim, K., Vilarrasa, V., Makhnenko, R. (2018). CO_2 Injection Effect on Geomechanical and Flow Properties of Calcite-Rich Reservoirs. Fluids 2018, 3, 66; doi:10.3390/fluids3030066.

Kulik, D.A., Wagner, T., Dmytrieva, S.V. et al. GEM-Selektor geochemical modeling package: revised algorithm and GEMS3K numerical kernel for coupled simulation codes. Comput Geosci 17, 1–24 (2013). https://doi.org/10.1007/s10596-012-9310-6

Kulik, D.A., Improving the structural consistency of C-S-H solid solution thermodynamic models, Cement and Concrete Research, Volume 41, Issue 5, 2011, Pages 477-495, ISSN 0008-8846, https://doi.org/10.1016/j.cemconres.2011.01.012.

Lasaga, A. C. (1984). Chemical kinetics of waterrock interactions. Journal of Geophysical Research: Solid Earth (1978–2012), 89(B6), 4009-4025.

Lebon, P., Bosgiraud, J.M., Foin, R. and Armand, G., The Full Scale Seal Experiment - A Seal Industrial Prototype for Cigéo – 13106, WM2013 Conference, February 24 – 28, 2013, Phoenix, Arizona, USA.

Li, X. L., Neerdael, B., Raymaekers, D., and Sillen, X., “The construction of the HADES Underground Research Laboratory and its role in the development of the Belgian concept for a deep geological repository”, Geological Society of London Special Publications, vol. 536, no. 1, 2023. doi:10.1144/SP536-2022-101.

Lothenbach, B., Winnefeld, F. (2006) Thermodynamic modelling of the hydration of Portland cement, Cement and Concrete Research, 36 (2), 209-226Luo Z., W. Li, K. Wang, S.P. Shah, Research progress in advanced nanomechanical characterization of cement-based materials, Cement and Concrete Composites. 94 (2018) 277–295. https://doi.org/10.1016/j.cemconcomp.2018.09.016.

Lu, R., Nagel, T., Poonoosamy, J., Naumov, D., Fischer, T., Montoya, V., Kolditz, O., & Shao, H. (2022). A new operator-splitting finite element scheme for reactive transport modeling in saturated porous media. Computers & Geosciences, 163, 105106.

Luraschi P, Gimmi T, Van Loon L R, et al. Evolution of HTO and 36Cl− diffusion through a reacting cement-clay interface (OPC Paste-Na montmorillonite) over a time of six years[J]. Applied geochemistry, 2020, 119: 104581.

Mäder U., Bernard, E., CI-D Experiment: Synthetic high-pH pore water and start of fluid circulation. Mt. Terri URL Technical Note TN-2020-51, 2018.

Maghous S., Dormieux L. and Barthelemy J. (2009) Micromechanical approach to the strength properties of frictional geomaterials. European Journal of Mechanics-A/Solids 28 (1):179-188.

María Cruz Alonso, José Luis García Calvo, Jaime Cuevas, María Jesús Turrero, Raúl Fernández, Elena Torres, Ana I. Ruiz, Interaction processes at the concrete-bentonite interface after 13 years of FEBEX-Plug operation. Part I: Concrete alteration, Physics and Chemistry of the Earth, Parts A/B/C, Volume 99, 2017, Pages 38-48, ISSN 1474-7065.

Merah A., B. Krobba, Effect of the carbonatation and the type of cement (CEM I, CEM II) on the ductility and the compressive strength of concrete, Constr. Build. Mater. 148 (2017) 874–886. https://doi.org/10.1016/j.conbuildmat.2017.05.098.

Nardi, A.; Idiart, A.; Trinchero, P.; de Vries, L. M.; Molinero, J. (2014). Interface COMSOL-PHREEQC (iCP), an efficient numerical framework for the solution of coupled Multiphysics and geochemistry. Computers &Geosciences. 69, 10–21.

NEA (2012). Cementitious Materials in Safety Cases for Geological Repositories for Radioactive Waste: Role, Evolution and Interactions. NEA/RWM/R(2012)3/REV.

Neeft, E., Weetjens, E., Vokal, A., Leivo, M., Cochepin, B., Martin, C., Munier, I., Deissmann, G., Montoya, V., Poskas, P., Grigaliuniene, D., Narkuniene, A., García, E., Samper, J., Montenegro, L., Mon, A. (2020).

Treatment of chemical evolution in National Programmes, D 2.4 of the HORIZON 2020 project EURAD. EC Grant agreement no: 847593.

Neeft E., Jacques D., Deissmann G., (2022): Initial State of the Art on the assessment of the chemical evolution of ILW and HLW disposal cells. D 2.1 of the HORIZON 2020 project EURAD. EC Grant agreement no: 847593.

Neeft, E., de Bruin, T., van Kleef, R., Phung, Q.T., Perko, J., Seetharam, S., Mijnendonckx, K., Li, X., Hausmannová, L., Vašíček, R., Večerník, P., Hlaváčková, V., Černá, K., Černoušek, T., Helson, O., Bourbon, X., Zghondi, J., Vidal, T., Sellier, A., Shao, J., Rougelot, T., Jantschik, K., Kulenkampff, J., Deissmann, G., Griffa, M., Churakov, S., Gimmi, T., and Ma, B., (2021). Selected experiments for assessing the evolution of concrete, their mechanical safety function and performance targets. Final version as of 28.01.2022 of deliverable D16.3 of the HORIZON 2020 project EURAD. EC Grant agreement no: 847593., http://www.ejp-eurad.eu/.

Neji, M., Dewitte, C., Durville, B., Influence of porosity network on the chemo-mechanical evolution of low-pH cementitious materials subjected to calcareous attack, Construction and Building Materials, Volume 405, 2023, 133313, ISSN 0950-0618, https://doi.org/10.1016/j.conbuildmat.2023.133313.

Obrecht, C., Kuznik, F., Tourancheau, B., Roux, J.J., A new approach to the lattice Boltzmann method for graphics processing units, Computers & Mathematics with Applications, Volume 61, Issue 12, 2011, Pages 3628-3638, ISSN 0898-1221, https://doi.org/10.1016/j.camwa.2010.01.054.

Olivella, S., Vaunat, J., Rodriguez-Dono, A. (2021). CODE_BRIGHT 2021 Tutorial Manual. VIII. Tutorial example: Sequential Excavation Method - SEM . Universitat Politècnica de Catalunya. Department of Civil and Environmental Engineering.Ibrahim et al, 2023.

Page C.L., Initiation of chloride-induced corrosion of steel in concrete: role of the interfacial zone, Mater. Corros. 60 (2009) 586–592

Parkhurst, D.L. (1995): User's guide to PHREEQC: A computer program for speciation, reaction-path, advective-transport, and inverse geochemical calculations. US Department of the Interior, US Geological Survey.

Patel, R. A., Perko, J., Jacques, D., De Schutter, G., Van Breugel, K., & Ye, G. (2014). A versatile pore-scale multicomponent reactive transport approach based on lattice boltzmann method: Application to portlandite dissolution. Physics and Chemistry of the Earth, Parts A/B/C, 70, 127–137.

Patel, R.A., Perko, J., Jacques, D., De Schutter, G., Ye, G. and Van Breugel, K. (2018) A three-dimensional lattice Boltzmann method based reactive transport model to simulate changes in cement paste microstructure due to calcium leaching. Construction and Building Materials 166, 158-170.

Patel, R.A., Churakov, S.V. and Prasianakis, N.I. (2021) A multi-level pore scale reactive transport model for the investigation of combined leaching and carbonation of cement paste. Cement & Concrete Composites 115.

Pernicova, R.; Citek, D.; Dobias, D.; Kolisko, J.; Mandlik, T.; Hausmannova, L. Development of a Low-pH Concrete Intended for Deep Geological Repository for Radioactive Waste. Buildings 2023, 13, 182.

Phung, Q.T., Maes, N., Jacques, D., Schutter, G., Ye, G., Perko, J, Modelling the carbonation of cement pastes under a CO2 pressure gradient considering both diffusive and convective transport, Construction and Building Materials, Volume 114, 2016, Pages 333-351, ISSN 0950-0618, https://doi.org/10.1016/j.conbuildmat.2016.03.191.

Pourbaix, M. (1963). Atlas d'équilibres électrochimiques. Gauthiers-Villars & Cie. Paris.

Qian Y.-H., d'Humières D. and Lallemand P. (1992) Lattice BGK models for Navier-Stokes equation. EPL (Europhysics Letters) 17(6): 479.

Rumelhart, D.E., Hinton, G.E., Williams, R.J., Learning representations by back-propagating errors, Nature 323: 533-536

Safi, M.A., Prasianakis, N., Turek, S., Benchmark computations for 3D two-phase flows: A coupled lattice Boltzmann-level set study, Computers & Mathematics with Applications, Volume 73, Issue 3, 2017, Pages 520-536, ISSN 0898-1221, https://doi.org/10.1016/j.camwa.2016.12.014.

Savage, D., Cloet, V. (2018). A review of cement-clay modelling. Nagra Report NAB 18-24, Nagra, Wettingen, Switzerland.

Schmidt, T., Lothenbach, B., Romer, M., Neuenschwander, J., & Scrivener, K. (2009). Physical and microstructural aspects of sulfate attack on ordinary and limestone blended Portland cements. Cement and Concrete Research, 39(12), 1111-1121. https://doi.org/10.1016/j.cemconres.2009.08.005

Seigneur, N., Kangni-Foli, E., Lagneau, V., Dauzères, A., Poyet, S., Le Bescop, P., L'Hôpital, E., d'Espinose de Lacaillerie, J.-B., Predicting the atmospheric carbonation of cementitious materials using fully coupled two-phase reactive transport modelling, Cement and Concrete Research 130 (2020) 105966. https://doi.org/10.1016/j.cemconres.2019.105966.

Seigneur, N., De Windt, L., Poyet, S., Socié, A., Dauzères, A., Modelling of the evolving contributions of gas transport, cracks and chemical kinetics during atmospheric carbonation of hydrated C3S and C-S-H pastes, Cement and Concrete Research 160 (2022) 106906. https://doi.org/10.1016/j.cemconres.2022.106906.

Seymour LM, Maragh J, Sabatini P, Di Tommaso M, Weaver JC, Masic A. Hot mixing: Mechanistic insights into the durability of ancient Roman concrete. Sci Adv. 2023 Jan 6;9(1):eadd1602. doi: 10.1126/sciadv.add1602. Epub 2023 Jan 6. PMID: 36608117; PMCID: PMC9821858.

Shen W., Shao J.-F., Liu Z., Oueslati A. and De Saxcé G. (2020) Evaluation and improvement of macroscopic yield criteria of porous media having a Drucker-Prager matrix. International Journal of Plasticity 126:102609.

Shen WQ, D Kondo, L Dormieux, JF Shao (2013), A closed-form three scale model for ductile rocks with a plastically compressible porous matrix. Mechanics of Materials, 59:73-86

Shen WQ, Shao JF, Burlion N, Liu ZB (2020), A microstructure-based constitutive model for cement paste with chemical leaching effect, Mechanics of Materials 150, (2020), 103571

Shi, H, Rougelot, T., Shao, J., NEJI, M., Dewitte, M., Ma, B., Griffa, M., Churakov, S., Initial synthesis of experimental data for calibration and validation of multiscale models in Task 4, EURAD, WP MAGIC.

Socié, A., Seigneur, N., Bary, B., Poyet, S., Touzé, G., A fully coupled Hydraulic Mechanical Chemical approach applied to cementitious material damage due to carbonation, Npj Mater Degrad 7 (2023) 1–11. https://doi.org/10.1038/s41529-023-00378-x.deliverable 16-8

Soylev T.A., Francois R., Quality of steel-concrete interface and corrosion of reinforcing steel, Cem. Concr. Res. 33 (2003) 1407–1415.

Stavropoulou, E., Briffaut, M., Dufour, F., Camps, G., Time-dependent behaviour of the Callovo-Oxfordian claystone-concrete interface, Journal of Rock Mechanics and Geotechnical Engineering, Volume 12, Issue 1, 2020, Pages 89-101, ISSN 1674-7755.

Sukop, M.C., Huang, H., Lin, C.L., Deo, M.D., Oh, K and Miller, J.D., Distribution of multiphase fluids in porous media: Comparison between lattice Boltzmann modeling and micro-x-ray tomography, Phys. Rev. E 77, 026710 –b2008

Szabó-Krausz, Z., Aradi, L.E., Király, C., Kónya, P., Török, P., Szabó, C., Falus, G., (2021) Signs of in-situ geochemical interactions at the granite–concrete interface of a radioactive waste disposal, Applied Geochemistry, 126, 104881.

Thouvenot, P., Bildstein, O., Munier, I., Cochepin, B., Poyet, S., et al. Modeling of concrete carbonation in deep geological disposal of intermediate level waste (2013) EPJ Web of Conferences, EDP Sciences, International Workshop NUCPERF 2012: Long-Term Performance of Cementitious Barriers and Reinforced Concrete in Nuclear Power Plant and Radioactive Waste Storage and Disposal (RILEM Event TC 226-CNM and EFC Event 351), 56, pp.05004.

Van Breugel, K. (1995a) Numerical-simulation of hydration and microstructural development in hardening cement-based materials .1. Theory. Cement and Concrete Research 25, 319-331.

Van Breugel, K. (1995b) Numerical-simulation of hydration and microstructural development in hardening cement-based materials .2. Applications. Cement and Concrete Research 25, 522-530.

Varzina, A., Cizer, O., Yu, L., Liu, S., Jacques, D., and Perko, J. (2020). A new concept for pore-scale¨ precipitation-dissolution modelling in a lattice boltzmann framework–application to portlandite carbonation. Applied Geochemistry, 123:104786.

Von Greve-Dierfeld, S., Lothenbach, B., Vollpracht, A. et al. Correction to: Understanding the carbonation of concrete with supplementary cementitious materials: a critical review by RILEM TC 281-CCC. Mater Struct 54, 87 (2021). https://doi.org/10.1617/s11527-021-01658-1

Wang, H. (2000). Theory of linear poroelasticity with applications to geomechanics and hydrogeology.

Wang, J., Y.C. Ersan, N. Boon, and N. De Belie, Application of microorganisms in concrete: a promising sustainable strategy to improve concrete durability. Appl Microbiol Biotechnol, 2016. 100(7): p. 2993-3007

Yang, Y., Xuhai Tang, Hong Zheng, Quansheng Liu, and Zhijun Liu. (2018). Hydraulic fracturing modeling using the enriched numerical manifold method. Applied Mathematical Modelling 53 462-486.

Zadler B J, Le Rousseau J H L, Scales J A, et al. Resonant ultrasound spectroscopy: theory and application[J]. Geophysical Journal International, 2004, 156(1): 154-169.